TECHNISCHE UNIVERSITÄT WIEN
Vienna | Austria

Diplomarbeit

Mathematical modelling of quorum quenching in chemostats and biofilms

zur Erlangung des akademischen Grades

Diplom-Ingenieurin

im Rahmen des Studiums

Technische Mathematik

eingereicht von

Viktoria Eva Freingruber
Matrikelnummer: 01163226

ausgeführt am Institut für Analysis und Scientific Computing
der Fakultät für Mathematik und Geoinformation
der Technischen Universität Wien

Betreuung:
Univ.Prof. Dipl.-Math. Dr.rer.nat. Hermann Eberl
Ao.Univ.Prof.i.R. Dipl.-Ing. Dr.sc.med. Dr.techn. Dr.rer.nat. Frank Rattay

Wien, am 01.04.2019

(Unterschrift Verfasserin) (Unterschrift Betreuer)

Abstract

Quorum sensing is a method of cell-to-cell communication based on local signal density and is used by bacteria to express group behaviours, e.g. virulence or resistance against antibiotics.
This work's aim is to perform simulation-based investigations of the quorum quenching mechanism, a special way of quorum sensing inhibition where the signal molecules necessary for the communication are degraded. Two models for quorum quenching in bacterial populations are introduced. The first model is realised in a chemostat setting and is described by a system of non-linear ordinary differential equations. The second one is a two-dimensional biofilm model represented by a system of non-linear reaction-diffusion equations.
The one-dimensional chemostat model is treated analytically and thereafter, computer simulations are conducted using MATLAB. A sensitivity analysis of with respect to certain key parameters is performed. Subsequently, simulation experiments are carried out to better understand characteristic properties of the quorum quenching mechanism.
For the two-dimensional model a simulation-based parameter study for quorum quenching key parameters was conducted. Thereafter, the spatial effects of quorum quenching for different parameter sets are examined.
Subsequently, the two-dimensional biofilm model is applied to an existing model in which resistance to antibiotics is triggered by quorum sensing.
In this work it is demonstrated that existing models of quorum sensing in bacterial populations can be extended to include quorum quenching, both in a chemostat setting and spatially structured biofilms. The simulations suggest that the efficiency of quorum quenching to suppress bacterial communication is dependent on several factors, however, the performance constant of the reaction between quorum sensing and quorum quenching molecules seems to be a key parameter for this. Furthermore, there might be certain circumstances under which the models introduced here could be substantially simplified, for example because it might not be necessary to track the quorum quencher explicitly.

Zusammenfassung

Quorum Sensing (QS) ist eine Art der interzellulären Kommunikation zwischen Bakterien basierend auf der lokalen Konzentration eines speziell dafür emittierten Signalmoleküls. QS dient der Ausprägung von Gruppenverhalten und induziert unter anderem Virulenz oder Antibiotikaresistenz.
Das Ziel dieser Arbeit ist es, Quorum Quenching (QQ) - eine spezielle Art der QS Inhibition bei welcher die zur Kommunikation notwendigen Signalmoleküle abgebaut werden - zu untersuchen. Zwei QQ-Modelle für bakterielle Populationen werden vorgestellt, ein Chemostatmodell, repräsentiert durch ein System nichtlinearer, gewöhnlicher Differentialgleichungen und ein zweidimensionales Biofilmmodell, beschrieben durch nichtlineare Reaktions-Diffusions-Gleichungen.
Das Chemostatmodell wird analysiert bevor Simulationsexperimente mit MATLAB durchgeführt werden. Weiters wird eine Sensitivitätsanalyse bezüglich bestimmter Simulationsparameter ausgeführt. Im Anschluss werden Simulationsexperimente vorgenommen um charakteristische Eigenschaften des QQ-Mechanismus besser zu verstehen.
Für das zweidimensionales Modell wird eine simulationsbasierte Parameterstudie für die QQ-Hauptparameter umgesetzt. Anschließend werden die räumlichen Effekte des Mechanismus untersucht. In weiterer Folge wird das zweidimensionale Modell auf ein existierendes Modell, in welchem Antibiotikaresistenz durch QS ausgelöst wird, angewandt.
In dieser Arbeit wird demonstriert, dass existierende Modelle von bakteriellen Populationen, sowohl in planktonischen Chemostatmodellen als auch in zweidimensionalen Biofilmmodellen, mit QQ erweitert werden können. Die Simulationsergebnisse suggerieren die Abhängigkeit der Effizienz von QQ von mehreren Faktoren, wobei sich jedoch die Performance-Konstante der Reaktion zwischen QS- und QQ-Molekülen als Schlüssel- parameter herausgestellt hat. Weiters gibt es gewisse Umstände, unter welchen eine signifikante Vereinfachung der vorgestellten Modelle vorgenommen werden könnte, zum Beispiel falls eine explizite Verfolgung des Quorum Quencher nicht notwendig ist.

Acknowledgements

All of this - that thesis as well as the successful completion of my studies - was made possible by some people whom I would like to thank at this point.

First of all I would like to thank Hermann Eberl for his dedicated support, ceaseless encouragement and his valuable advice throughout the whole process of this project. I enjoyed our conversations on a variety of topics and I am grateful for the opportunity to learn and grow in such an international environment that was offered to me through my visitorship at the "Thematic Program on Emerging Challenges in Mathematical Biology" at the Fields Institute in Toronto. During my time in Canada I got to know many interesting people who encouraged me to keep studying. I learnt much more about mathematical biology and about my own desired path than I could have imagined. I would like to warmly thank you for making this possible, Hermann!

I would like to thank Frank Rattay for the trust and freedom that he gave to me and for the opportunity of a double-supervised project.

A special thanks goes to Maryam Ghasemi who not only provided the foundation for this work but also supported me with her expertise in biofilm modelling and Fortran90 coding any time I needed advice. Thank you very much for your motivation and your encouraging words, Maryam!

I also would like to thank the Fields Institute and the University of Guelph for providing the spatial, financial and computational resources to conduct my thesis project abroad.

Ein besonders großer Dank geht an meine Familie: Eva und Gerhard, danke für eure endlose Unterstützung in jeglicher Hinsicht. Danke Verena, dass wir uns wortlos verstehen. Danke, Maria und Helga, für all die warmen Mahlzeiten und euren Glauben an mich. Vielen Dank euch allen, dass ihr mir die Möglichkeit geboten habt zu dem Menschen zu werden der ich heute bin.

Fabian, najlepša hvala za pomoč pri študiju in čustveno podporo. Vedno znaš narisati nasmeh na moj obraz in spremeniti življenje v pustolovščino, tudi med najtežjimi študijskimi obdobji.

Last but not least: Thank you, Mariella and Stephan for our shared laughters, all the ups and downs during our studies and the motivation you gave me when I needed it. It was a pleasure to study with you!

Thank you, Danke, Hvala!

Viktoria

Contents

Chapter 1

Introduction

"Nature is written in the mathematical language."
(G. Galilei)

1.1 Motivation

Bacteria are the most successful life form on earth in terms of biomass and variety, as well as extent of habitats colonised and they almost entirely proliferate in biofilms, making them ubiquitous [6]. In order to gain advantages over other species that populate the biofilm, microbial organisms perform beneficial group behaviours. These are initiated by "Quorum Sensing" (QS) - a way of cell-to-cell communication based on the local population density [17]. Nowadays it is known that QS essentially depends on the transport of the signal molecules which are necessary for the communication [15, 16]. Group behaviours are initiated by gene expressions that can be triggered by quorum sensing [23, 43]. Examples for quorum sensing induced behaviours comprise the expression of bioluminescence, virulence or antimicrobial resistance [23, 43]. The latter two constitute problems that are yet to be resolved. A promising new strategy is to suppress quorum sensing by "quorum quenching", a method to degrade the quorum sensing molecules (QSMs) required for the communication [8, 14, 23, 34].

The aim of this work is to investigate the interplay between the quorum sensing and the quorum quenching mechanism by extending existing quorum sensing models for quorum quenching. In chapter 2, a chemostat model will be introduced and analysed in order to gain knowledge about the mechanism itself without considering any spatial aspects. In chapter 3, a two-dimensional biofilm model will be considered to explore the spatial aspects of the system. The spatial model is then applied to a model with antibiotics exposure to investigate the interac-

tion between antibiotics and quorum quenching molecules during the treatment of harmful biofilms (section 3.5).

1.2 Bacterial biofilms

Bacterial biofilms are microbial communities that are attached to an abiotic or biotic surface and encapsulated in an extracellular polymeric substance (EPS). The gel-like surrounding enables the performance of many reactions relevant for various bacterial activities in different processes, such as waste water treatment, food processing or medicine. Bacterial biofilms are ubiquitious in nature and industry since almost 99% of microbial life proliferates in such colonies. For simplification, "biofilm" will always refer to a bacterial biofilm in this thesis. The process of biofilm development has multiple stages (Figure 1.1). First, free floating planktonic cells land on a surface and attach to it. When a certain population density is reached, the colony starts to produce EPS. The EPS provides mechanical stability and protection from outer stresses. Thus it enables the growth and the maturation of the biofilm. The shape and size of the biofilm is highly dependent on outer conditions, as shear stress or nutrient limitation. The biofilm usually consists of multiple types of bacteria, nutritious substrates, yeast, algae, fungi and end products of the microbials' metabolisms [29].

While some biofilms are beneficial for nature or human beings, others can be harmful (e.g. pathogenic bacteria) [26, 40]. It is assumed that about 65% of infectious diseases are related to bacterial communities proliferating in biofilms [25]. Moreover, it has been reported that bacteria within biofilms are around 1000 times more resistant to antibiotics than bacteria in planktonic form [33].

1.3 Quorum sensing

Bacteria not only form and proliferate in colonies, they also start to express certain beneficial group behaviours. This phenomenon is enabled by cell-to-cell communication, called "quorum sensing" and was first observed in the bioluminescence of the bacterium *Vibrio fischeri* that - among others - plays a crucial role in the survival strategy of the Hawaiian bobtail squid *Euprymna scolopes* [43]. The bioluminescent system was documented in the early 1970s by Nealson

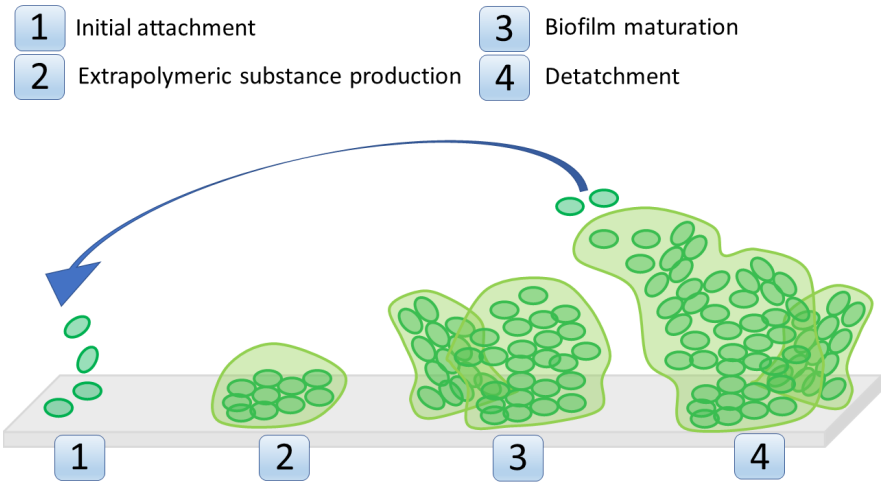

Figure 1.1: Biofilm formation: 1) Initial attachment 2) Extracellular polymeric substance production 3) Maturation 4) Detachment

et al. [31]. Only in 1994, the communication system was related to population density by Fuqua et al. [17].

In accordance with the usage of "Quorum" as the minimal number of votes necessary to make decisions as a group [1], it is used in biology to refer to a threshold of bacterial population density that "switches on" the group behaviour. Quorum sensing is a complex chemical process based on the local concentration of released signal molecules and is used by many bacteria to modulate gene expression [23, 43].

"Ordinary" cells are called down-regulated and those, performing the group behaviour are called up-regulated. The communication works with a signal molecule, the autoinducer (AI) that is produced and released by bacterial cells. From a biological point of view, there are several different mechanisms that enable quorum sensing [8, 23, 28, 43]. One of the best studied mechanisms is the system based on acyl-homoserine-lactones (AHL) as AI, used by many gram-negative bacteria (Figure 1.2) [43].

In [28, 34, 43] quorum sensing is described in detail. Gram-negative bacteria produce an AHL synthase, the LuxI-type protein, that catalyses the synthesis of AHL at a basal rate. The produced AHL diffuses out of the cell and away, if the cell density is relatively low. If the local biomass density, however, is high,

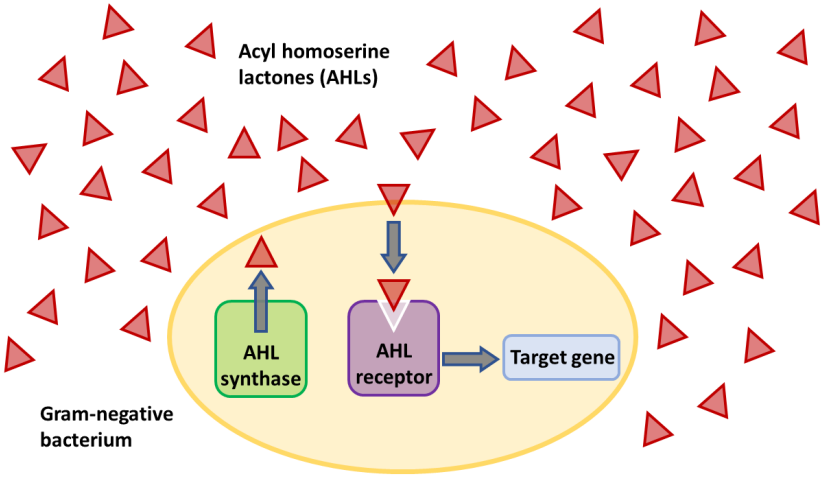

Figure 1.2: Quorum sensing mechanism in gram-negative bacteria

the AHL accumulates in the local environment until it reaches a certain threshold at which they bind to receptors, the LuxR-type proteins. This molecule then modulates the gene expression, resulting in the group behaviour, such as bioluminescence, EPS production, enhanced AHL production, the expression of virulence or antimicrobial resistance. This process is called up-regulation.

This work focusses on quorum sensing in gram-negative bacteria, using AHL as an autoinducer.

Quorum sensing based behaviours have significant, however sometimes harmful impacts and appear in various areas, such as food spoiling, aquaculture, water purification and medicine [23]. Quorum sensing also enables the performance of bacterial behaviours, as virulence or antimicrobial resistance [34]. A promising new strategy to cope with these problems is Quorum Sensing Inhibition (QSI).

Meanwhile it is very well understood that QS is not simply dependant on the local bacterial population size but that convection and diffusion are able to disrupt cell-to-cell communication even though population size is "big" or enable communication in "small" populations by transporting signal molecules in the environment [15, 16].

1.4 Quorum sensing inhibition

The quorum sensing mechanism can be disrupted in different ways. One could interfere by inhibiting QSM production, blocking the QSM receptor or accelerating the degredation of QSMs. The last possibility is also referred to as "Quorum Quenching" (QQ) [23]. This work will focus on a quorum quenching system applied to gram-negative bacteria using AHL as auto inducer. AHL molecules differ in length and substitution of their acyl chain, but have the same homoserine lactone moiety. Quorum quenching molecules (QQMs) appear naturally and are used by microbial species to gain an advantage in competitive environments. QQ molecules could be detected in (at least) 10 different bacterial species, including 4 *Bacillus spp.*, *Agrobacterium tumefaciens*, *Arthrobacter sp.*, *Klebsiella pneumoniae*, *Pseudomonas aeruginosa*, *Ralstonia sp.* and *Variovorax paradoxus*. The fact that the genes encoding AHL-degradation molecules are wide spread within bacterial species, might indicate the prevalence of that feature in many other prokaryeutic organisms. So far, these molecules can be categorised into two distinct groups of AHL-degrading molecules, the acyl-homoserine lactonase (AHL-lactonase) and the acyl-homoserine lactone acylase (AHL-acylase) [8].

AHL-lactonase degrades AHL by hydrolising its lactone bond (Figure 1.3). Aiia from Bacillus sp. 240B1 is a well-studied AHL-lactonase and shows high enzymatic activity against many tested AHLs [8].

AHL-acylase degrades AHL by hydrolising the amide linkage between the fatty acid chain and the homoserine lactone moiety (Figure 1.3). There is not much known about AHL-acylase [8].

Not only prokaryeutic organisms, but also eukaryots use quorum sensing and quorum quenching to gain beneficial effects in competitive surroundings [23]. In [23] detailed lists of eukaryotes, prokaryotes, their QS and QSI molecules are provided.

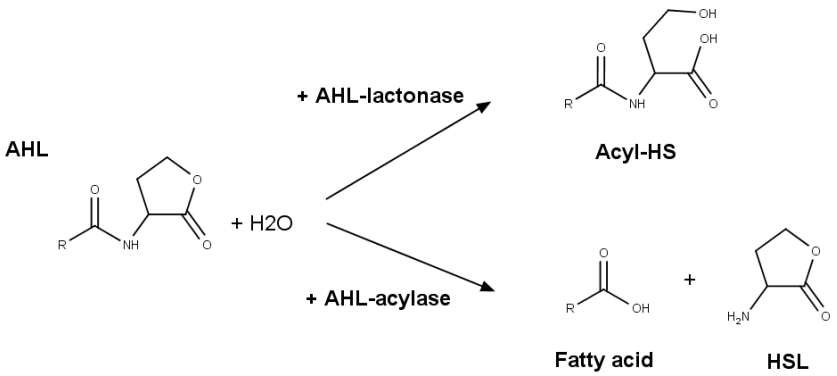

Figure 1.3: Quorum Quenching mechanism with AHL-lactonase and AHL-acylase

1.5 The chemostat model

The chemostat was introduced by Novick and Szilard in 1950 [32]. A chemostat is a closed environment where microbial reactions occur under controlled conditions. It has a continuous inflow and an equally rated outflow, keeping the volume constant. The feed contains nutrients and other substances that are supposed to enter the system from outside. The chemostat is well-stirred and thus only changes in time, but not in space need to be considered (see Figure 1.4).

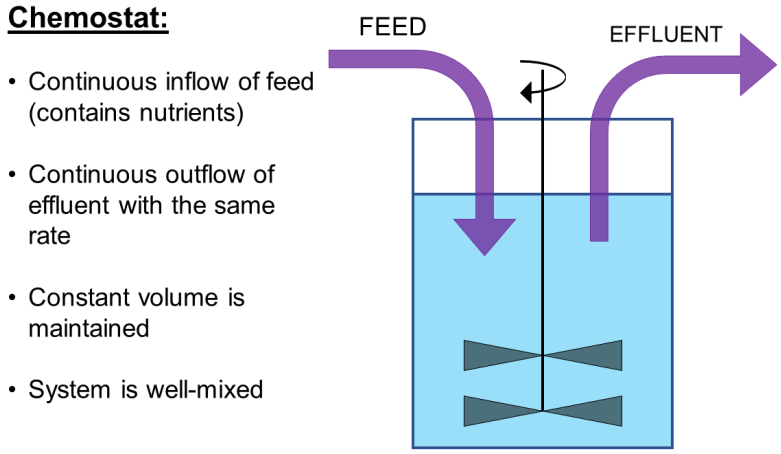

Figure 1.4: General chemostat setup

System (1.1) displayed below describes a simple chemostat model with one species, referred to as N and one growth limiting nutrient C:

$$\begin{cases} \frac{\mathrm{d}N}{\mathrm{d}t} = \underbrace{f(C(t))N(t)}_{\text{nutrient dependend growth term}} - \underbrace{qN(t)}_{\text{outflow}} \\ \frac{\mathrm{d}C}{\mathrm{d}t} = \underbrace{q(C^{\infty} - C(t))}_{\text{in-/ outflow}} - \underbrace{\frac{1}{Y} f(C(t))N(t)}_{\text{nutrient consumption term}} . \end{cases} \tag{1.1}$$

The dilution rate, i.e. the ratio between inflow rate and volume, is referred to as q and C^{∞} represents the nutrient concentration in the feed. The growth function f depends on the nutrient concentration within the chemostat. The consumption rate is the fraction between growth rate and yield coefficient Y which is the ratio of mass of microorganisms and mass of nutrients utilised [21]. Commonly, it is

assumed that f follows Monod kinetics [30]:

$$\begin{cases} \frac{\mathrm{d}N}{\mathrm{d}t} = \mu N \frac{C}{k+C} - qN(t) \\ \frac{\mathrm{d}C}{\mathrm{d}t} = q(C^\infty - C(t)) - \frac{\mu}{Y} N \frac{C}{k+C}. \end{cases} \tag{1.2}$$

This system (1.2) has at most two non-negative equilibria:
The *washout equilibrium* $(0, C^\infty)$ that is asymptotically stable if $C^\infty < \frac{qk}{\mu - q}$ and unstable otherwise. This equilibrium always exists.
The *non-trivial equilibrium* $(Y(C^\infty - \frac{qk}{\mu-q}), \frac{qk}{\mu-q})$, $C^\infty > \frac{qk}{\mu-q}$ exists only if the washout equilibrium is unstable. The non-trivial equilibrium is always stable if it exists. These stability results can be obtained with the linearisation of the system

$$J(C, N) = \begin{pmatrix} \mu \frac{C}{k+C} - q & \mu N \frac{k}{(k+C)^2} \\ -\frac{\mu}{Y} \frac{C}{k+C} & -q - \frac{\mu}{Y} \frac{k}{(k+C)^2} N \end{pmatrix}.$$

1.6 Mathematical modelling of biofilms

Rising evidence for biofilms' ubiquity incited attention in diverse disciplines, leading to the development of various mathematical models for biofilms. There exist continuum, as well as discrete approaches.

1.6.1 Continuum models

A basic biofilm model contains terms for biomass growth, transport and consumption. These models can be either formulated with ordinary differential equations (ODEs) or partial differential equations (PDEs) in one or more spatial dimensions. Although, ODE and one-dimensional PDE models do not offer much information on the shape and spatial development, they can be used to analyse a system globally if spatial resolutions are not required. After it became clear that biofilms are highly complex spatial formations [6], also multi-dimensional models were developed.

In multi-dimensional PDE models, the domain observed is parted into two sections (Figure 1.5). The biofilm itself, where the biomass $N(x, t)$ is greater than

zero and the bulk liquid around it, where the biomass is equal to zero:

$$\Omega_1(t) := \{x \in \Omega \quad | \quad N(x,t) > 0\}$$
$$\Omega_0(t) := \{x \in \Omega \quad | \quad N(x,t) = 0\}.$$

The domain contains two types of components, dissolved substrates as nutri-

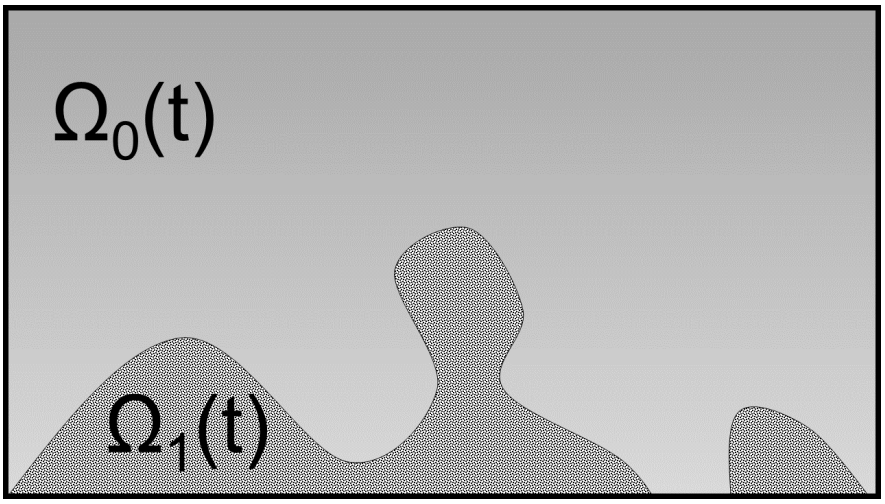

Figure 1.5: Domain of a biofilm model: Liquid Phase Ω_0 and Biofilm Ω_1

ents, signal molecules, antibiotics or metabolic products and particulate cells as active and inert bacterial cells. The model needs to contain terms for growth, consumption and transport [29]. While the transport of dissolved substrates can be modelled with diffusion, the spreading of the biomass is more complex and depends on physical and environmental conditions, as shear stress or nutrient availability [10, 38]. Before continuum approaches to the biofilm development were developed, discrete models were used to describe the biofilm growth. These usually are based on probabilistic rules for the spreading mechanism, but often lack in accuracy for many reasons [10]. Therefore Eberl et al. [10] proposed a prototype continuum model for the growth and spreading of a biofilm:

$$\begin{cases} \dfrac{\partial C}{\partial t} = \nabla \cdot (d_C(N)\nabla C) - f(C,N) \\ \dfrac{\partial N}{\partial t} = \nabla \cdot (d_N(N)\nabla M) - g(C,N). \end{cases} \tag{1.3}$$

where the consumption term $f(C,N) = k_1 N \frac{C}{k_2+C}$ is represented by Monod kinetics and the biomass production term is defined as $g(C,N) = k_3(f(C,N) - k_4 N)$ and $k_{1,2,3,4} \geq 0$. $C(t,x)$ is the nutrient concentration that changes due to diffu-

$N(t,x)$	Biomass density
$C(t,x)$	Nutrient concentration
$d_{C,N}$	Diffusion coefficients for C and N
$f(C,N)$	Nutrient consumption rate
$g(C,N)$	Biomass production rate

sion. $N(t,x)$ represents the biomass density that grows by nutrient consumption. The authors developed a diffusion coefficient for the biomass that satisfies the following criteria:

- There exists a sharp boundary between biofilm and liquid phase.
- Spreading of the biomass is significant if a certain density N_{max} is approached and this bound cannot be exceeded.

The diffusion coefficient

$$d_N(N) := \big(\frac{\epsilon}{N_{max} - N}\big)^b N^a \tag{1.4}$$

is zero for $N = 0$ and almost zero when N is significantly smaller than N_{max}, but diverges for $N \to N_{max}$. The constants a, b are greater than 1. The nutrient's diffusion coefficient $d_C(N)$ is also density dependent, but in a non-critical way.
Originally, this model also considered a flow field in the liquid phase, represented by the Navier Stokes equation. Due to high complexity of the system, the authors assumed the hydrostatic case $u \equiv 0$, resulting in the system introduced above. In this case the shear stress can be neglected.
Furthermore, it is assumed that $d_C(M) = d_C$ is constant, leading to the simplified system:

$$\begin{cases} \dfrac{\partial C}{\partial t} = d_C \nabla^2 C - f(C,M) \\ \dfrac{\partial N}{\partial t} = \nabla \cdot \big[\big(\dfrac{\epsilon}{N_{max} - N}\big)^b N^a \nabla N\big] + g(C,M). \end{cases} \tag{1.5}$$

This system was refined and numerically treated in [9, 11, 19] and analysed in [12]. In [12] it was shown that $N < N_{max} = 1$ which ensures the well-posedness of the problem. The non-linear density-dependent diffusion coefficient for the biomass was also used in biofilm models considering quorum sensing [15, 16, 19] and in biofilm models with quorum sensing and under antibiotics exposure [18, 20].

1.6.2 Discrete models

Discrete approaches usually use bottom-up models such that the biofilm is built from the bacterial unit's scope of action. These approaches also use ordinary differential equations for the growth terms, but discrete rules for the transport. There are three main model types. These are Cellular Automaton (CA) models, hybrid differential-discrete CA models and Individual-based models, which are agent based models [26, 40].

1.7 Modelling of quorum sensing and quorum quenching

1.7.1 Modelling of quorum sensing

Since the discovery of the quorum sensing mechanism in 1994 [17], mathematical models have been developed and improved. There exist multi-dimensional models in form of PDE systems as well as ODE models.

Quorum sensing in planktonic lifeforms can be modelled with a system of ODEs since spatial effects can be fully ignored here. Ward et al. formulated a model for quorum sensing in bacteria in 2001 [41]. The biomass now has to be divided into two different types, down- and up-regulated cells, where the up-regulated cells are those who underwent the changes in gene expressions.

$$\begin{cases} \dfrac{\mathrm{d}N_d}{\mathrm{d}t} = r(N_d + (2-\gamma)N_u)F(N_d+N_u) - \alpha G(A)N_d + \beta N_u \\ \dfrac{\mathrm{d}N_u}{\mathrm{d}t} = r(\gamma-1)N_u F(N_d+N_u) + \alpha G(A)N_d - \beta N_u \\ \dfrac{\mathrm{d}A}{\mathrm{d}t} = \kappa_u N_u + \kappa_d N_d - \alpha G(A)N_d - \lambda A \end{cases} \tag{1.6}$$

N_d and N_u represent the down- and the up-regulated populations, and A is the signal molecule. $F(.)$ is a suitable growth function and $G(A)$ the up-regulation function. At the time this work was published, there was little known about the kinetics of this process. Therefore the authors assumed $G(A) = A$ to be linear. However, they mentioned that for larger A, Monod kinetics $G(A) = \frac{A}{1+k_a A}$ might be more suitable. For the down-regulation, the term βN_u was used. Up- and down-regulated cells are assumed to produce signal molecules at different rates

κ_u and κ_d and Signal molecules decay naturally with rate λ. It is furthermore assumed that one up-regulated cell divides into γ up-regulated and $(2-\gamma)$ down-regulated cells. γ is highly dependent on the signal molecule concentration inside and outside of the cell during the division process, the authors refer to experimental data and use $\gamma \approx 1$.

Quorum sensing in biofilms is often modelled using partial differential equations in multiple dimensions, so that the complex spatial development can be pursued. Ghasemi et al. in [18] extended the quorum sensing models [13, 15, 35]. The model in [18] is given by

$$\begin{cases} \frac{\partial N_d}{\partial t} = & \nabla \cdot (D(N)\nabla N_d) + \mu N_d \frac{C}{K_C + C} + \psi N_u \frac{\tau^n}{\tau^n + A^n} \\ & -\omega N_d \frac{A^n}{\tau^n + A^n} - K N_d \\ \frac{\partial N_u}{\partial t} = & \nabla \cdot (D(N)\nabla N_u) + \mu N_u \frac{C}{K_C + C} - \psi N_u \frac{\tau^n}{\tau^n + A^n} \\ & +\omega N_d \frac{A^n}{\tau^n + A^n} - K N_u \\ \frac{\partial C}{\partial t} = & \nabla \cdot (D_C(N)\nabla C) - \nu N_d \frac{C}{K_C + C} - \nu N_u \frac{C}{K_C + C} \\ \frac{\partial A}{\partial t} = & \nabla \cdot (D_A(N)\nabla A) + \alpha N_\infty (N_d + N_u) + \beta N_\infty N_u \frac{A^n}{\tau^n + A^n} - \gamma A. \end{cases} \tag{1.7}$$

N_d and N_u being again the down- and the up-regulated biomass density, C the nutrient concentration and A the signal molecule concentration. N is the total biomass, $N = N_d + N_u$. The substrates C and A only move due to diffusion, since the hydrostatic case is considered and thus convection can be neglected. For the diffusion coefficients $D_{C,A} = d_{C,A}(1 + M(\rho_{C,A} - 1))$, non-critical linear terms were used, where $d_{C,A} > 0$ and $0 < \rho_{C,A} \leq 1$ are the diffusion coefficients in water and the ratio of diffusivity between biofilm and water respectively. The diffusion coefficient for the biomass is defined as $D(N) = \delta N^a (1 - N)^{-b}$ with $a, b > 1$, similar to [10]. For the switching between the two types of bacteria, so called Hill equations $\frac{A^n}{\tau^n + A^n}$ or $\frac{\tau^n}{\tau^n + A^n}$ are used. These functions converge to the Heaviside function for $n \to \infty$ and equal the Monod equation for nutrient consumption for $n = 1$. Usually a value $2 \leq n \leq 3$ is used [15, 16].

1.7.2 Modelling of quorum quenching

Due to the recency of the strategy to treat harmful biofilms with quorum quenching molecules, the range of mathematical models is still very limited.
In [42] a quorum sensing inhibition model was introduced by Wei et al. in 2016. The authors expanded the quorum sensing models introduced in [27] and [44] and developed a complex ODE model considering the whole AHL production process and all three possibilities of QSI.

$$
\begin{cases}
\dfrac{\mathrm{d}[A]}{\mathrm{d}t} = & \underbrace{\left(c_A + \dfrac{k_A[C]}{K_C + [C]}\right)\dfrac{K_{QSILasI}}{K_{QSI_{LasI}} + [QSI_{LasI}]}}_{\text{inhibition of AHL production}} - k_0[A] \\
& - k_1[R][A] + k_2[RA] - \underbrace{k_{cat}[A][QSI_d]\dfrac{[A]}{K_M + [A]}}_{\text{degradation of AHL molecules}} \\
\dfrac{\mathrm{d}[R]}{\mathrm{d}t} = & c_R + \dfrac{k_R[C]}{K_C + [C]} - k_3[R] - k_1[R][A] \\
& + k_2[RA] - \underbrace{k_8[R][QSI_{anlg}] + k_9[RQSI_{anlg}]}_{\text{blockade of AHL receptor}} \\
\dfrac{\mathrm{d}[RA]}{\mathrm{d}t} = & k_1[R][A] - k_2[RA] - 2k_4[RA]^2 + 2k_5[C] \\
\dfrac{\mathrm{d}[C]}{\mathrm{d}t} = & k_4[RA]^2 - k_5[C] \\
\dfrac{\mathrm{d}[QSI_{LasI}]}{\mathrm{d}t} = & -k_6[QSI_{LasI}] \\
\dfrac{\mathrm{d}[QSI_d]}{\mathrm{d}t} = & -k_7[QSI_d] \\
\dfrac{\mathrm{d}[QSI_{anlg}]}{\mathrm{d}t} = & k_9[RQSI_{anlg}] - k_8[R][QSI_{anlg}] - k_{10}[QSI_{anlg}] \\
\dfrac{\mathrm{d}[RQSI_{anlg}]}{\mathrm{d}t} = & k_8[R][QSI_{anlg}] - k_9[RQSI_{anlg}].
\end{cases}
\tag{1.8}
$$

The variable A represent the AHL molecules, R the LasR complex (responsible for the AHL reception), RA the complex formed by LasR and AHL, C the dimerized complex and c_A and c_B stand for the base level transcription for A and R respectively. QSI_{LasI} stands for the QSI molecule that inhibits AHL production and QSI_d for the QQ molecule. The AHL receptor is blocked by molecules that act as antagonists for AHL and are referred to as QSI_{anlg}, and $RQSI_{anlg}$ is the binding product of LasR and QSI_{anlg}. In combination they are responsible for the third inhibition process. $[X]$ denotes the concentration of component X. The

Table 1.1: Parameter description for QSI-QQ model (1.8) from [42]

K_M	Michaelis constant
$K_{QSI_{LasI}}$	Constant for QSI of AHL prod.
K_C	LasR and AHL half saturation concentration
k_R	LasR max. prod. rate
k_A	AHL max. prod. rate
$k_{0,3,6,7,10}$	decay rates
k_1	LasR-AHL binding rate
k_2	LasR-AHL unbinding rate
k_4	formation rate of LasR-AHL complex
k_5	deformation rate of LasR-AHL complex
k_8	$LasR - QSI_{anlg}$ binding rate
k_9	$LasR - QSI_{anlg}$ unbinding rate

authors integrated this QS-QSI model in a multiscale environment where also bacterial cells in a biofilm on mesoscopic scale are investigated.

In [14] combination strategies of quorum sensing inhibition and quorum quenching in suppressing quorum sensing in *P.aeruginosa* are investigated. The authors present a model describing the LasR/I circuit. The quorum quenching function for degrading the AHL molecules is not given explicitly. The assumptions $\eta'(QQ) > 0$ and $\eta''(QQ) \leq 0$ are made for that term.

Aside from these two publication, there can be found hardly anything concerning quorum quenching models. However, there are some biological papers on specific AHLs, their QQ molecules and reaction kinetics, including [7] and [39]. In both publications, Michaelis Menten kinetics $Qk_{cat}\frac{A}{K+A}$ used to fit the experimental data, where Q stands for the QQM, A for the AHL, k_{cat} for the reaction rate and K for the Michaelis constant. This assumption is consistent with the model assumption in [42], suggesting the retention of this term in future models.

1.8 Objectives

There is only little literature about mathematical quorum quenching (QQ) or quorum sensing inhibition (QSI) models. In [14] the authors show that quorum quenching can boost the effectiveness of quorum sensing inhibition and vice versa. However, their simulations show that when the therapy strategies are not combined, QSI could reduce the signal molecule by 35% and QQ could reduce it by almost 100%.
The effects of quorum quenching or quorum sensing inhibition on a bacterial community has only been studied in [42], as far as it is known. The authors use a complex multiscale approach in order to capture the complex mechanisms involved.

Modelling quorum sensing inhibition requires an involved model of the cell signalling pathways on a molecular scale. Combining this approach with a mesoscopic biofilm model on cellular scale would create a highly complex system, as in [42]. Considering only the QQ mechanism allows to build the model on a mesoscopic cell-level such that both, information on the bacterial colony and their signal molecules can be obtained.

The aim of this work is to fill that empty gap in the literature with a model that treats the simple but effective mechanism of quorum quenching with effect on a bacterial colony as well as its signal molecules without using a multiscale approach.

1.9 Outline of the thesis

In the second chapter a planktonic chemostat model in form of an ODE system is introduced. The goal of this section is to investigate the quorum quenching mechanism itself and to suitably integrate a new equation with adequate parameters for the quorum quenching in well-studied models for quorum sensing systems.
In the third chapter, the system is investigated in a two-dimensional domain. A system of diffusion-reaction-equations is introduced and analysed. The focus in this chapter is the spatial development of the biofilm and the chemical communication process.
The fourth chapter consists of the discussion of the results and the conclusion.

Chapter 2

Quorum quenching chemostat model

"All models are wrong, but some models are useful."
(G. Box)

2.1 Introduction

In this chapter a system of ordinary differential equations representing a QS-QQ-chemostat model is introduced. The aim of this chapter is to investigate and analyse the quorum quenching mechanism applied to a planktonic colony that coordinates gene expressions with quorum sensing. For further explanation of a standard chemostat model see section 1.5.
The model includes two types of bacteria, as there are down-regulated and up-regulated cells as well as three dissolved substrates: the nutrients, quorum quenching molecules (QQM) and quorum sensing molecules (AHL or QSM). While the latter is produced by the bacterial cells, the former two are added to the system with the feed. Down-regulated cells refer to the standard type and up-regulated cells follow the group behaviour. The following variable names will be used for these components:

N_d	Down-regulated bacteria, "normal" or non-resistant type
N_u	Up-regulated bacteria, resistant type
C	Nutrients
A	Quorum sensing molecules (QSMs)
Q	Quorum quenching molecules (QQMs).

2.2 Modelling

2.2.1 Model assumptions

Our model derivation will be based on the following assumptions:

1. **Chemostat:**
   The system is regarded in a chemostat setup. Assumptions for the general chemostat setup follow [32]. The inflow and outflow rates are constant and equal and the contents are well-stirred, resulting in a homogeneous spatial distribution.
   Nutrients and QQM are added with the feed at rate q. All the components flow out of the system equally with rate q.

2. **Consumption based cell growth:**
   Both, down- and up-regulated cells grow according to Monod kinetics [30] with maximum growth rates μ_d and μ_u and half saturation concentration k_C. Following the assumptions in [41] and [2], an up-regulated cell divides into γ up-regulated and $(2-\gamma)$ down-regulated cells.
   Nutrients are used up accordingly with yield coefficients y_d and y_u.

3. **Up- and down-regulation:**
   The up-regulation and the down-regulation behave according to the Hill equation with Hill constant n and threshold for the up-regulation k_A [20]. The maximum rates for the up- and the down-regulation are denoted by α and β respectively.

4. **Production of QSMs:**
   Signal molecules are produced by both down- and up-regulated cells at a basal rate κ_0 [20].
   The production of signal molecules is accelerated when the system becomes up-regulated. This effect is again modelled with the Hill function for the up-regulation and has maximal production rate κ_1 [20].

5. **QSM-QQM reaction:**
   The reaction of quorum sensing and quorum quenching is modelled with saturation kinetics with maximum reaction rate ν, half saturation rate k_Q and reaction ratio between QSM and QQM r. [7, 39, 42].

6. **Initial conditions:**
   Initially, only down-regulated cells and nutrients are in the chemostat.

2.2.2 Model equations

Based on the assumptions (A1-A6) above, the model equations read as follows:

$$
\begin{cases}
\dfrac{\mathrm{d}N_d}{\mathrm{d}t} = \underbrace{\mu_d N_d \dfrac{C}{k_C + C} + (2-\gamma)\mu_u N_u \dfrac{C}{k_C + C}}_{\text{growth terms (A2)}} \underbrace{- qN_d}_{\text{outflow (A1)}} \\
\qquad \underbrace{- \alpha N_d \dfrac{A^n}{k_A^n + A^n}}_{\text{up-regulation (A3)}} + \underbrace{\beta N_u \dfrac{k_A^n}{k_A^n + A^n}}_{\text{down-regulation (A3)}} \\
\dfrac{\mathrm{d}N_u}{\mathrm{d}t} = \underbrace{(\gamma-1)\mu_u N_u \dfrac{C}{k_C + C}}_{\text{growth term (A2)}} \underbrace{- qN_u}_{\text{outflow (A1)}} \\
\qquad + \underbrace{\alpha N_d \dfrac{A^n}{k_A^n + A^n}}_{\text{up-regulation (A3)}} \underbrace{- \beta N_u \dfrac{k_A^n}{k_A^n + A^n}}_{\text{down-regulation (A3)}} \\
\dfrac{\mathrm{d}C}{\mathrm{d}t} = \underbrace{q(C^\infty - C)}_{\text{in-/ outflow (A1)}} \underbrace{- \dfrac{\mu_d}{y_d}\dfrac{C}{k_C + C}N_d - \dfrac{\mu_u}{y_u}\dfrac{C}{k_C + C}N_u}_{\text{nutrient consumption (A2)}} \\
\dfrac{\mathrm{d}A}{\mathrm{d}t} = \underbrace{\kappa_0(N_u + N_d)}_{\text{basic signal production (A4)}} + \underbrace{\kappa_1 N_u \dfrac{A^n}{k_A^n + A^n}}_{\text{enhanced signal production by up-reg. cells (A4)}} \\
\qquad \underbrace{- \nu Q \dfrac{A}{k_Q + A}}_{\text{QS-QQ reaction (A5)}} \underbrace{- qA}_{\text{outflow (A1)}} \\
\dfrac{\mathrm{d}Q}{\mathrm{d}t} = \underbrace{q(Q^\infty - Q)}_{\text{in-/ outflow (A1)}} \underbrace{- \dfrac{\nu}{r} Q \dfrac{A}{k_Q + A}}_{\text{QS-QQ reaction (A5)}}
\end{cases}
\tag{2.1}
$$

with initial conditions according to A6

$$\begin{cases} N_d(0) = N_d^0 \geq 0 \\ C(0) = C^0 \geq 0 \\ N_u(0) = A(0) = Q(0) = 0. \end{cases} \tag{2.2}$$

2.2.3 Analytical treatment

Existence and uniqueness of a solution

The system (2.1) - (2.2) consists of non-linear, autonomous, first-order differential equations and can more generally be written as

$$\frac{\mathrm{d}y}{\mathrm{d}t} = f(y) \tag{2.3}$$

$$y(0) = y_0 \tag{2.4}$$

where $y(t) = (N_d(t), N_u(t), C(t), A(t), Q(t))^T$, $y_0 = (N_d^0, N_u^0, C^0, A^0, Q^0)^T$ and $f \in C(\mathbb{R}^5, \mathbb{R}^5)$.

Proposition 2.2.1. *Let* $S := \mathbb{R}_0^+ \times \mathbb{R}_0^+ \times [0, C^\infty] \times \mathbb{R}_0^+ \times [0, Q^\infty]$ *and let all the parameters used in* (2.1) *be positive and the initial values* (2.2) *be non-negative. The initial value problem* (2.1) - (2.2) *with initial values* $(N_d^0, N_u^0, C^0, A^0, Q^0) \in S$ *has a unique solution which remains in* S *for all* $t > 0$*. Moreover, there exist constants* c_1 *and* c_2 *such that*

$$N_d + N_u + A \leq c_1 e^{(\bar{\mu} - q)t} + c_2$$

where $\bar{\kappa} = \kappa_1 + \kappa_2$ *and* $\bar{\mu} := \max(\mu_d, \mu_u)$.

Proof. Assume, there exists a solution. Then, the following properties are satisfied:
Non-negativity: Given that all the parameters are positive and the initial values are non-negative,

$$\left.\frac{\mathrm{d}N_d}{\mathrm{d}t}\right|_{N_d=0, N_u, C, A, Q \geq 0} = \frac{\mu_u(2-\gamma)N_u C}{k + C} + \frac{\beta N_u k_A^n}{k_A^n + A^n} \geq 0.$$

Thus, N_d does not decrease for $N_d = 0$ and $C, A, Q \geq 0$. Similarly,

$$\left.\frac{\mathrm{d}N_u}{\mathrm{d}t}\right|_{N_u=0,N_d,C,A,Q\geq 0} \geq 0, \qquad \left.\frac{\mathrm{d}C}{\mathrm{d}t}\right|_{C=0,N_d,N_u,A,Q\geq 0} \geq 0,$$
$$\left.\frac{\mathrm{d}A}{\mathrm{d}t}\right|_{A=0,N_d,N_u,C,Q\geq 0} \geq 0, \qquad \left.\frac{\mathrm{d}Q}{\mathrm{d}t}\right|_{Q=0,N_d,N_u,C,A\geq 0} \geq 0.$$

Since the tangent condition in [4, §10.XV] is satisfied, it follows that $\mathbb{R}^5_{+,0}$ is positively invariant with respect to the system above, i.e. the model preserves non-negativity.

Upper Bound: First, upper bounds for C and Q are derived:

$$\left.\frac{\mathrm{d}C}{\mathrm{d}t}\right|_{C=\tilde{C}\geq C^\infty} = q(C^\infty - \tilde{C}) - \frac{\mu_d}{y_d}\frac{\tilde{C}}{k+\tilde{C}}N_d - \frac{\mu_u}{y_u}\frac{\tilde{C}}{k+\tilde{C}}N_u \leq 0,$$

$$\left.\frac{\mathrm{d}Q}{\mathrm{d}t}\right|_{Q=\tilde{Q}\geq Q^\infty} = q(Q^\infty - \tilde{Q}) - \nu_2\frac{\tilde{Q}}{k_Q+\tilde{Q}}A \leq 0.$$

C decreases for values $\tilde{C} \geq C^\infty$. Thus, $\max(C^\infty, C^0)$ is an upper bound for C. Similarly, $Q \leq \max(Q^\infty, Q^0)$.
Again, with the tangent condition [4, §10.XV], the positive invariance of S with respect to the system considered follows. Now, the existence discussion can be restricted to S. Since the Jacobi matrix of f is continuous, it follows that f is locally lipschitz continuous and thus, a solution exists on some interval $t \in [0, t_f]$.

Let $N := N_d + N_u$, $N^0 := N_d^0 + N_u^0$, $\bar{\kappa} = \kappa_1 + \kappa_2$ and $\bar{\mu} := \max(\mu_d, \mu_u)$. Then

$$\frac{\mathrm{d}N}{\mathrm{d}t} \leq (\bar{\mu} - q)N$$

and thus

$$N \leq N^0 e^{(\bar{\mu}-q)t}.$$

Similarly, for A:

$$\frac{\mathrm{d}A}{\mathrm{d}t} \leq \bar{\kappa}N.$$

Therefore,

$$A \leq \frac{\bar{\kappa}N_0}{\bar{\mu}-q}e^{(\bar{\mu}-q)t} + c_2$$

and

$$N + A \leq c_1 e^{(\bar{\mu}-q)t} + c_2 \qquad \forall t \geq 0,$$

where $c_1 = N^0\big(1 + \frac{\bar{\kappa}}{\bar{\mu}-q}\big)$ and $c_2 = A^0 - \frac{\bar{\kappa}N^0}{\bar{\mu}-q}$.
Thus, there is no blow up in finite time and a global solution exists according Theorem A.0.3. Furthermore, the solution is unique.

□

Remark. No solution can satisfy $N_d(t) = 0$ and $N_u(t) > 0$ (or $N_u(t) = 0$ and $N_d(t) > 0$) for any $t > 0$ since $\frac{\mathrm{d}N_d}{\mathrm{d}t}\Big|_{N_d=0,N_u>0} = \frac{\mu_u(2-\gamma)N_uC}{k+C} + \frac{\beta N_u k_a^n}{k_a^n+A^n} > 0.$

Proposition 2.2.2. *With conditions and assumptions from Theorem 2.2.1, the solution y for the initial value problem* (2.1) - (2.2) *depends continuously on the initial values and on the model parameters.*

Proof. This results from Theorem A.0.6 □

Steady state analysis

In a chemostat model, the washout equilibrium always exists. This state describes an equlibrium that is attained as soon as the dilution rate q is too high for the population to proliferate. In that case, only the in-feed components remain in the system and the population itself is washed out. A non-trivial equilibrium at which all the components are present at their steady states is more interesting for biological analyses, but often difficult to calculate explicitly.

Proposition 2.2.3. *The* ***washout equilibrium*** $(0, 0, C^\infty, 0, Q^\infty)$ *always exists and is asymptotically stable if*

$$q > \max\left(\frac{C^\infty\mu_d}{k_C + C^\infty}, \frac{C^\infty(\mu_u(\gamma-1)-\beta) - k_C\beta}{k_C + C^\infty}\right). \tag{2.5}$$

Proof. The Jacobian matrix evaluated at $(0, 0, C^\infty, 0, Q^\infty)$ is

$$J = \begin{pmatrix} \frac{\mu_d C}{k_C + C^\infty} - q & \frac{\mu_u(2-\gamma)C^\infty}{k_C + C^\infty} + \beta & 0 & 0 & 0 \\ 0 & \frac{\mu_u(\gamma-1)C^\infty}{k_C + C^\infty} - \beta - q & 0 & 0 & 0 \\ \frac{-\mu_d C^\infty}{y_d(k_C + C^\infty)} & \frac{-\mu_u C^\infty}{y_u(k_C + C^\infty)} & -q & 0 & 0 \\ \kappa_1 & \kappa_2 & 0 & -q - \frac{\nu_1 Q^\infty}{k_Q} & 0 \\ 0 & 0 & 0 & \frac{-\nu_2 Q^\infty}{k_Q} & -q \end{pmatrix}.$$

The corresponding eigenvalues are:

$$\begin{aligned} \lambda_{1,2} &= -q \\ \lambda_3 &= -q - \frac{Q^\infty \nu_1}{k_Q} \\ \lambda_4 &= -q + \frac{C^\infty \mu_d}{k_C + C^\infty} \\ \lambda_5 &= -q - \beta + \frac{C^\infty \mu_u(\gamma-1)}{k_C + C^\infty} \end{aligned}$$

Given the non-negativity of Q^∞ and the positivity of all the other parameters used, it follows immediately that $\lambda_{1,2,3} < 0$. For λ_4 to be negative, $q > \frac{C^\infty \mu_d}{k_C + C^\infty}$ has to be satisfied. For λ_5 to be negative, $q > \frac{C^\infty(\mu_u(\gamma-1)-\beta) - k_C\beta}{k_C + C^\infty}$ must be fulfilled. □

Interestingly, the stability condition is determined by the growth rate of the down-regulated cells μ_d when $\gamma \leq 1$. Only when $\gamma > 1$ there is a chance that the stability condition is dependant on the growth rate for the up-regulated cells.

Remark. For the parameters used for simulation experiments, given in Table 2.2 the washout equilibrium is unstable.

Simulations indicate the existence of a non-trivial equilibrium for the system, however, this remains to be proven.

2.3 Simulation

For simulation experiments and further discussion of results, the entire system was non-dimensionalised (section A). The denotation for the parameters was kept

although the parameters now represent compositions of the previous parameters. For further details see section A.
The new system reads as follows:

$$\begin{cases} \frac{\mathrm{d}N_d}{\mathrm{d}t} = & \mu_d N_d \frac{C}{k_C + C} + \mu_u (2-\gamma) N_u \frac{C}{k_C + C} - N_d \\ & -\alpha N_d \frac{A^n}{1 + A^n} + \beta N_u \frac{1}{1 + A^n} \\ \frac{\mathrm{d}N_u}{\mathrm{d}t} = & \mu_u (\gamma - 1) N_u \frac{C}{k_C + C} - N_u \\ & +\alpha N_d \frac{A^n}{1 + A^n} - \beta N_u \frac{1}{1 + A^n} \\ \frac{\mathrm{d}C}{\mathrm{d}t} = & (1 - C) - (m_d N_d + m_u N_u) \frac{C}{k_C + C} \\ \frac{\mathrm{d}A}{\mathrm{d}t} = & (N_u + N_d) + \kappa N_u \frac{A^n}{1 + A^n} - \nu_1 Q \frac{A}{k_Q + A} - A \\ \frac{\mathrm{d}Q}{\mathrm{d}t} = & (1 - Q) - \nu_2 Q \frac{A}{k_Q + A} \end{cases}$$

Remark. The variables C and Q were scaled with respect to their inflow concentrations respectively. Thus, changing the QQM inflow concentrations is now reflected by adapting $\nu_1 := \frac{\nu Q^\infty}{q k_A}$(, whereas $\nu_2 := \frac{\nu}{qr}$ is independent of the old QQM inflow concentration). Also note that the independent time variable was scaled with the dilution rate q and the latter is now implicitly given within the other parameters.

2.3.1 Parameters

Many assumptions on parameter values were adopted (and adapted) from [20], even though the authors consider a spatial model. The amount of literature about reaction kinetics between quorum sensing molecules and quorum quenching molecules is scarce and the information presented varies significantly. In [7, 14, 42] quorum quenching and quorum sensing inhibition models are introduced. In [7, 39, 42] measurements for the reaction kinetics are provided (Table 2.1). Although these works share the approach of using Michaelis Menten

kinetics $\frac{k_{cat}A(t)}{K+A(t)}$, the parameter values fitted varied in the following ranges

Table 2.1: Ranges for parameter values found in the literature [7, 39]

Reaction rate	k_{cat}	$[0.038, 37.63]s^{-1}$
Michaelis constant	K	$[0.036, 7.51]mM$
Performance constant	k_{cat}/K	$[0.97, 14.1]mM^{-1}s^{-1}$

Another parameter set for the QSM-QQM reaction is given in [42] with $k_{cat} = 0.1s^{-1}$ and $K = 0.1\mu M$. The performance constant is $10^3 mM^{-1}s^{-1}$ which is much higher than the performance constants found in [7, 39] and was therefore not integrated into Table 2.1. The differences in these findings can be attributed to distinct experimental conditions and the use of various QSMs and QQMs. This fact makes the choice for suitable reaction parameters rather difficult. Even though the absolute values for these two parameters k_{cat} and K change substantially, the ratio of these two values k_{cat}/K remains in the interval $[0.97, 14.1]mM^{-1}s^{-1}$.
The value k_{cat}/K is often referred to as performance constant and reflects the enzymatic performance. A higher value generally implies a higher catalytic efficiency [24]. Another parameter that characterises an enzyme reaction is $1/K$ which represents the affinity of enzymes to a substrate - the greater $1/K$ the more affinity enzymes show for the substrate [24]. According to [37], 'kinetically perfect' enzymes have ratios between

$$\frac{k_{cat}}{K} \in [10^8, 10^{10}]M^{-1}s^{-1} \quad \hat{=} \quad [10^5, 10^7]mM^{-1}s^{-1} \tag{2.6}$$

The average performance constant for moderately efficient enzymes is

$$\frac{k_{cat}}{K} \approx 10^5 M^{-1}s^{-1} \quad \hat{=} \quad 10^2 mM^{-1}s^{-1} \tag{2.7}$$

which exceeds the range of the values used in the research up to now. Following this information, the enzyme reactions in the measurements given in [39, 7] are quite inefficient.
Moreover, in coherence with the properties of the Michaelis Menten kinetics

$$k_{cat}Q(t)\frac{A(t)}{K+A(t)} \approx \frac{k_{cat}}{K}A(t)Q(t) \tag{2.8}$$

for $A << K$.

As it will be seen in the base case simulation this is the case if K is chosen in consistency with the literature, since $A(t) < 550$ in the base case (Figure 2.1b). This is equivalent to $550 \cdot k_A = 0.0275mM$ considering the original source for the parameter values [20].
Therefore, it will be distinguished between two different cases. In the first one (**Case 1 - Low affinity**), K will be chosen in the upper part of the interval given in Table 2.1 such that $A << K$, meaning the enzyme reaction rate corresponds to (2.8). In that case only the ratio k_{cat}/K is relevant and thus further investigation concerning the actual value of k_{cat} will be neglected. The only requirement is $K >> A(t)$. In this scenario a broad range of performance constants k_{cat}/K will be tested.
For the second case (**Case 2 - High affinity**) K will be chosen in the range of A, such that the full scope of the Michaelis Menten reaction kinetics can be observed. Here the actual values of K and k_{cat} play an important role. In that scenario it will be further distinguished between different values for k_{cat}/K. An emphasis is put on the following two situations described below.
In order to investigate the quorum quenching mechanism based on the information given in the literature, $\frac{k_{cat}}{K} = 8.7mM^{-1}s^{-1}$ is chosen in the range of the measurements provided.
In addition to that, considering the possibility of a moderately efficient reaction, $\frac{k_{cat}}{K}$ will also be varied in higher intervals.

Remark. The reaction rate k_{cat} and the Michaelis constant K represent the values before the non-dimensionalisation. Thus, $k_{cat} = \nu$, which affects the new parameters ν_1 and ν_2 and $k_Q = K/k_A$.

2.3.2 Computational setup

All the simulations in this chapter were conducted using MATLAB. For the numerical solution of the ODE system the MATLAB routine *ode15s* was used. The initial conditions were defined to be

$$(N_d^0, N_u^0, C^0, A^0, Q^0) = (1/5, 0, 4, 0, 0) \tag{2.9}$$

for all following simulations. To enable initial cell growth the nutrient concentration was set to a greater value than the nutrient feed concentration.

Table 2.2: Description of parameters for the chemostat model (before non-dimensionalisation)

Parameter description	Parameter	Value	Unit	Source
Dilution rate (Scaling factor)	q	0.6	d^{-1}	assumed
Threshold for the up-regulation (Scaling factor)	k_A	50	nM	[20]
Basic production rate of QSM	κ_0	5500	$nMd^{-1}g^{-1}m^3$	[20]
Nutrient inflow concentration (Scaling factor)	C^∞	4	gm^{-3}	assumed
QQM inflow concentration (Scaling factor)	Q^∞	will be varied	gm^{-3}	-
Max. growth rate of down-reg. cells	μ_d	6	d^{-1}	[20]
Max. growth rate of up-reg. cells	μ_u	4	d^{-1}	[20]
Number of N_u being produced when one N_u divides	γ	$0, 1, 2$	-	[41]
Half saturation concentration	k_C	1	gm^{-3}	[20]
Max. up-regulation rate	α	2.5	d^{-1}	[20]
Max. down-regulation rate	β	2.5	d^{-1}	[20]
Enhanced production rate of QSM	κ_1	55000	$nMd^{-1}g^{-1}m^3$	[20]
Ratio between enhanced and base QS production rates	κ	10	–	[20]
Yield coefficient for N_d	y_d	1	–	assumed
Yield coefficient for N_u	y_u	2/3	–	assumed
Hill coefficient	n	2.5	–	[20]
QSM-QQM reaction rate for A	ν_1	will be varied	d^{-1}	[7, 39, 42]
QSM-QQM reaction rate for Q	ν_2	will be varied	d^{-1}	[7, 39, 42]
Half saturation rate for A in reaction kinetics	k_Q	will be varied	nM	[7, 39, 42]

2.3.3 Typical simulation

In order to generate a reference case the quorum sensing system without quorum quenching molecules is examined first.

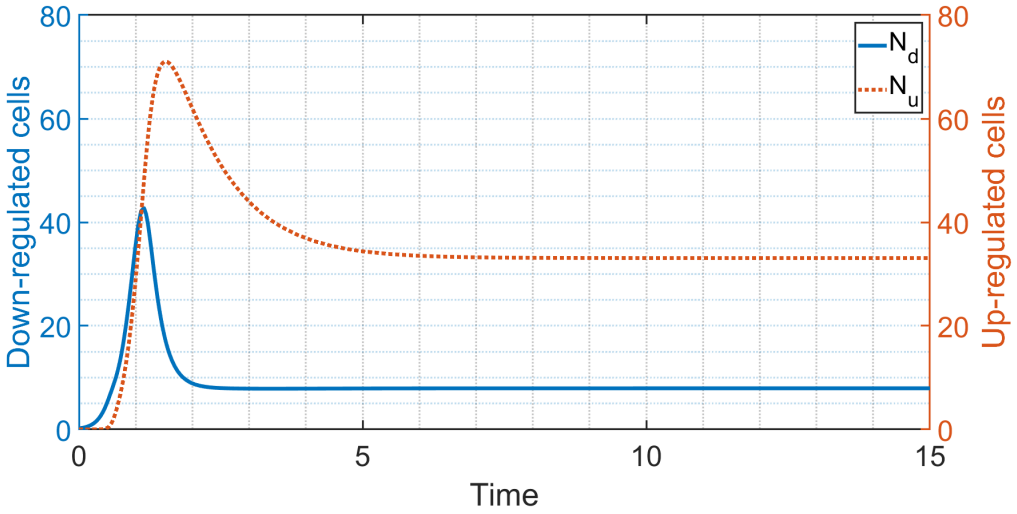

(a) Down- and up regulated cells N_d and N_u

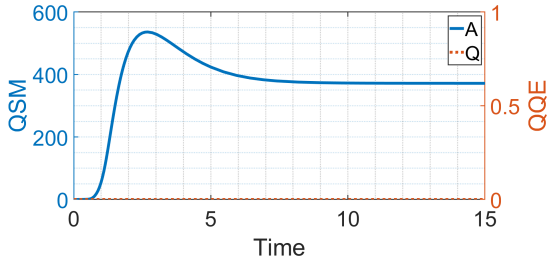

(b) QSM A and QQM $Q = 0$

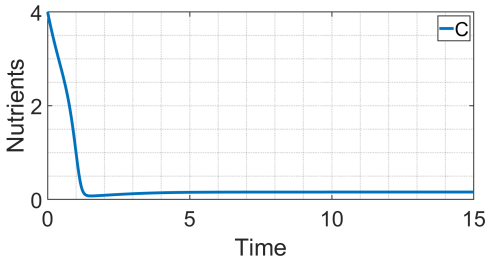

(c) C

Figure 2.1: Typical simulation of the quorum sensing model (without QQM, $Q^{\infty} = 0$)

In Figure 2.1 the development of the four active components, which are the down- and up-regulated bacterial cells (Figure 2.1a), the quorum sensing molecule (Figure 2.1b) and the nutrients (Figure 2.1c) are displayed.
The down-regulated population grows and achieves its peak at $t = 1.15$ where $N_d = 42.72$, then drops steeply to their equilibrium $N_d^* = 7.94$. The growth of the up-regulated type begins slowly but accelerates around $t = 0.55$. The up-regulated cells exceed the down-regulated type at $t = 1.15$, attain their maximum $N_u = 71.02$ at $t = 1.53$ and then also decrease to a steady state at approximately $N_u^* = 33.08$.
The quorum sensing molecules A are produced moderately at the beginning of

the simulation, but as soon as the threshold for the up-regulation is exceeded at $t = 0.55$, the QSMs rise steeply until the maximum $A = 536.17$ is attained at $t = 2.70$. They gradually decline to the equilibrium $A^* = 371.85$.
The nutrients C start at their initial condition $C = 4$ and are consumed rapidly until $t = 1.53$ where the minimum $C = 0.075$ is reached. The nutrients slowly accumulate again until C equilibrates at $C^* = 0.16$.

The components N_d, N_u, A and C reach their steady states at approximately $t = 2.5$, $t = 6.5$, $t = 8.5$ and $t = 4.5$ respectively.

2.3.4 Local sensitivity analysis

In order to assess the sensitivity of the model with respect to its parameter values the steady states of the dependent variables were compared. For the first sensitivity analysis the latin hypercube sampling method [22] was used. This method is meant to provide a good overview of how uncertainty in parameter values affect the outcome, but does not supply detailed information on the influence of individual parameters. Therefore, an one-per-one sensitivity analysis will be conducted afterwards to gain comprehensive results for each parameter. In both methods it is distinguished between the "scaling parameters" that were used for the non-dimensionalisation of the system and the remaining "parameters". Note that scaling parameters have a direct influence on some other parameters in the non-dimensional system. Moreover, there will be analyses for both, the system without quorum quenching, meaning $Q^\infty = 0$, and with quorum quenching. For all the visualisations boxplots of the steady state values are used.

Table 2.3: Table of parameters and scaling factors used for the sensitivity analysis

Number	1	2	3	4	5	6
Parameter	μ_d	μ_u	k	α	β	n
Value	10	20/3	1	25/6	25/6	2.5
Number	7	8	9	10	11	12
Parameter	κ	m_d	m_u	ν_1	ν_2	k_Q
Value	10	15/100	15/100	$10^6/3$	5000/6	2
Number	1	2	3	4	5	
Scaling Parameter	q	κ_0	C^∞	k_A	Q^∞	
Value	0.6	500	4	50	2000	

Latin hypercube sampling

As mentioned above, this method provides a general overview of how uncertainty in parameter values affects the result. The idea of this method is to divide the range of each parameter in equally probable intervals and to sample the values for all parameters in their respective ranges at the same time. To compare different cases the parameters were varied within $[P \pm 0.05P]$ and $[P \pm 0.4P]$ around their reference values P (see Table 2.3). The number of samples was set to $n = 1000$. Simulations with different parameter ranges were also conducted, although with similar outcomes and hence, will not be discussed further. For demonstration only the two intervals mentioned are used.

In Figure 2.2 and Figure 2.3 the steady states of N_d, N_u, C and A can be found for simulations without quorum quenching. While in Figure 2.2 the parmeters 1-9 and the scaling parameters 1-4 (Table 2.3) were varied within $\pm 5\%$ of their reference value, the range was extended to $\pm 40\%$ in Figure 2.3. When parameters 1-9 are varied within $\pm 5\%$ of their reference value, steady states N_d^*, N_u^*, C^* and A^* fluctuate approximately between $[m(N_d^*) \pm 12.5\%]$, $[m(N_u^*) \pm 10\%]$, $[m(C^*) \pm 10\%]$ and $[m(A^*) \pm 13\%]$ where $m(.)$ denotes the median respectively. These observations do not change significantly when the scaling parameters 1-4 are varied. When the values for parameters 1-9 are sampled in $[P \pm 0.4P]$ the ranges for N_d^*, N_u^*, C^* and A^* are approximately $[m(N_d^*) - 60\%, [m(N_d^*) + 300\%]$, $[m(N_u^*) - 50\%, m(N_u^*) + 230\%]$, $[m(C^*) - 50\%, m(C^*) + 200\%]$ and $[m(A^*) - 50\%, m(A^*) + 270\%]$ respectively (Figure 2.3). When the scaling parameters are varied, the boxplots for down-regulated cells N_d and nutrients C remain almost constant. The up-regulated cells N_u and A, however, are more sensible with respect to the input variables. The broader ranges for the steady states for the second sensitivity analysis can be explained by the separation of the outcomes into the up- and the down-regulated section.

The medians in all those plots, however, do not seem to move significantly. Only the ranges of the boxes and whiskers are spread in a greater area when the interval around the standard value is increasing. Even though the latter observation is rather predictable it motivates to further investigate the influence of single parameters.
In Figure 2.4a, Figure 2.4b and Figure 2.5 the system with the quorum quenching

mechanism is considered. Again, for the variation within $P \pm 5\%P$ the steady states remain in a small range except for some outliers, whereas they change more significantly in the case $P \pm 40\%P$. The medians stay almost constant throughout the two cases, but the range of the boxes and whiskers, again, vary. The outliers can be explained with a switch between an up-regulated and a down-regulated final state.

One-per-one sensitivity analysis

The previous method does not provide any information on the influence of single parameters. Therefore, an additional one-per-one sensitivity analysis was conducted. Several ranges for the variation of each parameter were tested with similar outcomes (Figure 2.6a, Figure 2.6b). Hence, the variation intervals $[P \pm 0.05P]$ and $[P \pm 0.4P]$ was chosen for following exemplary figures.
For every parameter 500 uniformly distributed values were sampled in the range of its according interval. The default values for each parameter can again be found in Table 2.3.

Again, the system without quorum quenching mechanism will be investigated first. Figure 2.6 shows the sensitivity of the steady states of N_d, N_u, C and A respectively. The bacterial cells are most sensitive to the growth rates μ_d, μ_u and to the consumption rates whereas the consumption rate by up-regulated cells is more critical. The down-regulated cells are furthermore sensitive to changes of the up-regulation rate α. The half-saturation rate barely affects the steady state of the bacteria. The steady states of C are highly sensitive to the half-saturation concentration k_C and the growth rate for the up-regulated cells μ_u and a little bit less sensitive to the growth rate of the down-regulated type μ_d. Also, the up-regulation rate α has a small impact on the steady states of C. The steady state of the quorum sensing molecule A is sensitive to both of the growth rates μ_d and μ_u, the QSM production ratio κ and the consumption by up-regulated cells m_u. The half saturation k_C, the up-regulation rate α and the consumption rate for the down-regulated cells m_d have only little influence on the steady state of A.

The sensitivity analysis was also conducted for the scaling parameters q, κ_0, C^∞ and k_A (Table 2.3). While C seems to be unaffected by κ_0 and k_A, all of the four scaling values almost equally affect the other components N_d, N_u, A

(Figure 2.6c).
Now the whole system with quorum quenching is regarded. When the parameters are varied only in the small range around its reference value $[P \pm 5\%]$ only some parameters affect the outcome. The down-regulated type is influenced by μ_d, k and m_d, the up-regulated type by μ_d, α, β, n, m_d, ν_1 and k_Q, the nutrients C are only affected by μ_d and k and the QSM A by μ_d, m_d, ν_1 and k_Q (Figure 2.7a). In Figure 2.7b the greater range of the parameter variation results in more fluctuation within the equilibria. The relatively large area covered by the boxes when parameters are varied in $[P \pm 40\%]$ is due to the mix of final up- and down-regulated states. Parameters μ_d, μ_u, κ, m_u, ν_1 and ν_2 can thus modify the final result. The two parameters β and n do not seem to have an effect at all.

In general it can be observed that uncertainty in some special parameters such as β and n result in a damped fluctuation of outcomes. Input fluctuations in other parameters such as μ_d, k, m_d, $\nu_{1,2}$ and k_Q are amplified in the steady state outcomes. Reasons for this will be discussed in section 2.5.

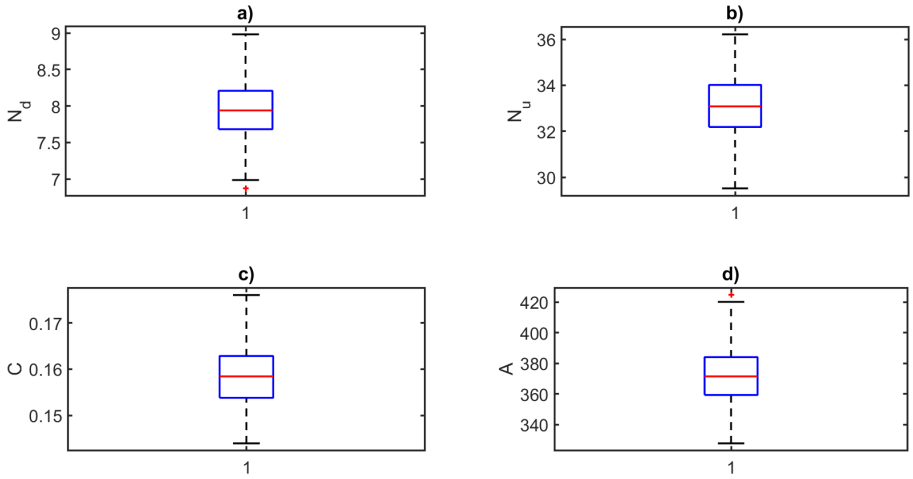

(a) Parameters 1-9

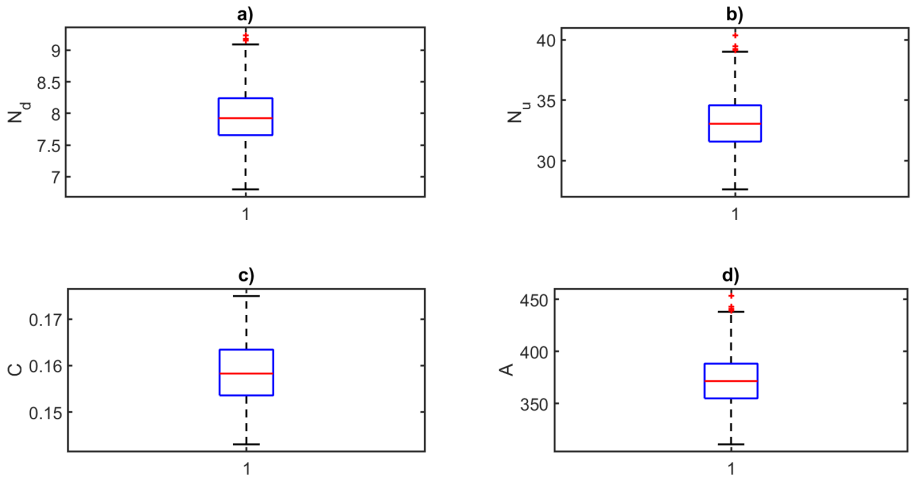

(b) Scaling parameters 1-4

Figure 2.2: Latin Hypercube Sampling in the range of $[P \pm 0.05P]$ for a) parameters 1-9 and b) scaling parameters 1-4 - Simulation without quorum quenching - Sensitivity of steady states for N_d, N_u, C and A (see Table 2.3)

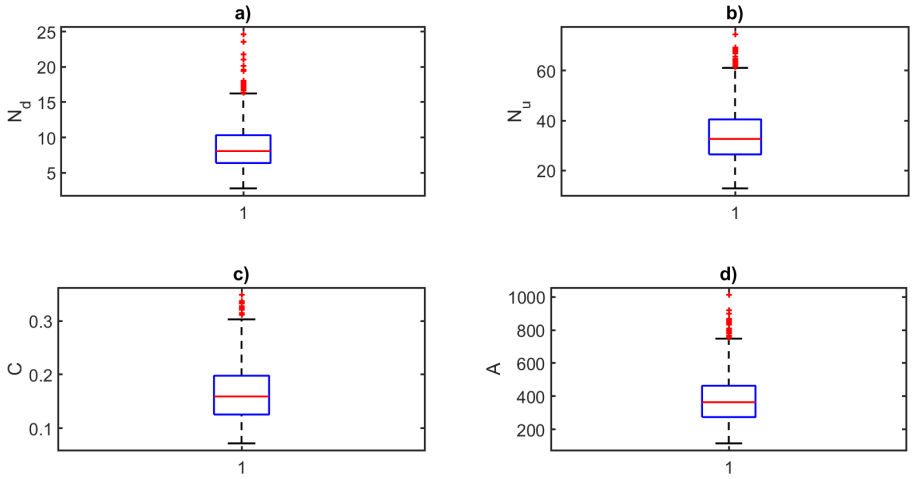

(a) Parameters 1-9

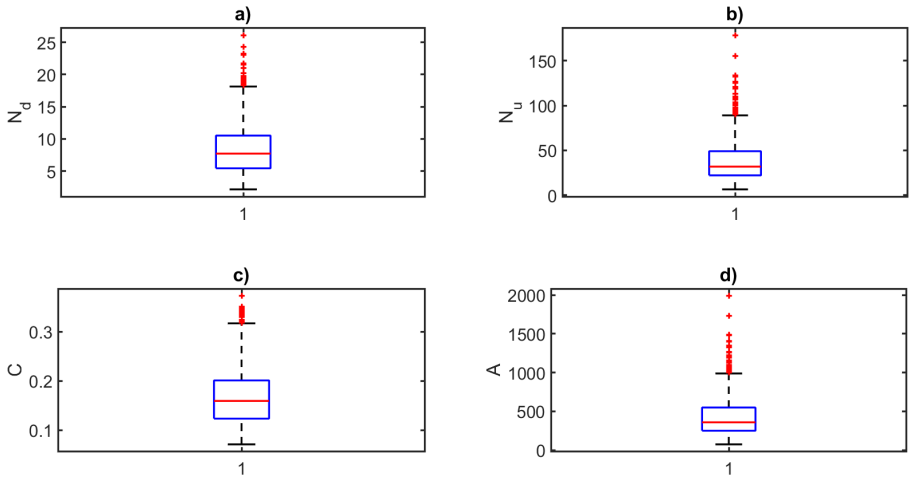

(b) Scaling parameters 1-4

Figure 2.3: Latin Hypercube Sampling in the range of $[P \pm 0.4P]$ for a) parameters 1-9 and b) scaling parameters 1-4 - Simulation without quorum quenching - Sensitivity of steady states N_d, N_u, C and A (see Table 2.3)

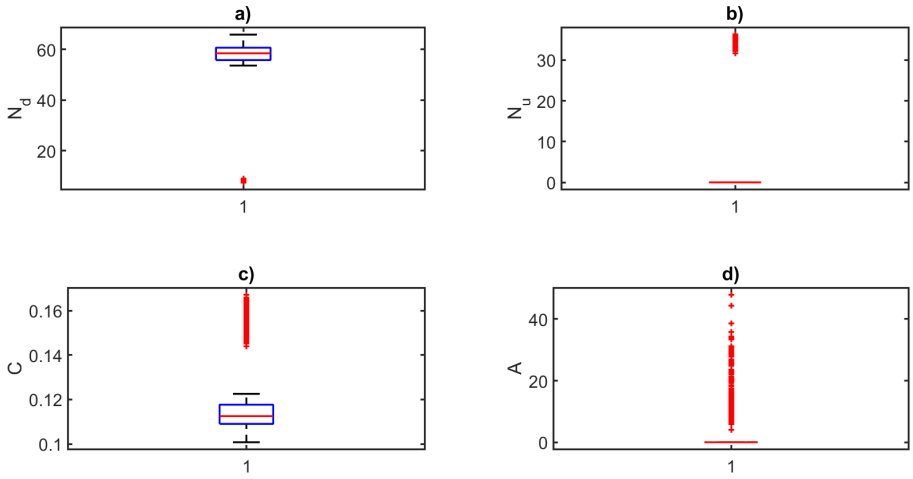

(a) $P \pm 0.05P$

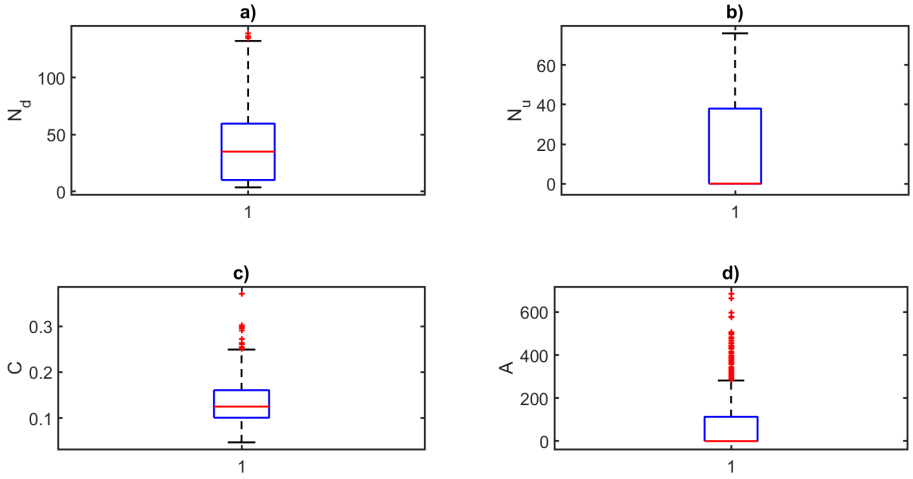

(b) $P \pm 0.4P$

Figure 2.4: Latin Hypercube Sampling in the range $[P \pm 0.05P]$ - Simulation with quorum quenching - Sensitivity of steady states with respect to parameters 1-12 (see Table 2.3) - Steady states for N_d, N_u, C, A

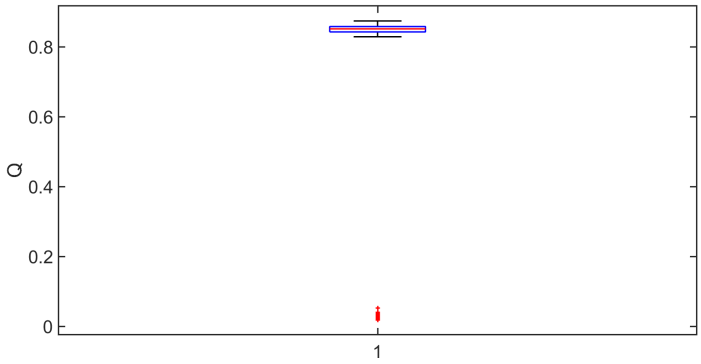

(a) ±5%

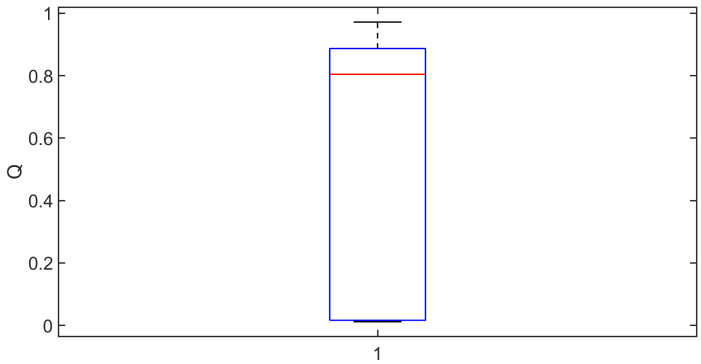

(b) ±40%

Figure 2.5: Latin Hypercube Sampling in the range a) $[P \pm 0.05P]$ b) $[P \pm 0.4P]$ - Simulation with quorum quenching - Sensitivity of steady states with respect to parameters 1-12 (see Table 2.3) - Steady states for Q

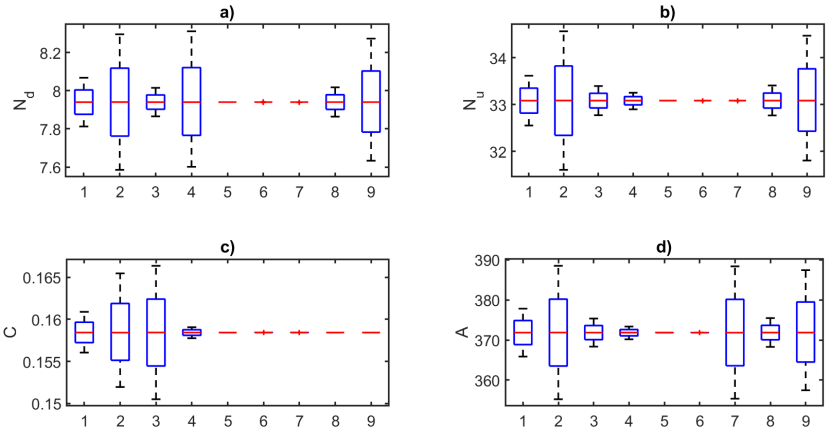

(a) Parameters 1-9, $[P \pm 0.05P]$

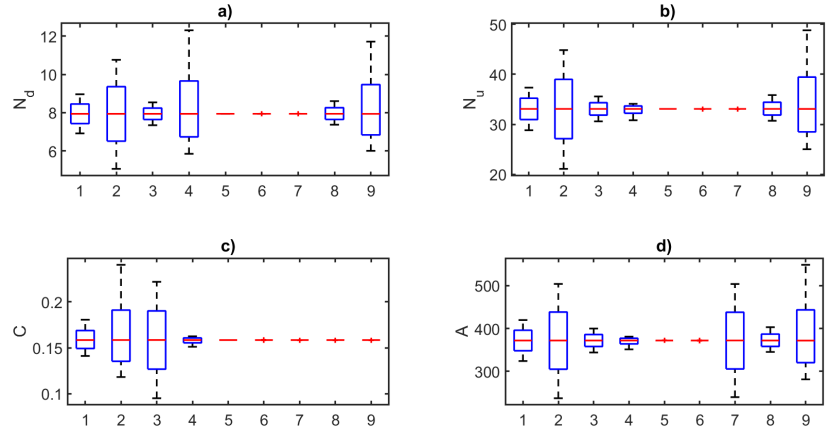

(b) Parameters 1-9, $[P \pm 0.4P]$

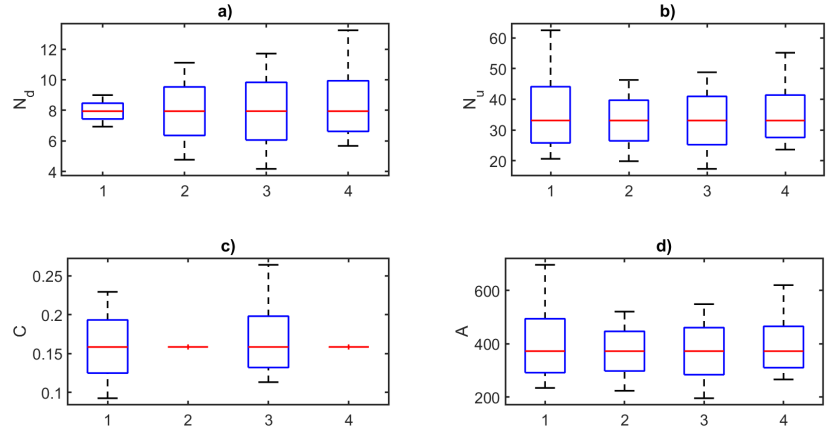

(c) Scaling parameters 1-4, $[P \pm 0.4P]$

Figure 2.6: One-per-one SSA - Simulations without quorum quenching - Sensitivity of steady states with respect to a) parameters 1-9 in $[P \pm 0.05P]$, b) parameters 1-9 in $[P \pm 0.4P]$ and c) scaling parameters 1-4 in $[P \pm 0.4P]$ (see Table 2.3) - Steady states for N_d, N_u, C, A

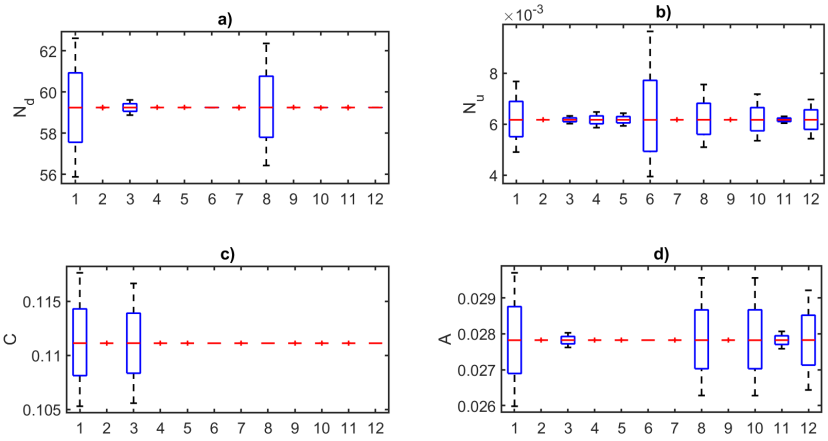

(a) Parameters 1-12, $[P \pm 0.05P]$

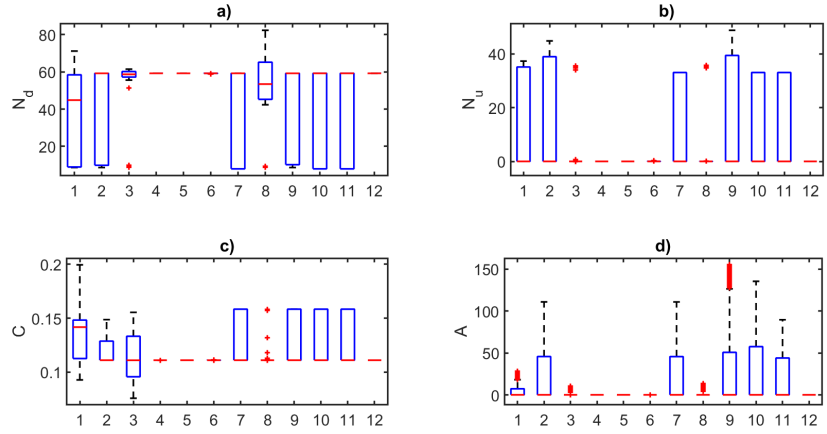

(b) Parameters 1-12, $[P \pm 0.4P]$

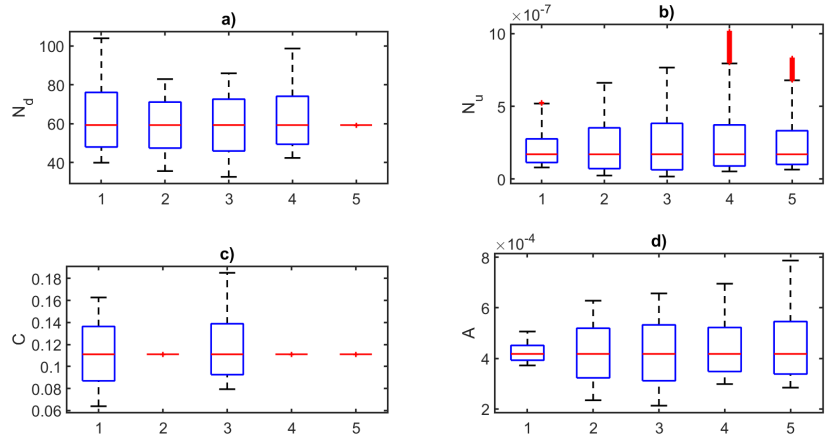

(c) Scaling parameters 1-5

Figure 2.7: One-per-one SSA - Simulation with quorum quenching - Sensitivity of steady states with respect to parameters 1-12 in a) $[P \pm 0.05P]$, b) $[P \pm 0.4P]$ and c) scaling parameters 1-5 in $[P \pm 0.4P]$ (see Table 2.3) - Steady states for N_d, N_u, C, A

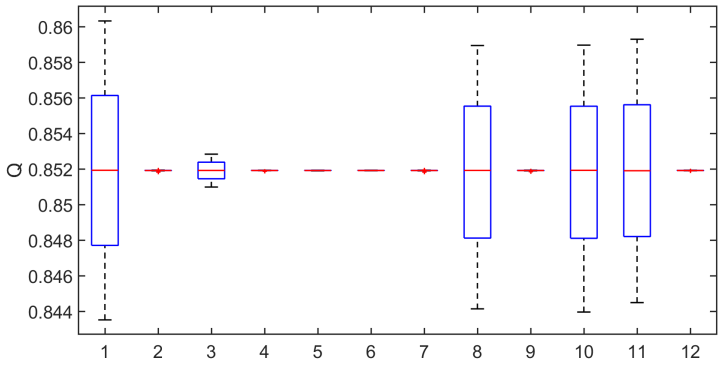

(a) ±5%

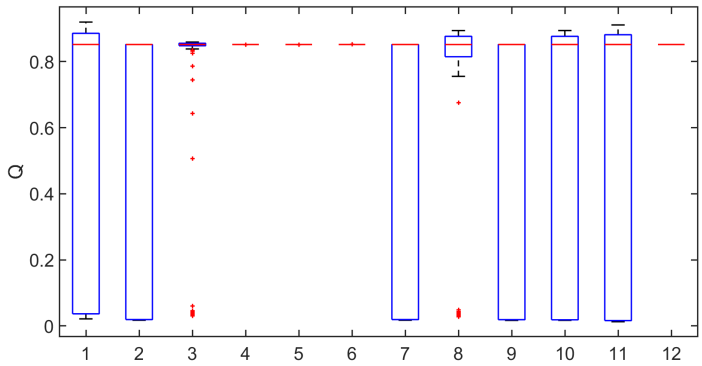

(b) ±40%

Figure 2.8: One-per-one SSA in the range a) $[P \pm 0.4P]$ b) $[P \pm 0.4P]$ - Simulation with quorum quenching - Sensitivity of steady states with respect to scaling parameters 1-12 (see Table 2.3) - Steady states for Q

2.4 Results

2.4.1 Case 1: Low QQM affinity to the substrate

The main question to answer will be how different QQM inflow concentrations affect the outcome of the system considering a variety of parameter combinations for the reaction term. First, it was assumed that $A << K$, thus the Michaelis constant was set to $k_Q = K/k_A = 1000000/k_A$. The performance constant for the first simulation was chosen to lie within the interval provided in the literature (Table 2.1), $k_{cat}/K = 8.7mM^{-1}s^{-1}$.

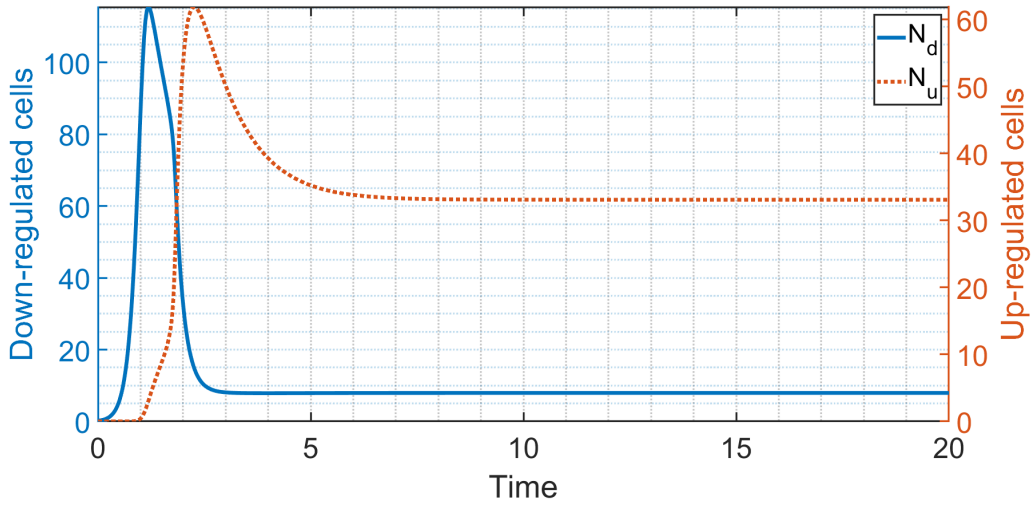

(a) Down- and up-regulated cells

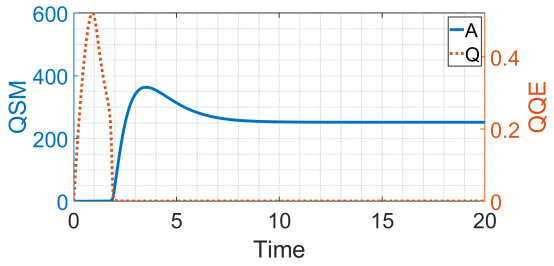

(b) QSMs and QQMs

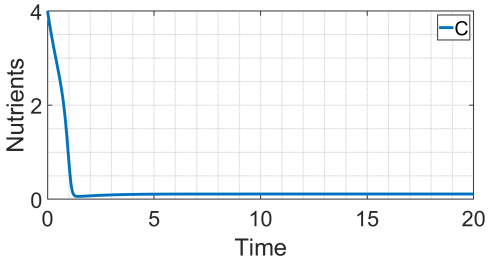

(c) Nutrients

Figure 2.9: Typical quorum quenching simulations with $Q^{\infty} = 600$ – a) down- and up-regulated cells N_d and N_u, b) QSMs A and QQMs Q and c) nutrients C – With Michaelis constant: $k_Q = 1000000/k_A >> A$ and performance constant $k_{cat}/K = 8.7mM^{-1}s^{-1}$

In Figure 2.9 and Figure 2.10 two typical simulations of the quorum quenching

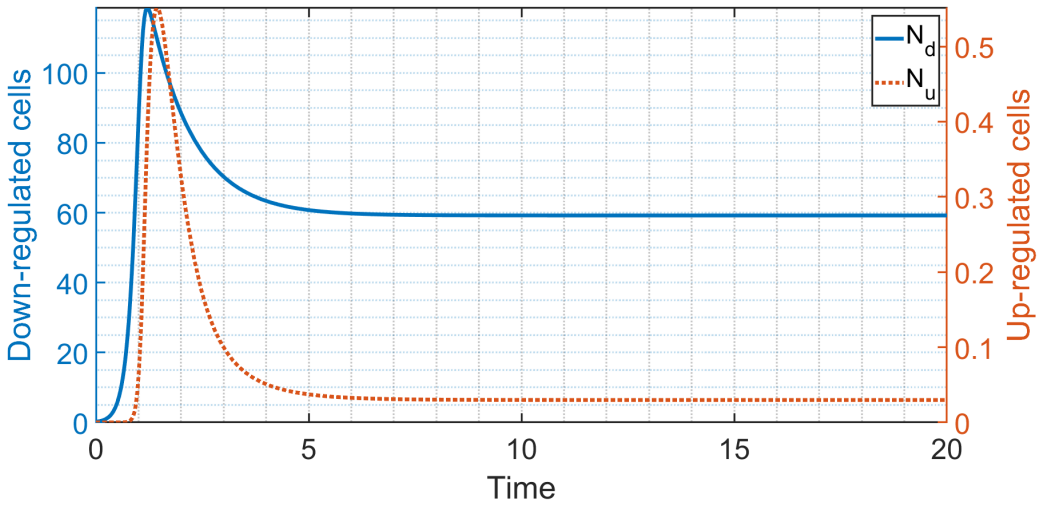

(a) Down- and up-regulated cells

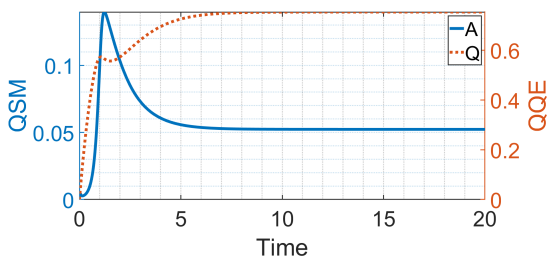

(b) QSMs and QQMs

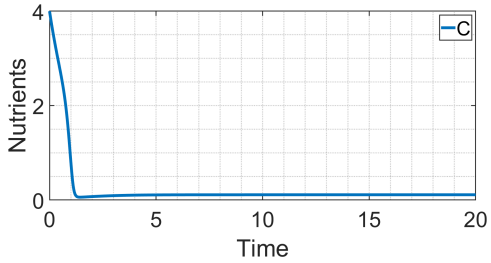

(c) Nutrients

Figure 2.10: Typical quorum quenching simulations with $Q^{\infty} = 1200$ – a) down- and up-regulated cells N_d and N_u, b) QSMs A and QQMs Q and c) nutrients C – With Michaelis constant: $k_Q = 1000000/k_A >> A$ and performance constant $k_{cat}/K = 8.7mM^{-1}s^{-1}$

model are displayed. Please note the different scales for down- and up-regulated cells and QSMs and QQMs respectively.

In Figure 2.9, the amount of QQM is too small to prevent the up-regulation of the colony eventually. The down-regulated cell type dominates the system as long as there are enough QQM to suppress the emergence of QSM. As soon as the QQM are used up, the amount of QSM rises sharply and so does the up-regulated population. The down-regulated community sank fast to its equilibrium. The steady state of the system is reached at approximately $t = 8$.

In Figure 2.10 however, there are sufficient QQM in the system to prohibit the up-regulation. At first the QSMs and the up-regulated cells are increasing but at approximately $t = 1.5$ they drop to their steady state. The down-regulated cells rise until they reach their peak shortly after $t = 1$ and then too decrease to

their final state. The amount of QQMs increases fast, then sinks at the time the QSMs are reaching their peak, but then again grow slowly to their equilibrium. These outcomes (Figure 2.9 and Figure 2.10) were also observed in several other simulations with similar settings.

The steady states were reached later in the simulations with QQMs than the steady states of the simple QS-system. For comparison the times when the steady state are approached are listed in Table 2.4.

Table 2.4: Times when steady states are reached for all components

Case	N_d	N_u	C	A	Q
Base case (Figure 2.1)	2.5	6.5	4.5	8.5	-
$Q^\infty = 600$ (Figure 2.9)	3	7	4.5	9	2
$Q^\infty = 1200$ (Figure 2.10)	7	7	4.5	7	7

When comparing the development of each trajectory it can be observed that the nutrient's trajectory $C(t)$ stays constant across different simulations. Initially their concentration is higher than the nutrient feed concentration, they are used up before $t = 1$ and enable initial growth of the biomass. Thereafter, nutrients are limited which reflects biologically relevant systems as many bacterial pathogens proliferate in nutrient limiting environments.
The down-regulated component N_d is overruled by up-regulated cells at $t = 1$ in the base case (Figure 2.1). When QQMs are added, the growth of up-regulated cells is prohibited long enough for the down-regulated part to grow up to almost a 3-fold of the base case. The peak of the up-regulated cells N_u depends on the amount of QQMs added and almost equals the base case (Figure 2.1) for the up-regulated outcome (Figure 2.9) and reduces to approximately a 1/120 part of the base case peak for the down-regulated outcome.

Moreover, it can be demonstrated that the QQM inflow does not significantly affect the steady states of the two cell types and the nutrient. This effect was already insinuated in the sensitivity analysis Figure 2.7c. For this reason, 500 values for Q^∞ were randomly picked in the range of $[10^0, 10^5]$ such that the decadal logarithm of the sample is uniformly distributed. In Figure 2.11 and Figure 2.12 the equilibria of all components were plotted against Q^∞. Figure 2.11 demonstrates the consistency of those two outcomes over a broad range for Q^∞ whereas Figure 2.12 displays sharp switch between these states. Both visualisations are

based on the same set of simulations. No matter how low or high the QQM inflow concentration is, the system either stays up-regulated as in Figure 2.9 or the up-regulation is completely suppressed by a sufficiently high dose of QQM as in Figure 2.10. Only in a small interval for Q^{∞} the steady states are in a transition area between these two possible events.

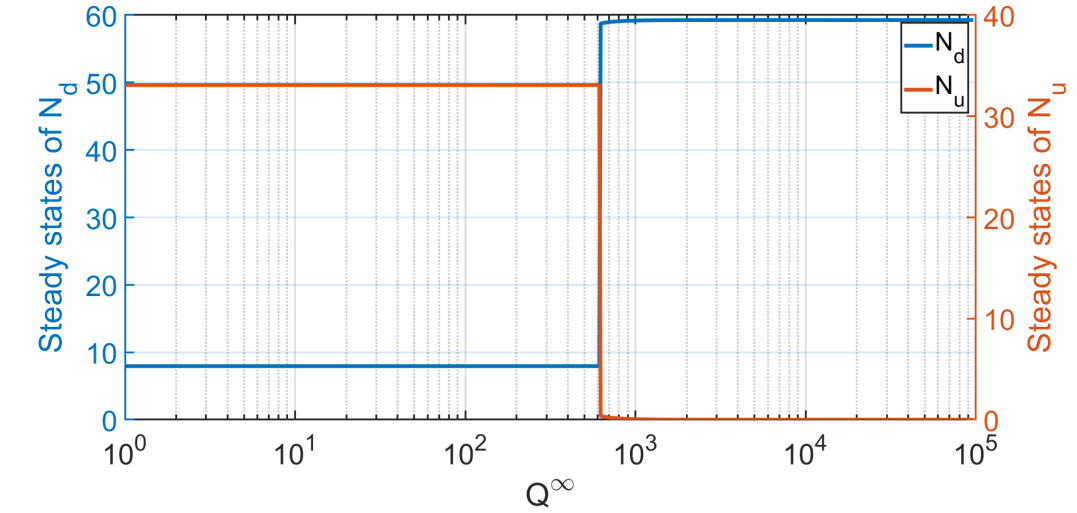

(a) Down- and up-regulated cells

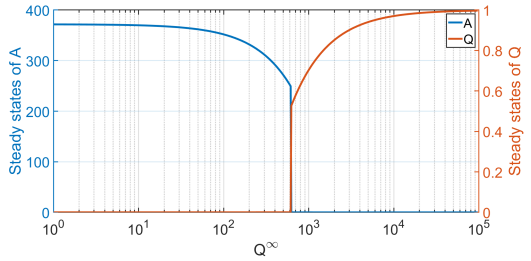

(b) QSMs and QQMs

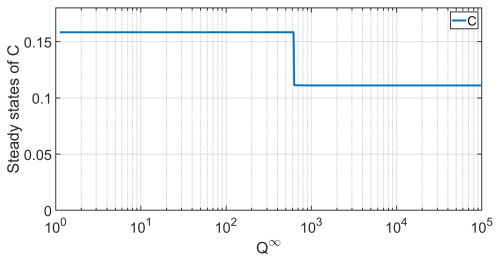

(c) Nutrients

Figure 2.11: Steady states depending on various values for $Q^{\infty} \in [10^0, 10^5]$ for a) down- and up-regulated cells, b) QSMs and QQMs and c) nutrients – With Michaelis constant: $k_Q = 1000000/k_A >> A$ and performance constant $k_{cat}/K = 8.7mM^{-1}s^{-1}$

In order to demonstrate this phenomenon also for other performance constant, both Q^{∞} and the performance constant k_{cat}/K were varied between $[400, 800]$ and $[10^0, 10^3]$ respectively. In Figure 2.13 the steady state values for N_d, N_u, C, A and Q are plotted against k_{cat}/K and Q^{∞}. Again, a sharp boundary between the system's two states can be observed. The steady state values for the nutrients, the down- and the up-regulated cells do not vary significantly within the down-

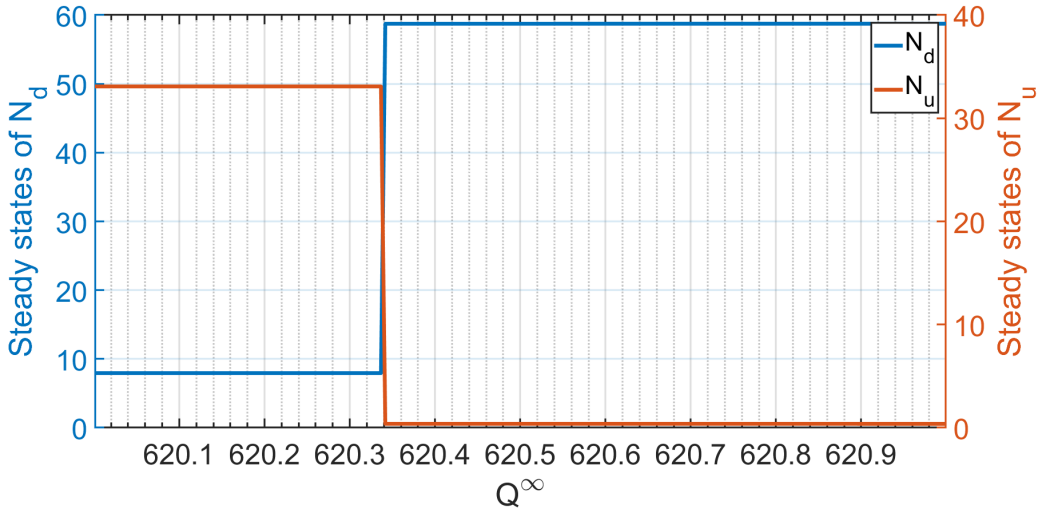

(a) Down- and up-regulated cells

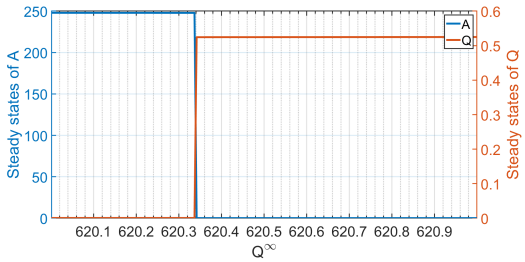

(b) QSMs and QQMs

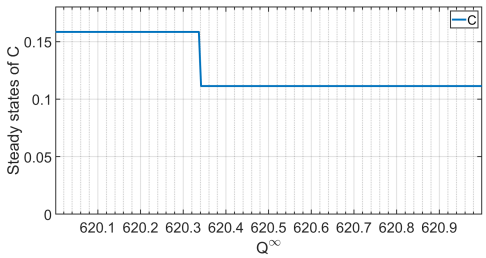

(c) Nutrients

Figure 2.12: Steady states depending on various values for $Q^{\infty} \in [620, 621]$ for a) down- and up-regulated cells, b) QSMs and QQMs and c) nutrients – With Michaelis constant: $k_Q = 1000000/k_A >> A$ and performance constant $k_{cat}/K = 8.7mM^{-1}s^{-1}$

regulated or up-regulated outcome. In the case of up-regulation, the equilibria of QSMs vary between 200 and 250 depending on Q^{∞} (Figure 2.13d). The equilibria of the QQM stay constant when the system ends up being up-regulated and range between 0.3 and 0.6 in the down-regulated event.

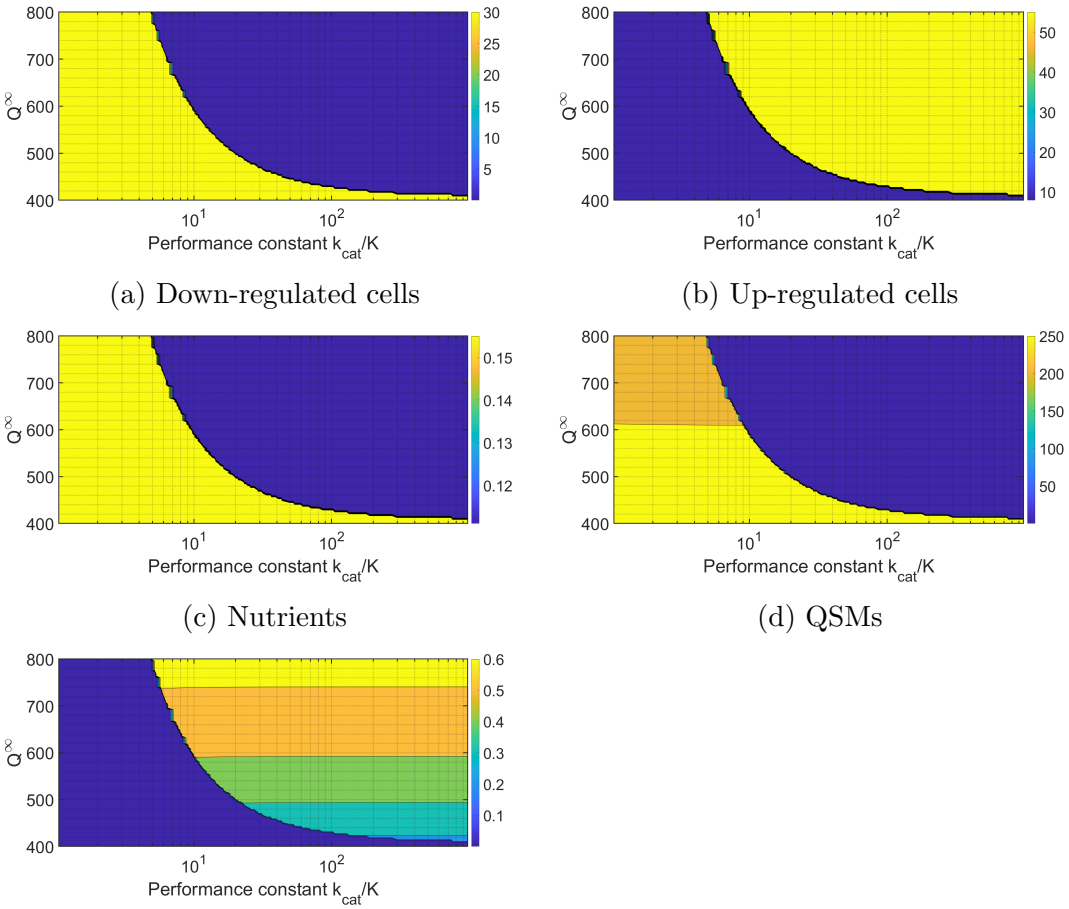

(a) Down-regulated cells

(b) Up-regulated cells

(c) Nutrients

(d) QSMs

(e) QQMs

Figure 2.13: Steady states depending on various values for Q^∞ and k_{cat}/K for a) down-regulated cells, b) up-regulated cells, c) nutrients, d) QSMs and e) QQMs

2.4.2 Case 2: High QQM affinity to the substrate

In various simulations it was verified for the previous case where $A << K$ that the magnitude of the values itself does indeed not affect the steady states or the qualitative development of the components, but the ratio alone determines everything. Now, it will be shown that even for some K in the range of A, the steady states for N_d, N_u and C do not alter if K is varied while k_{cat}/K is kept constant. In Figure 2.14 four simulations with very different reaction parameters k_{cat} and K but constant ratio $k_{cat}/K = 8.7$ are displayed as an example. While the K used for Figure 2.14a clearly exceeds the range of A, the K values chosen for Figure 2.14b, Figure 2.14c and Figure 2.14d are near or in the range of A. Nonetheless, the steady states for N_d, N_u, C and A stay quite constant within those examples. Only the value for the Q equilibrium differed in the last simulation Figure 2.14d. Apart from the shape and width of the peak in the down-regulated cells, the simulations in Figure 2.14 look very similar in terms of time of up-regulation and shape of trajectories. These observations suggest that the performance constante k_{cat}/K plays a crucial role for the eventual state of the biomass types even if K is chosen near to A.

To check this hypothesis, 300 values for $k_{cat}/K \in [10^0, 10^3]$ and 400 values for $K \in [10^1, 10^6]$ were again randomly picked, such that the decadal logarithms of the samples are uniformly distributed. The equilibria can be found in (Figure 2.15). The blue area in Figure 2.15a represents the up-regulated final state, the yellow the final down-regulated one. In Figure 2.15b and Figure 2.15c it is vice versa. While the upper half of all the images represent the case where $A << K$, the lower half puts K closer to A. Outside of the region $[10^1, 2 \cdot 10^1]$ for k_{cat}/K it seems that the outcome for N_d, N_u and C still only depends on the performance constant and not on the values for the reaction kinetics itself. The steady states for A and Q however are more affected by changes in K or k_{cat}/K. If the performance rate is very small, both A and Q end up having greater equilibria than in a more efficient case (Figure 2.15d, Figure 2.15e).
Furthermore, the sharp boundary between the up-regulated and the down-regulated final state - which was demonstrated for for $K >> A$ in Figure 2.11 and Figure 2.12 - could also be detected for K in the range of A (Figure 2.16). Interestingly, it seems that the sharp boundary between up- and down-regulated final state is not dependent on K but on k_{cat}/K.

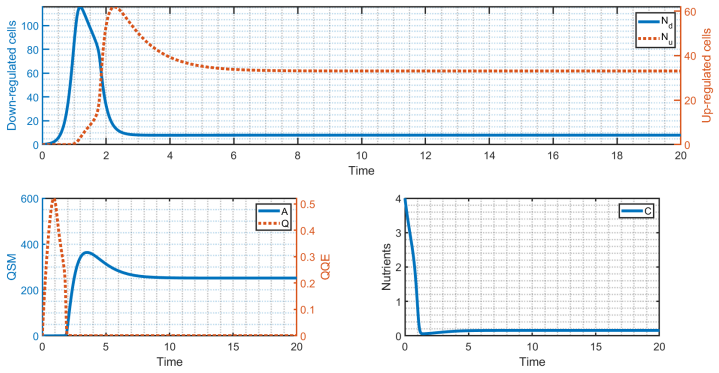

(a) $\nu = 1750000, \quad k_Q = 46562.36$

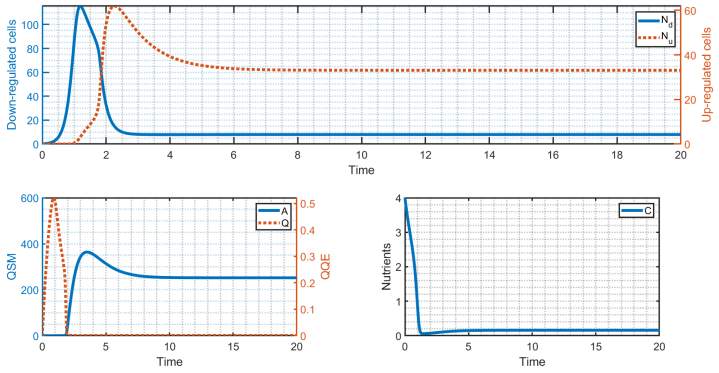

(b) $\nu = 9020.16, \quad k_Q = 720$

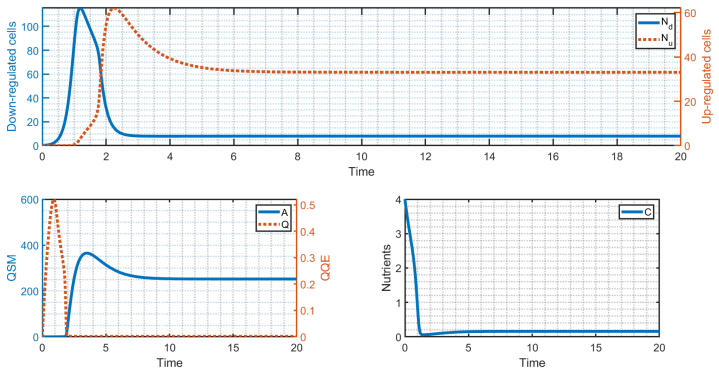

(c) $\nu = 5000, \quad k_Q = 133.0344$

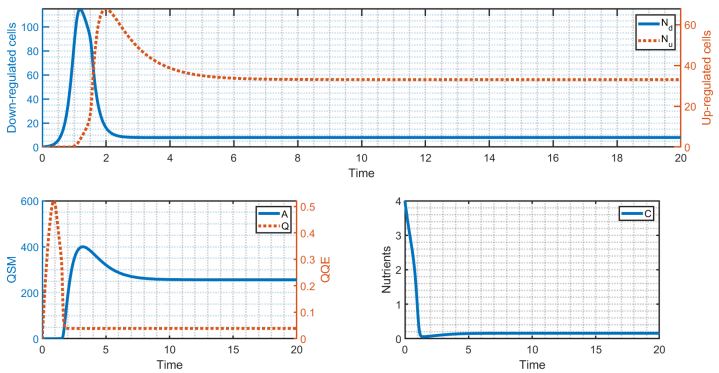

(d) $\nu = 50.112, \quad k_Q = 4$

Figure 2.14: Four exemplary simulations with constant ratio $k_{cat}/K = 8.7 s^{-1} m M^{-1}$, or equivalently $\nu/(50 k_Q) = 0.75168 d^{-1} n M^{-1}$

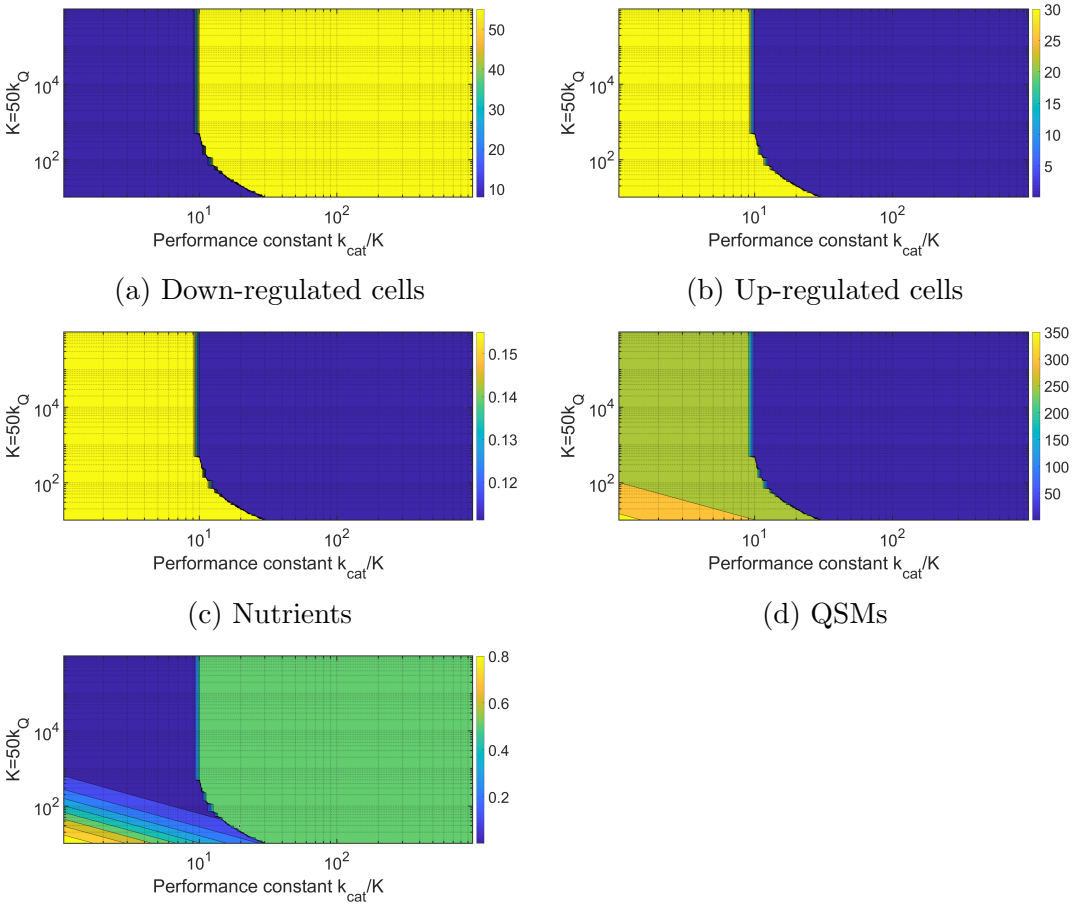

(a) Down-regulated cells

(b) Up-regulated cells

(c) Nutrients

(d) QSMs

(e) QQMs

Figure 2.15: Steady states depending on various values for k_{cat}/K and K for a) down-regulated cells, b) up-regulated cells, c) nutrients, d) QSMs and e) QQMs - $Q^{\infty} = 600$

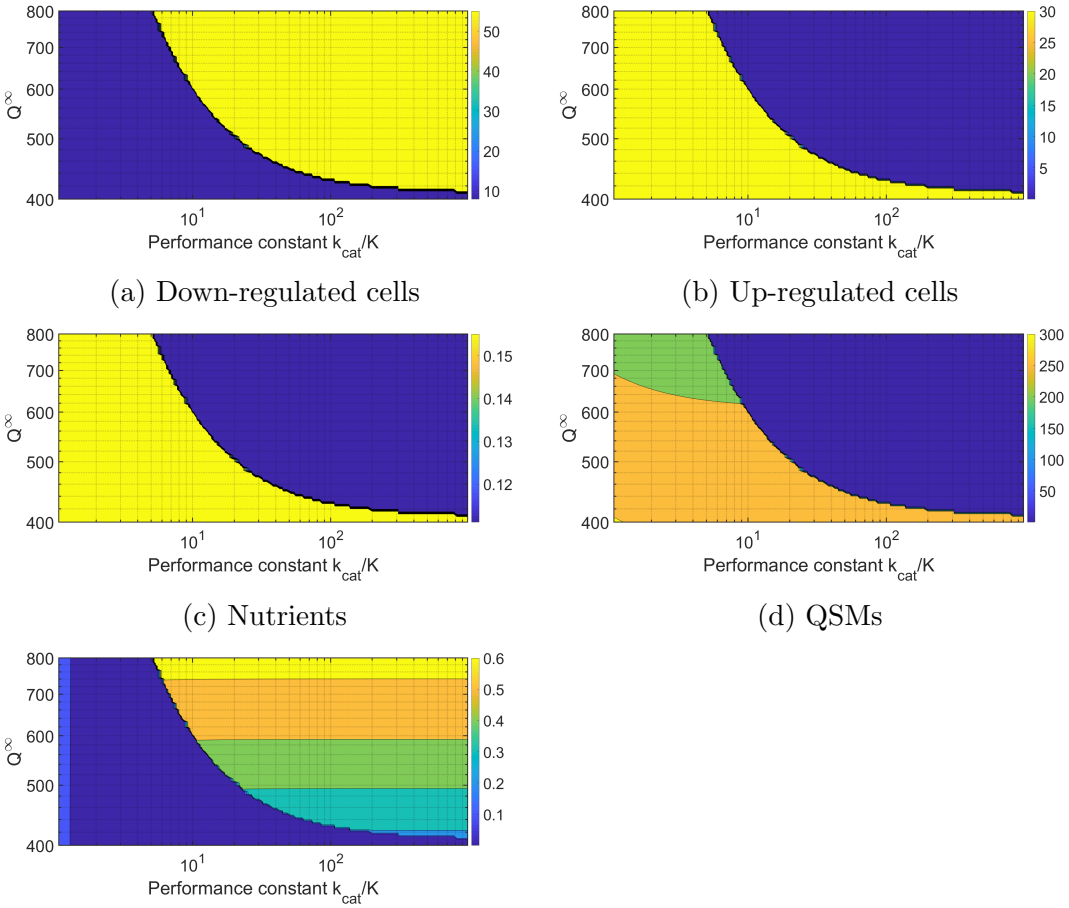

(a) Down-regulated cells

(b) Up-regulated cells

(c) Nutrients

(d) QSMs

(e) QQMs

Figure 2.16: Steady states depending on various values for k_{cat}/K and Q^{∞} for a) down-regulated cells, b) up-regulated cells, c) nutrients, d) QSMs and e) QQMs - $K = 500/k_A$

2.4.3 Boundary between up- and down-regulated equilibrium

Figure 2.13 and Figure 2.16 suggest that the amount of QQM necessary in order to suppress the up-regulation depends on the performance constant k_{cat}/K. The parameter K, however, seems to not be influencing this relation in a significant way. Therefore, a curve was fitted to the data between up- and down-regulated outcome for both, the low affinity and the high affinity case. For this purpose, the MATLAB curve fitting tool was used with the *ansatz*

$$Q^{\infty}(x) = ax^b + c$$

Table 2.5: Fitted coefficients to the ansatz $Q^{\infty} = ax^b + c$ for low affinity (2.4.1, Figure 2.13) and high affinity (2.4.2, Figure 2.16)

Low affinity		**High affinity**	
Coefficient	95% CI	Coefficient	95 % CI
$a = 1972$	$(1954; 1990)$	$a = 2107$	$(2084; 2129)$
$b = -1.032$	$(-1.037; -1.027)$	$b = -1.042$	$(-1.047; -1.036)$
$c = 408.8$	$(408.4; 409.1)$	$c = 408.9$	$(408.5; 409.2)$
Goodness of fit	$R^2 = 0.9997$	Goodness of fit	$R^2 = 0.9997$
	$SSE = 508$		$SSE = 518.3$

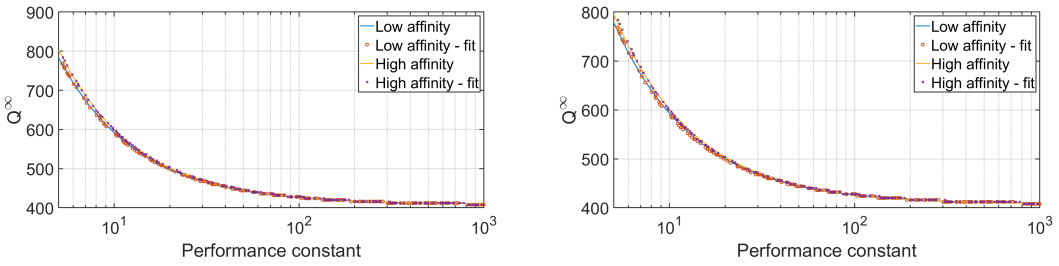

(a) b not fixed (b) $b = -1$ fixed

Figure 2.17: Fitted curves and underlying data for both, the high affinity and the low affinity case with a) free parameters a, b, c b) free parameters a, c and fixed $b = -1$

The performance constant was restricted to be ≥ 5 in this context. The two curves fitted to the data for low and high affinity approach each other with increasing performance constant. For smaller performance constants the functions are clearly separated, however, the maximum distance between them is 19.3545.

Since the exponent in the fitted function seems to be close to -1, the fit was repeated with fixed $b = -1$. Both fits, with fixed and unfixed b, are robust to changes in initial guesses of the parameter fitting procedure. The goodness of the second fit suggests that $b = -1$ can be chosen without loosing information and a simpler model for the fitting procedure can be chosen.

Table 2.6: Fitted coefficients to the ansatz $Q^{\infty} = ax^{-1} + c$ for low affinity (2.4.1, Figure 2.13) and high affinity (2.4.2, Figure 2.16)

Low affinity		**High affinity**	
Coefficient	95% CI	Coefficient	95 % CI
$a = 1860$	$(1854; 1865)$	$a = 1944$	$(1938; 1950)$
$c = 407.1$	$(406.8; 407.4)$	$c = 406.9$	$(406.6; 407.3)$
Goodness of fit	$R^2 = 0.9995$	Goodness of fit	$R^2 = 0.9994$
	$SSE = 879.8$		$SSE = 1041$

Following these results, the QQM inflow necessary in order to prevent up-regulation is proportional to the reciprocal of the performance constant, i.e. $1/x = K/k_{cat}$.

2.4.4 The effect of γ on the behaviour of the system

γ represents the number of up-regulated cells that are produced when a single up-regulated cell divides. In accordance to that, $(2 - \gamma)$ down-regulated cells are produced in the same process. The value of γ highly depends on the AHL concentration inside and around the dividing cell. If the AHL concentration is high enough, it is possible that the up-regulated cell divides into two up-regulated cells. In [20] it is assumed that $\gamma = 2$ whereas in [41] this parameter is treated as unknown. In [41] some measurements for that parameter were provided, however, these simulation experiments were conducted under very specific conditions and thus, can not be assumed generally.
Therefore, the following simulation experiments were designed in order to determine whether γ has an impact on the process of up-regulation and on the steady states. Although γ might be considered as a stochastic value in the interval $[0, 2]$, it is here assumed that γ can attain only the integer values $0, 1, 2$. For these simulations the parameter values given in table (Table 2.2) were used.

In Figure 2.18 three simulations without QQM, i.e. $Q^{\infty} = 0$ are displayed for $\gamma = 0, 1, 2$. While the nutrient concentration (Figure 2.18c) hardly changes for

different γ, the other components show changes. The QSM A (Figure 2.18b) and the up-regulated cell type N_u (Figure 2.18a) is increase with γ. For the down-regulated cells N_d (Figure 2.18a), the opposite holds. When $\gamma = 2$, the down-regulated cells almost completely vanish.

In Figure 2.19 three quorum quenching simulation with $Q^\infty = 600$, $K = 500$ and $k_{cat}/K = 8.7$ are displayed. Again, $\gamma \in \{0, 1, 2\}$. Apart from the fact that the down-regulated cells almost completely vanish again, the other components do not vary significantly. However, there is a sensitive interval for Q^∞ where γ determines whether the final state is up- or down-regulated Figure 2.20. In Figure 2.20a the up-regulation of the system with $\gamma = 0$ is suppressed and in Figure 2.20b there are enough quorum quenching molecules to act on both, the system with $\gamma = 0$ and $\gamma = 1$. The model where an up-regulated cell divides into two up-regulated cells is thus the most resistant against quorum quenching.

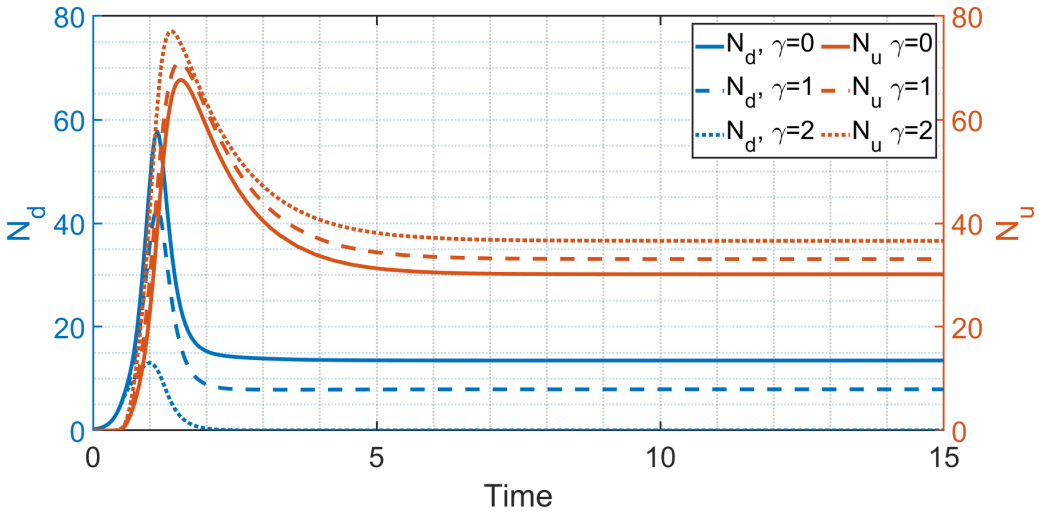

(a) Down- and up-regulated cells (N_d and N_u) for $\gamma = 0, 1, 2$

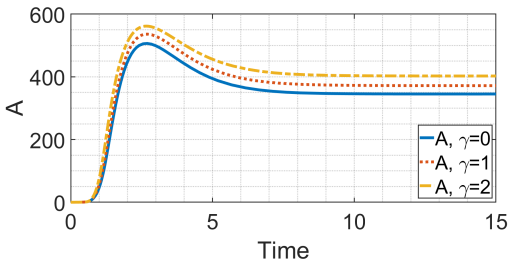

(b) QSM A for $\gamma = 0, 1, 2$

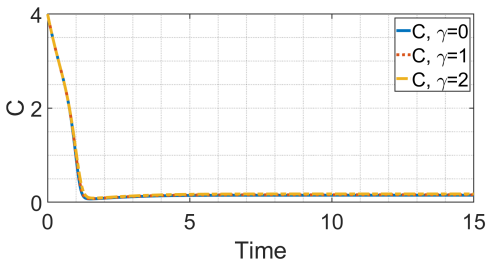

(c) Nutrient C for $\gamma = 0, 1, 2$

Figure 2.18: Simulation without QQM ($Q^\infty = 0$) for $\gamma = 0, 1, 2$

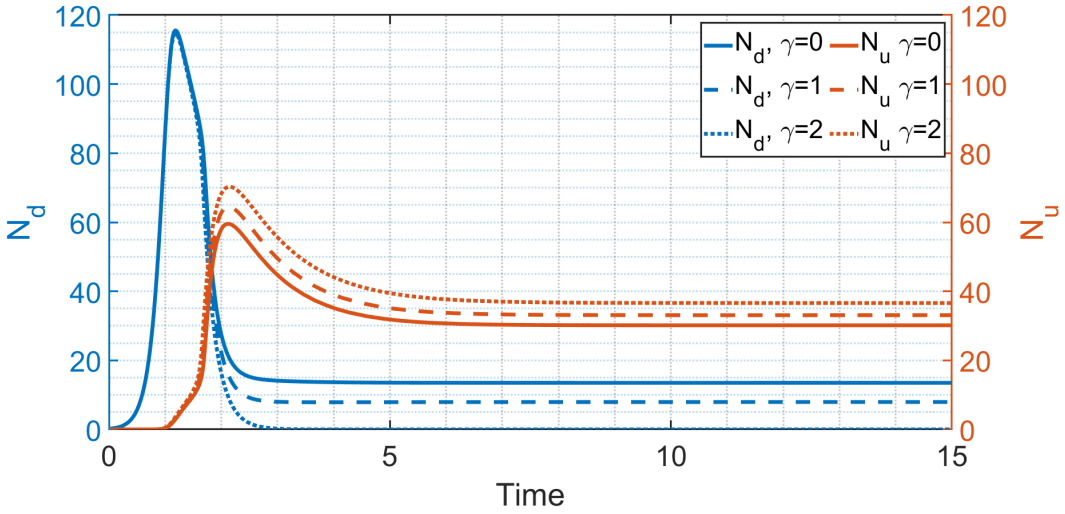

(a) Down- and up-regulated cells (N_d and N_u) for $\gamma = 0, 1, 2$

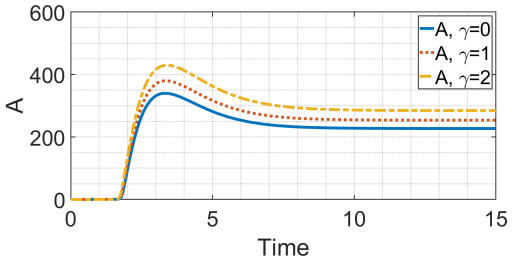

(b) QSM A for $\gamma = 0, 1, 2$

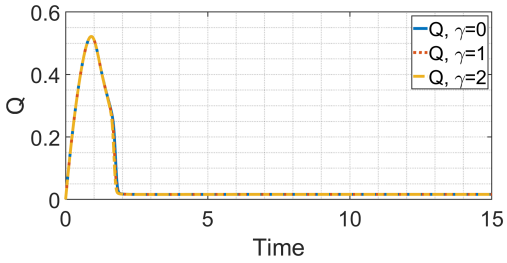

(c) QQM Q for $\gamma = 0, 1, 2$

Figure 2.19: Simulation with QQM for $\gamma = 0, 1, 2$ ($Q^\infty = 600$, $K = 500$, $k_{cat}/K = 8.7$)

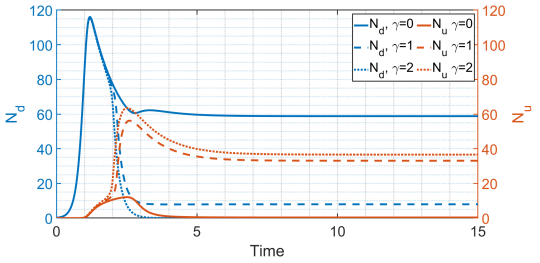

(a) $Q^\infty = 627.5$

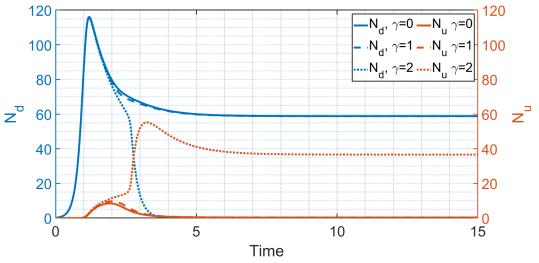

(b) $Q^\infty = 634.3$

Figure 2.20: Quorum Quenching simulations for N_d and N_u with $K = 500$, $k_{cat}/K = 8.7$, $\gamma = 0, 1, 2$

2.5 Discussion

The chemostat setting provided a good environment for the initial investigation of the quorum quenching mechanism. The simulations were fast and could be easily modified. Also, the properties of the ODEs used enabled the classification into the "up-regulated" and "down-regulated" state since the system equilibrated at some point.
In some way, this chapter's aim was to understand the reaction kinetics between quorum sensing - and quorum quenching molecules in order to make a good parameter choice when it comes to the more complex two-dimensional model.
Before simulations experiments were made a comprehensive sensitivity analysis was conducted. The parameters with the most influence on steady states of the system are the growth rate for down-regulated cells, the half saturation concentration for the growth by nutrient consumption, the consumption rate by down-regulated cells, the two reaction rates for the QSM and QQM as well as the half rate constant for the reaction. The down-regulation rate and the Hill exponent in the switch function between up- and down-regulated state seem not to have an influence at all. A reason for this is that down-regulation hardly ever occurs since the concentration of QSMs always exceeded the threshold for the switch.
The literature concerning quorum quenching models is very limited and parameter values given for the reaction kinetics between QS- and QQMs differ significantly. Therefore, a comprehensive investigation of many different, possible scenarios was necessary. In many biological articles, it was suggested that the ratio between the catalytic reaction rate and the Michaelis constant k_{cat}/K would properly reflect the efficiency of a(n) (enzyme) reaction [3, 24, 37]. For that reason, a main focus was set on modifying this so-called performance constant k_{cat}/K.
The simulation experiments were categorised into two cases: One case, where the QSMs show low reaction affinity to the QQM and a second case where the QSMs show high affinity. In both cases, however, similar quantitative results could be observed for the steady states (Figure 2.13, Figure 2.16). Interestingly, the transition between up- and down-regulated outcome is not continuous but rather abrupt. The parameter field gets divided into two sections - the up-regulated area and the down-regulated area. In either of those, the steady states change only in the QSM and the QQM. The equilibrium values for the nutrients, the down- and the up-regulated cell types stay almost constant in those sections.

This bifurcation is not only dependent on the QQM feed concentration, but also sensitive to the growth rates for down- and up-regulated cells, the ratio between enhanced and basic QSM production rate, the consumption rate of up-regulated cells and both the QSM-QQM reaction rates (Figure 2.7b, Figure 2.8b).
This switch-like behaviour is supported by many other simulations and is also consistent with the findings in [14]. Furthermore, it seems that the inflow amount of QQMs can be expressed in dependence of the performance constant. Hence, a curve was fitted to the low affinity case and to the high affinity case, respectively. These obtained functions, however, are almost equal and are able to describe the minimal amount of QQMs needed in order to prevent an up-regulation of the system. Although the functions are almost equal, in the case with higher reaction efficiency less QQMs were needed to prevent the up-regulation.
Another focus of the investigation was the question whether the phenotype of up-regulated cells is inherited. This parameter is highly dependent on the QSM concentration around and inside the cell during its division process. The number of up-regulated descendants from an up-regulated cell is of importance when it comes to optimising the QQM feed concentration in order to suppress total up-regulation. In [41] it was treated as unknown whereas it was treated as discrete value in the range $\{0, 1, 2\}$ here. It could be demonstrated that, in a certain interval for the QQM feed concentration, the inheritance of the phenotype determines the final state. In reality, this interval could be meaningless small or significantly large - an answer to that would need more biological expertise and thus, cannot be given at this point. It should, however, be remarked that this is an interesting result which could be subject to further research. In some (medical) cases, where quorum quenching is applied as an adjuvant to traditional antibiotics, a better quantification of inheritance of phenotypes could enable the right dosage for the treatment strategy. An interesting approach for the future would be to choose this parameter as a random variable.

Given that limited amount of literature on quorum quenching models and quorum quenching reaction kinetics, it cannot be concluded which parameters are suitable and which are not. A comprehensive biological study on both, quorum sensing and quorum quenching in a specific bacterial species that provides complete information on parameters would facilitate future work on this subject significantly. That way, all the parameters can be drawn from one source and do not need to be puzzled together from many different experiments.

Since medical treatment strategy with quorum quenching is not well established yet, there is also little information on how and in what doses quorum quenching molecules would be administered.
In a well mixed environment, quorum sensing could be successfully and sustainably prohibited when enough QQM were added to the system. That means that the majority of cells stayed down-regulated, i.e. non-resistant in a case where antimicrobial resistance is quorum sensing triggered.

Chapter 3

Spatial quorum quenching model

"I have deeply regretted that I did not proceed far enough at least to understand something of the great leading principles of mathematics, for men thus endowed seem to have an extra sense."
(Ch. Darwin)

3.1 Introduction

In this chapter, a system of reaction-diffusion equations representing a QS-QQ-biofilm model is introduced. The aim of this chapter is to investigate and analyse the quorum quenching mechanism applied to a spatially structured biofilm colony that coordinates gene expressions with quorum sensing. For further explanation of a standard biofilm model, see section 1.6. The model includes two types of bacteria, as there are down-regulated and up-regulated cells, and three dissolved substrates, the nutrients, quorum quenching molecules (QQM) and quorum sensing molecules (AHL or QSM). While the latter is produced by the bacterial cells, the former two are added to the system through the top boundary of the domain. Down-regulated cells refer to the standard type and up-regulated cells follow the group behaviour. The following variable names will be used for these components:

N_d	Volume fraction of down-regulated bacteria
N_u	Volume fraction of up-regulated bacteria
C	Concentration of nutrients
A	Amount of quorum sensing molecules (QSM)
Q	Amount of quorum quenching molecules (QQM)

3.2 Modelling

3.2.1 Model assumptions

The following assumptions were made in order to govern the equations:

1. **Domain (A1):** The considered region Ω is bounded and consists of two separated areas: The aqueous phase $\Omega_0(t)$ is characterised by the absence of biomass whereas the biofilm $\Omega_1(t)$ is the area where the biomass is located. Both subdomains are changing in time as the biofilm grows. Nothing can leave or enter the region through the bottom, left and right boundary. Nutrients and QQM can enter through the top boundary and QSM can leave the region there.

2. **Behaviour switch (A2):** There are two different types of biomass, down- and up-regulated cells. The former switch to an up-regulated state as soon as a specific threshold of QSM is reached locally around the cells. The up-regulated cells do not necessarily keep their state. As soon as the local QSM concentration drops below the threshold, they become down-regulated again. Both theses processes are modelled with Hill equations. For further information on the Hill equation see section 1.7.

3. **Signal production (A3):** Both of these cell types produce these signal molecules to "communicate" with each other. All cells produce signals at a base level, while up-regulated ones release them at an enhanced rate. The base level signal production is linearly dependent on the biomass. The enhanced signal production is modelled with the Hill equation.

4. **Cell growth and nutrient consumption (A4):** Cell growth by nutrient consumption is described with the Monod equation. We assume that down-regulated cells grow faster than up-regulated cells and both types have the same consumption rate. Biologically, this would mean that the group behaviour expressed by the up-regulated cells engage in an enhanced utilisation of the nutrients consumed and thus results in a decreased growth. Furthermore it is assumed, that the half saturation concentration is the same for both, up- and down-regulated cells.

5. **Natural decay (A5):** Both types of bacterial cells N_d and N_u as well as the QSM A decay naturally.

6. **QSM-QQM reaction (A6):** The reaction of quorum sensing molecules with quorum quenching molecules is modelled with Michaelis-Menten kinetics ([39], [42], [7]).

7. **Diffusivity of biomass (A7):** For the biomass, a density dependent diffusion coefficient was used. This coefficient disappears when the biomass is zero and blows up when the biomass approaches one. This enables the spatial growth of the colony and ensures its sharp contour.

8. **Diffusivity of substrates (A8):** The substrates, i.e. the nutrient, the QSM and the QQM, are subject to Fickian diffusion. The diffusion in the biofilm is assumed to be slower than diffusion in the aquaeous phase.

3.2.2 Model equations

In accordance with the assumptions above, the model equations read as follows:

$$
\begin{cases}
\dfrac{\partial N_d}{\partial t} = \nabla \cdot (D_N(N)\nabla N_d) + \underbrace{\mu_d N_d \dfrac{C}{k+C}}_{\text{growth term, A4}} - \underbrace{\alpha N_d \dfrac{A^n}{k_a^n + A^n}}_{\text{up-regulation, A2}} \\
\qquad\qquad + \underbrace{\beta N_u \dfrac{k_a^n}{k_a^n + A^n}}_{\text{down-regulation, A2}} - \underbrace{\sigma_N N_d}_{\text{decay, A5}} \\
\dfrac{\partial N_u}{\partial t} = \nabla \cdot (D_N(N)\nabla N_u) + \underbrace{\mu_u N_u \dfrac{C}{k+C}}_{\text{growth, A4}} + \underbrace{\alpha N_d \dfrac{A^n}{k_a^n + A^n}}_{\text{up-regulation, A2}} \\
\qquad\qquad \underbrace{- \beta N_u \dfrac{k_a^n}{k_a^n + A^n}}_{\text{down-regulation, A2}} \underbrace{- \sigma_N N_u}_{\text{decay, A5}} \\
\dfrac{\partial C}{\partial t} = \nabla \cdot (D_C(N)\nabla C) \underbrace{- \omega_d \dfrac{C}{k+C} N_d - \omega_u \dfrac{C}{k+C} N_u}_{\text{nutrient consumption, A4}} \\
\dfrac{\partial A}{\partial t} = \nabla \cdot (D_A(N)\nabla A) + \underbrace{\kappa_0 (N_u + N_d)}_{\text{base level signal prod., A3}} + \underbrace{\kappa_1 N_u \dfrac{A^n}{k_a^n + A^n}}_{\text{enhanced signal prod. by up-reg. cells, A3}} \\
\qquad\qquad \underbrace{- \sigma_A A}_{\text{decay, A5}} \underbrace{- \nu Q \dfrac{A}{k_Q + A}}_{\text{QS-QQ reaction, A6}} \\
\dfrac{\partial Q}{\partial t} = \nabla \cdot (D_Q(N)\nabla Q) \underbrace{- \dfrac{\nu}{r} Q \dfrac{A}{k_Q + A}}_{\text{QS-QQ reaction, A6}}
\end{cases}
$$

With boundary conditions on $\Omega = [0, L] \times [0, H]$ and diffusion coefficients according to (A1) and (A7 - A8) respectively:

$$\begin{cases} \dfrac{\partial N_d}{\partial n} = \dfrac{\partial N_u}{\partial n} = 0 \quad \text{at} \quad x = 0, L \quad \text{and} \quad y = 0 \\ \dfrac{\partial C}{\partial n} = \dfrac{\partial A}{\partial n} = \dfrac{\partial Q}{\partial n} = 0 \quad \text{at} \quad x = 0, L \quad \text{and} \quad y = 0 \\ N_d = N_u = 0 \quad \text{at} \quad y = H \\ C + \lambda \dfrac{\partial C}{\partial n} = C^{\infty} \quad \text{at} \quad y = H \\ A + \lambda \dfrac{\partial A}{\partial n} = 0 \quad \text{at} \quad y = H \\ Q + \lambda \dfrac{\partial Q}{\partial n} = Q^{\infty} \quad \text{at} \quad y = H \end{cases}$$

$$D_N(N) = d_N \frac{N^a}{(1-N)^b} \quad \text{(A7)},$$

$$D_{C,A,Q} = d_{C,A,Q}(1 + N(\rho_{C,A,Q} - 1)) \quad \text{(A8)}$$

Here, N refers to the total biomass: $N := N_d + N_u$. For the proof of the system's well-posedness the reader is referred to [20, 35, 36]. For a single species model [10], the well-posedness was shown in [12]. In [35] a model for quorum sensing in a patchy biofilm community was introduced and its well-posedness was proven.

3.3 Simulation

For simulation experiments and further result discussions, the whole system was non-dimensionalised (section B). The notation for the parameters was kept, although the parameters now represent compositions of the previous parameters.

For further details, see section B. The new system reads as follows:

$$\begin{cases} \frac{\partial N_d}{\partial t}(x,t) = \nabla(D_N(N)\nabla N) + \frac{C}{k+C}N_d - \alpha\frac{A^n}{1+A^n}N_d \\ \qquad\qquad + \beta\frac{1}{1+A^n}N_u - \sigma N_d \\ \frac{\partial N_u}{\partial t}(x,t) = \nabla(D_N(N)\nabla N) + \mu_u\frac{C}{k+C}N_d + \alpha\frac{A^n}{1+A^n}N_d \\ \qquad\qquad - \beta\frac{1}{1+A^n}N_u - \sigma N_u \\ \frac{\partial C}{\partial t}(x,t) = \nabla(D_C(N)\nabla C) - \omega_d\frac{C}{k+C}N_d - \omega_u\frac{C}{k+C}N_u \\ \frac{\partial A}{\partial t}(x,t) = \nabla(D_A(N)\nabla \tilde{A}) + \kappa_0(N_d+N_u) + \kappa_1 N_u\frac{A^n}{1+A^n} \\ \qquad\qquad - \sigma_A A - \nu_1\frac{A}{k_Q+A}Q \\ \frac{\partial Q}{\partial t}(x,t) = \nabla(D_Q(N)\nabla Q) - \nu_2\frac{A}{k_Q+A}Q \end{cases} \tag{3.1}$$

With boundary conditions on $\Omega = [0,1]\times[0,H/L]$ and diffusion coefficients:

$$\begin{cases} \frac{\partial N_d}{\partial n} = \frac{\partial N_u}{\partial n} = 0 \quad \text{at} \quad x = 0,1 \quad \text{and} \quad y = 0 \\ \frac{\partial C}{\partial n} = \frac{\partial A}{\partial n} = \frac{\partial Q}{\partial n} = 0 \quad \text{at} \quad x = 0,1 \quad \text{and} \quad y = 0 \\ N_d = N_u = 0 \quad \text{at} \quad y = H/L \end{cases} \qquad \begin{cases} C + \lambda\frac{\partial C}{\partial n} = C^\infty \quad \text{at} \quad y = H/L \\ A + \lambda\frac{\partial A}{\partial n} = 0 \quad \text{at} \quad y = H/L \\ Q + \lambda\frac{\partial Q}{\partial n} = 1 \quad \text{at} \quad y = H/L \end{cases}$$

$$D_N(N) = d_N\frac{N^a}{(1-N)^b} \quad \text{(A7)}, \qquad D_{C,A,Q} = d_{C,A,Q}(1+N(\rho_{C,A,Q}-1)) \quad \text{(A8)}$$

3.3.1 Computational setup

The code used is an extension of the one in [18] by Ghasemi et al. The model was implemented with Fortran90.

First, the model was non-dimensionalised (see section B). The domain $[0,1]\times[0,H/L]$ was discretised using a finite volume method with an uniformly distributed grid. Following [20], the time-adaptive, error-controlled embedded Rosenbrock-

Wanner method ROS3PRL was used. For the 2D visualisations the domain was divided into $n \times n = 256 \times 256$ grid cells, while $n \times n = 128 \times 128$ was sufficient for the lumped output variables.
Initially, a half-circle shaped colony of down-regulated cells N_d was placed on the right side of the bottom. Its center was set to $[2/3, 0]$ and the radius to $1/16$. This setup is displayed in Figure 3.1. To avoid a starve-out phenomenon, nutrients C are also present throughout the domain at the beginning. The initial conditions did not change across the different simulations. Unless otherwise stated, the parameter values in Table 3.2 are used. Simulations were stopped when the area occupied by biomass reached 25% of the total domain.

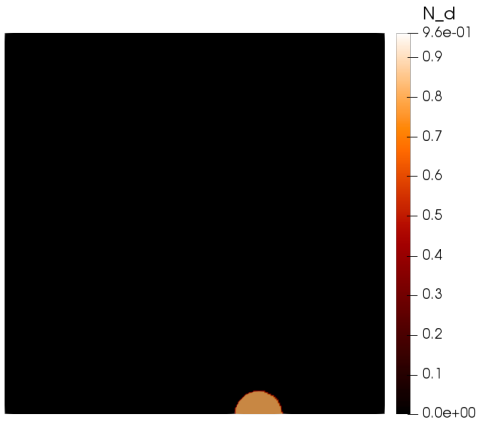

Figure 3.1: Initial simulation setup: Half-circle shaped colony of down-regulated cells N_d positioned at the right side of the domain

3.3.2 Typical simulation

First, the system without quorum quenching molecules will be introduced. In Figures 3.1, 3.2 and 3.3 the 2-dimensional quorum sensing system is displayed. These simulations will later serve as a reference case for the effect of quorum quenching on the system. In Figure 3.1 the initial condition is visualised. A half-circle shaped colony of down-regulated cells N_d is placed at the right bottom of the domain. In Figure 3.2a the situation at $t = 5$ was captured. It can be seen that the biofilm increased in size, but QSM and up-regulated cells are still negligible. Nutrients enter the system from the top boundary and thus their diffusion towards the colony can be observed. At $t = 10$ (Figure 3.2b) a significant

part of the cells already underwent the up-regulation process, meaning that the down-regulated cells vanished for the most part while the up-regulated ones dominate. The signal molecules also accumulated inside and around the colony with a concentration gradient pointing towards the colony. At $t = 15$ (Figure 3.3a) it can be observed that the ratio of down-regulated cells decreased again. Together with the up-regulated cells, also the signal molecules increased, still having its peak in the center of the colony and decreasing with the distance. The nutrients keep decreasing from the center of the biofilm towards the top boundary, this trend can also be observed at $t = 22$ (Figure 3.3b). At that time the biofilm, still being almost totally up-regulated, reached its final 25% of the whole area. The signals have occupied the whole domain and their gradient is pointing radially symmetric to the center of the colony.

In addition to the two-dimensional visualisations, the following lumped variable outputs will be used for displaying the total amount of each component:

$$I^*(t) := \int_\Omega I(x,t)\mathrm{d}x \quad \text{for} \quad I = N, N_d, N_u, C, A, Q$$

These output parameters give the total amount of biomass fraction of each type and the total amount of substratum, QSM and QQM at time t.
In Figure 3.4 the lumped biomass variables as well as the lumped QSM variable are plotted against time. The purple line represents the total biomass $N := N_d + N_u$ and increases continuously. The down-regulated biomass is represented by the blue dotted line and the up-regulated biomass by the green dashed line. As it can already be seen in the 2-dimensional visualisations, the down-regulated type dominates before $t = 5$. They start to decrease shortly before $t = 5$ whereas the up-regulated cells begin to grow faster at this time. At approximately $t = 8$ the volume fraction of N_d and N_u are equal. The down-regulated cells decrease to an almost non-existing state while the up-regulated cells become the dominant type in the system. The QSM start to accumulate at the same time as the up-regulated cell type begins to establish. After that, the QSM seem to grow linearly with time.

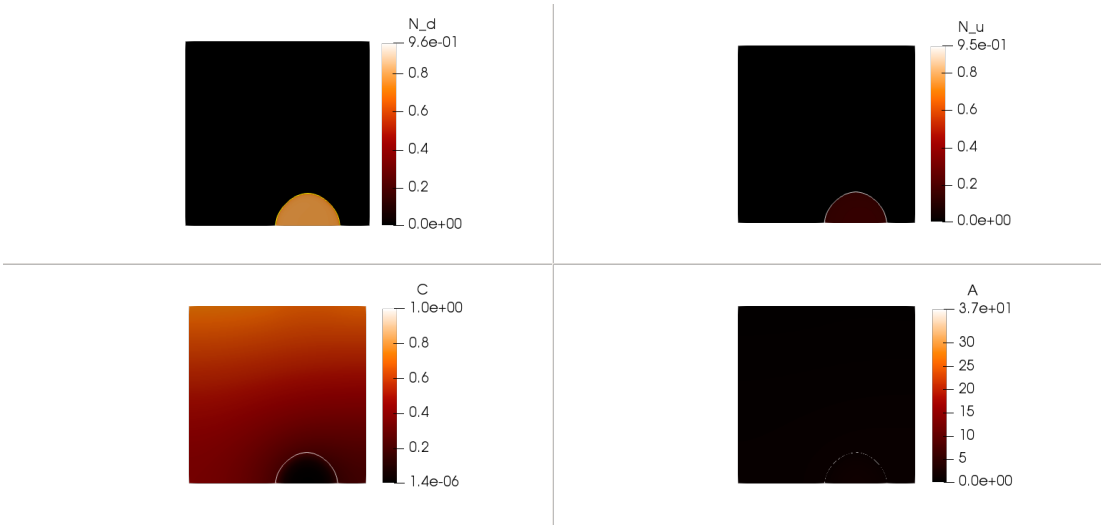

(a) $t = 5$

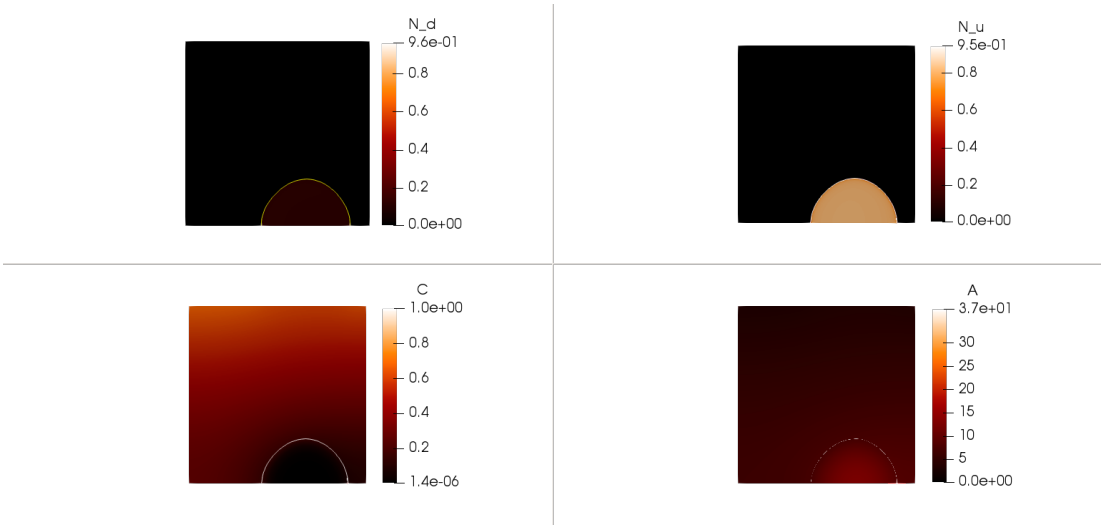

(b) $t = 10$

Figure 3.2: Illustrative Simulation (without the addition of QQM) at $t = 5$ - Upper line: Down-regulated cells N_d, up-regulated cells N_u, Lower line: Nutrients C, QSM A

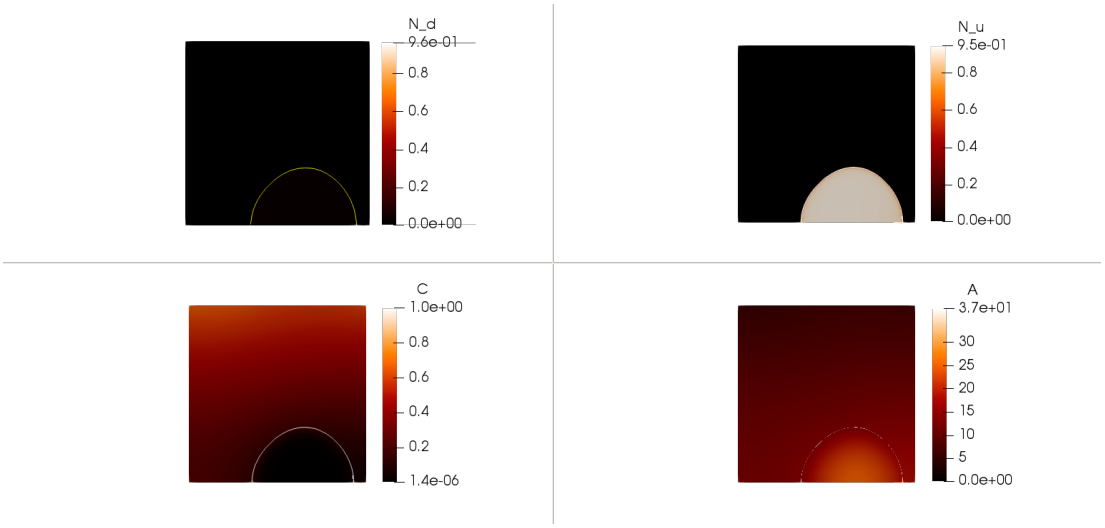

(a) $t = 15$

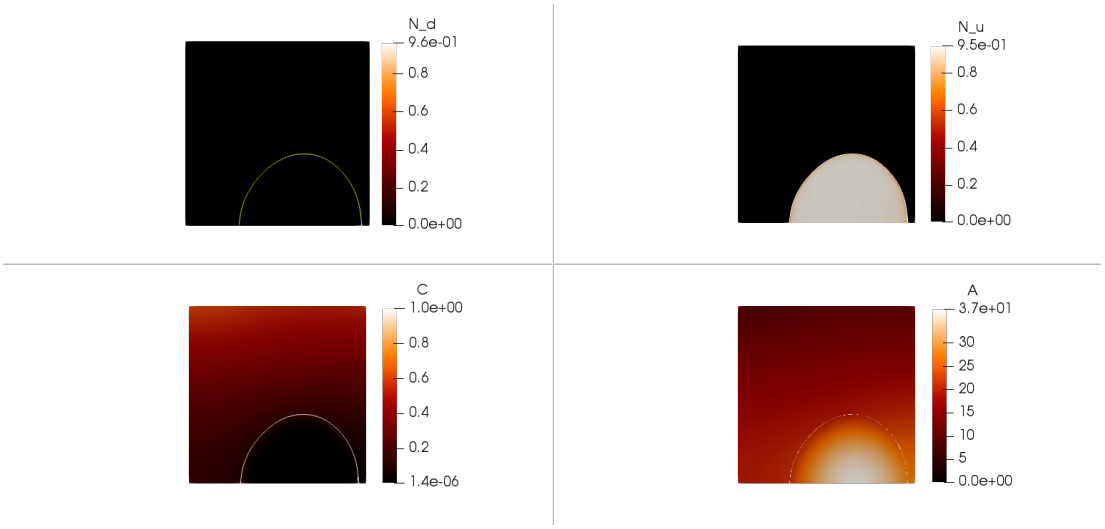

(b) $t = 22$

Figure 3.3: Illustrative Simulation (without the addition of QQM) - Upper line: Down-regulated cells N_d, up-regulated cells N_u, Lower line: Nutrients C, QSM A

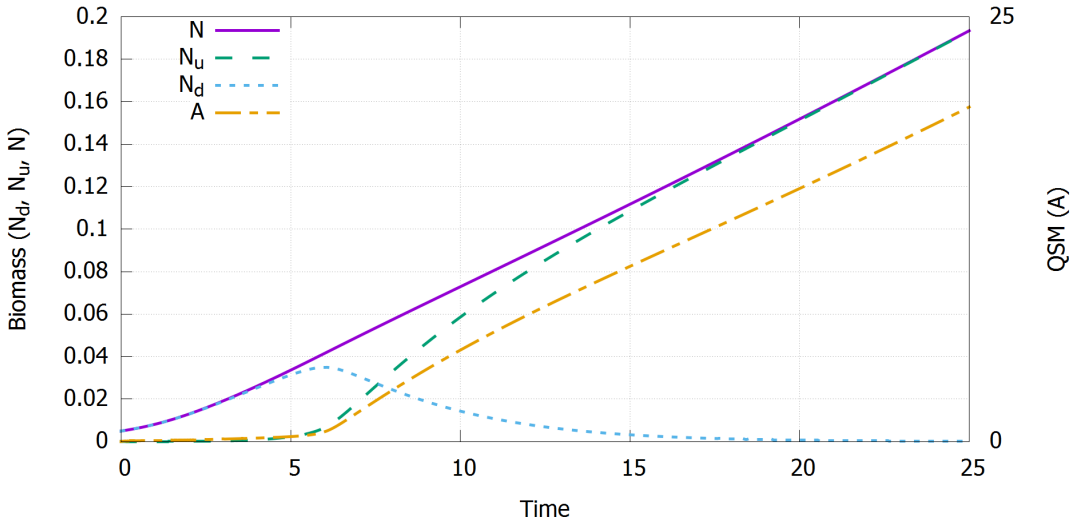

Figure 3.4: Lumped variables: Total biomass fraction $N = N_d + N_u$ (purple full line), down-regulated type N_d (blue dotted line), up-regulated type N_u (green dashed line) and the QSM A (orange dashed line)

3.3.3 Parameters

Again, almost all of the parameter values used in these simulations were adapted from [20]. If not stated differently, the standard parameter values given in Table 3.2 are used for simulations. The parameter for the QSM-QQM-reaction ν_1, ν_2, k_Q were newly added to the existing quorum sensing system given in [20]. The parameter values for those, however, differed significantly in the given literature [7, 39, 42]. For more detailed information please the reader is referred to subsection 2.3.1, where possible reasons for that variation and differences in the chemostat outcome are discussed. Since it could be demonstrated in the chemostat model that the performance constant k_{cat}/K has more influence on the outcome than the reaction affinity K the focus will be set on the performance constant in this chapter. Thus, two cases with different performance constants (PC) ν_1/k_Q will be considered.

Table 3.1: Different cases for the simulations

	small PC	large PC
ν $[d^{-1}]$	75.168	8640
k_Q $[nM]$	100	100
PC $[mM^{-1}s^{-1}]$	8.7	10^3

The main differences in the outcomes for small and large performance constant will be discussed in subsection 3.3.4.

Table 3.2: Description of parameters and their standard values (before non-dimensionalisation)

Parameter description	Parameter	Value	Unit	Source
Max. growth rate of down-reg. cells	μ_d	6	d^{-1}	[20]
Max. growth rate of up-reg. cells	μ_u	4	d^{-1}	[20]
Max. up-regulation rate	α	2.5	d^{-1}	[20]
Max. down-regulation rate	β	2.5	d^{-1}	[20]
Decay rate of cells	σ_N	0	d^{-1}	[20]
Decay rate of QSM	σ_A	0.12	d^{-1}	[20]
Half saturation concentration for growth	k	4	gm^{-3}	[20]
Threshold for the up-regulation	k_A	10	nM	[20]
Basic QS production	κ_0	5500	$nMd^{-1}m^3g^{-1}$	[20]
Enhanced QS production	κ_1	55000	$nMd^{-1}m^3g^{-1}$	[20]
Nutrient uptake rate	$\omega_{d,u}$	$10^4/0.63$	$gm^{-3}d^{-1}$	[20]
Exponent of Hill function for behaviour switch	n	2.5	-	[20]
Biofilm/water diffusivity ratio of nutrients, QSM and QQM	$\rho_{C,A,Q}$	0.1	-	[20]
Diffusion coefficient of nutrients in water	d_C	10^{-4}	m^2d^{-1}	[20]
Diffusion coefficient of QSM in water	d_A	0.00007758	m^2d^{-1}	[20]
Diffusion coefficient of QQM in water	d_Q	0.000007758	m^2d^{-1}	assumed
Concentration boundary layer thickness	λ	0.0005	m	[20]
Max. reaction rate QS-QQ	$\nu_{(1,2)}$	will be varied	d^{-1}	[7, 39, 42]
Reaction ratio QS/QQ	r	25	-	assumed
Michaelis constant for QS-QQ reaction	k_Q	will be varied	nM	[7, 39, 42]
Substratum concentration in bulk	C^∞	20	gm^{-3}	–
QQM concentration in bulk	Q^∞	will be varied	gm^{-3}	–
Concentration boundary thickness layer	λ	0.0005	m	assumed

3.3.4 Parameter study

To demonstrate the differences between a small performance constant (SPC) and a large performance constant (LPC) two different simulations are displayed with lumped variables (defined in subsection 3.3.2) as well as in 2D visualisations. The parameter values used for the reaction kinetics can be found in Table 3.1.

Figure 3.5 displays three different simulations. Case 1 refers to a reference case without the addition of QQM, for Case 2 the parameter set with a large performance constant (LPC) was used and for Case 3 the small performance constant (SPC) was assumed. When a SPC is used, the up-regulation process starts only shortly after the reference case without QQM (Case 1) at around $t = 7$ whereas it begins around $t = 13.5$ with a LPC. With a LPC the total biomass reaches 25% of the domain at $t \approx 24$, with a SPC this proportion is only reached after the observed time $t = 25$.

In Figure 3.6 two-dimensional visualisations of the ratio of up-regulated cells and total cells $R := \frac{N_u}{N_d+N_u}$ as well as the QSM A are displayed at different times. Figure 3.7 shows the QQM Q and the location of the reaction $\nu Q \frac{A}{k_Q+A}$, again in two dimensions and at different times. The case with a large performance constant is always shown on the left and the one with a small performance on the right hand side of each subfigure.

In accordance with the observation from the lumped variables, Figure 3.6 shows the delayed up-regulation when a LPC is used. That means, a LPC allows the QQM to successfully suppress the signalling strategy. Apart from this expected difference, two more can be found.

The location of the reaction (Figure 3.7) for the SPC starts and stays mainly within the biofilm as the QQM are added from $t = 0$ and have time to diffuse down to the colony before a significant production of QSM begins. With advancing time, the QSM diffuse out of the colony and the reaction also spreads radially in those regions. The maximal activity, however, can be found inside the colony for all observed t.
Apart from the absolute magnitude of the reaction, the LPC scenario resembles the SPC case for $t \leq 12$. The QQM diffuse into the domain fast enough so that

the reaction has its peak inside and around the colony, where the QSM is produced and released. The radially decreasing distribution of the QSM with origin in the biofilm is displayed in Figure 3.6. Due to the reaction being very efficient, the QQM are used up in those regions switch-like between $t = 12$ and $t = 13$. The location of the reaction abruptly shifts to the top boundary where QQM are entering the domain.

Also, the concentration of QQM Q hardly decreases with a SPC (Figure 3.5, Figure 3.7). Although there are enough QSM in the systems for the quenching molecules to react with, the performance of the reaction is too low to break down the molecules. As a result, the system gets up-regulated almost as fast as in the case where no QQM are added.
When a LPC is used, the QQM and QSM react more efficiently and the QQM are used up at a certain point and the QSM can establish within and around the biofilm and spread to the whole domain.

As the aim of this work is to examine the whole QS-QQ-system, parameters with a larger performance constant will be chosen for further simulations in order to explore the full range of possible outcomes. Nonetheless, a sensitivity analysis for different parameters, regardless of their reaction performance constant will be conducted in the following section.

The nutrients C hardly change across the different simulations as they are consumed by both types of bacteria at the same rate. Thus their evolution is similar to the typical simulation given in subsection 3.3.2. At the end of each simulations nutrients are accumulated at the top boundary with around half of the bulk concentration and are almost used up inside and around the colony so they act growth limiting. This phenomenon is justified as many bacterial colonies actually grow in nutrient limiting systems.

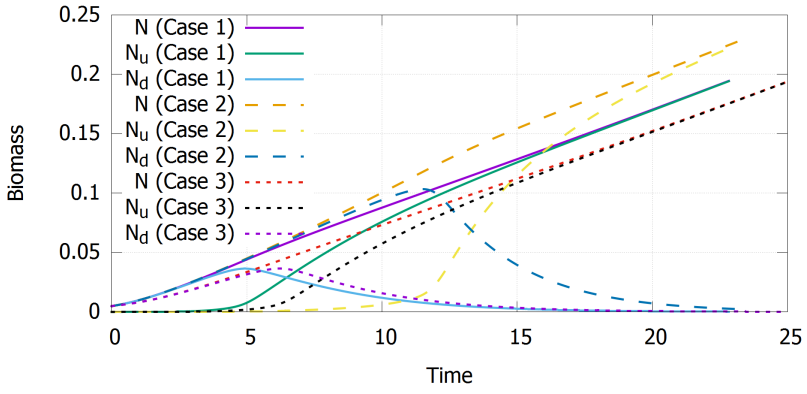

(a) Biomass N, N_d, N_u

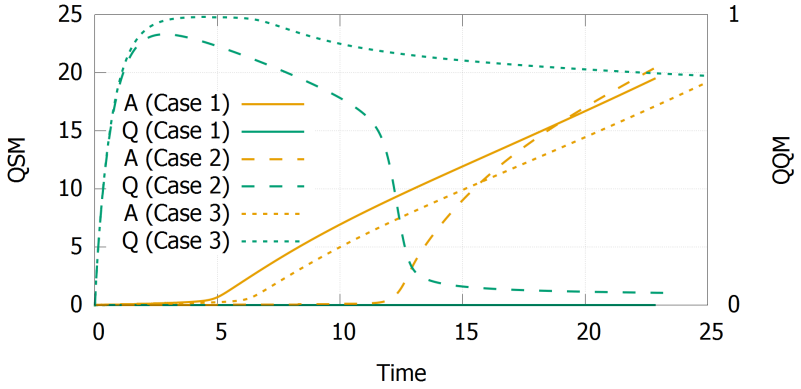

(b) QSM A and QQM Q

Figure 3.5: Lumped variables - Case 1: without QQM, Case 2: LPC - Case 3: SPC (for parameter values see Table 3.1)

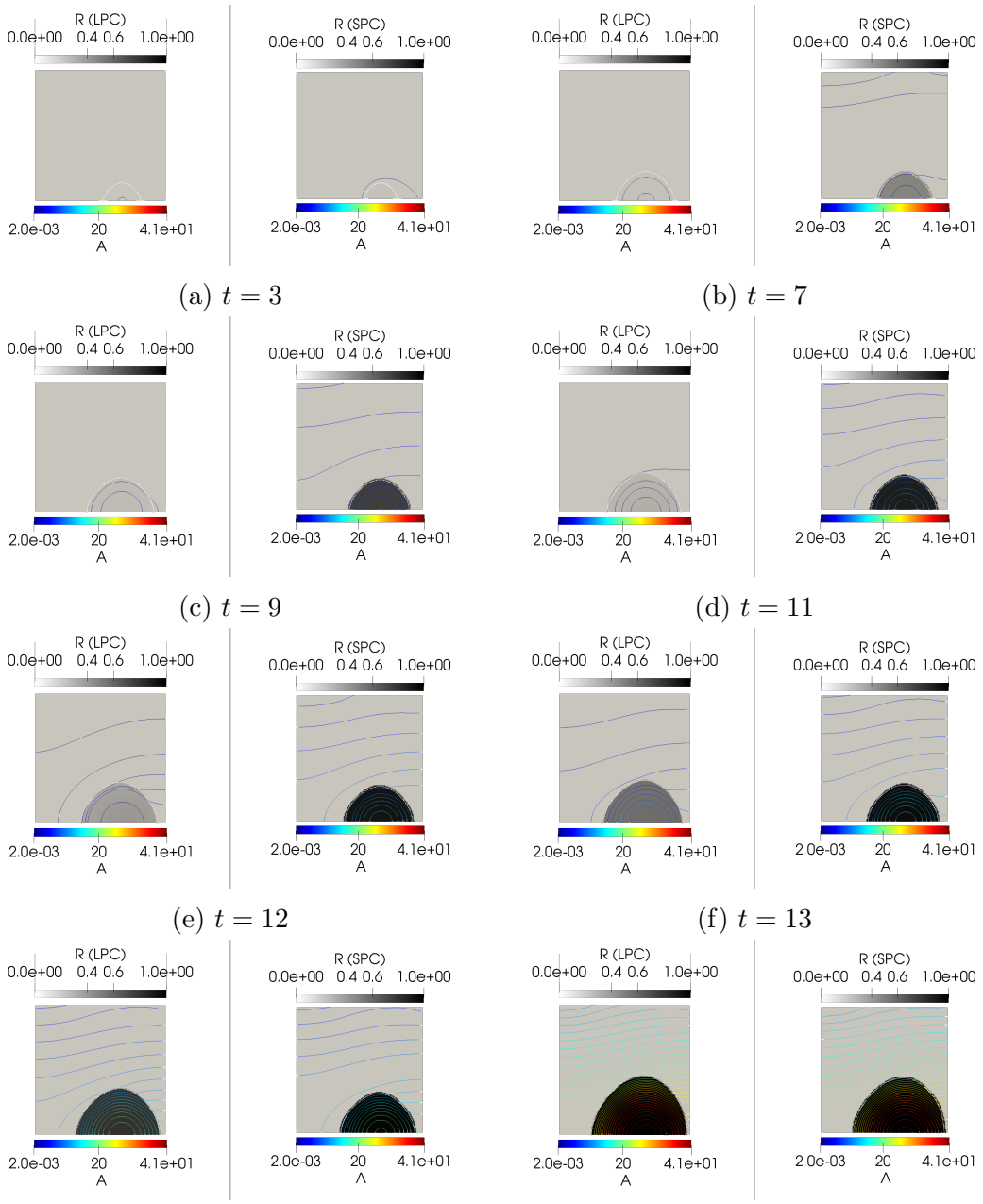

(a) $t = 3$ (b) $t = 7$

(c) $t = 9$ (d) $t = 11$

(e) $t = 12$ (f) $t = 13$

(g) $t = 15$ (h) $t = 24$ (LPC), $t = 26$ (SPC)

Figure 3.6: Ratio of up-regulated cells $R := N_u/(N_d + N_u)$ and QSM A for both, a small (SPC) and a large performance constant (LPC) at different times

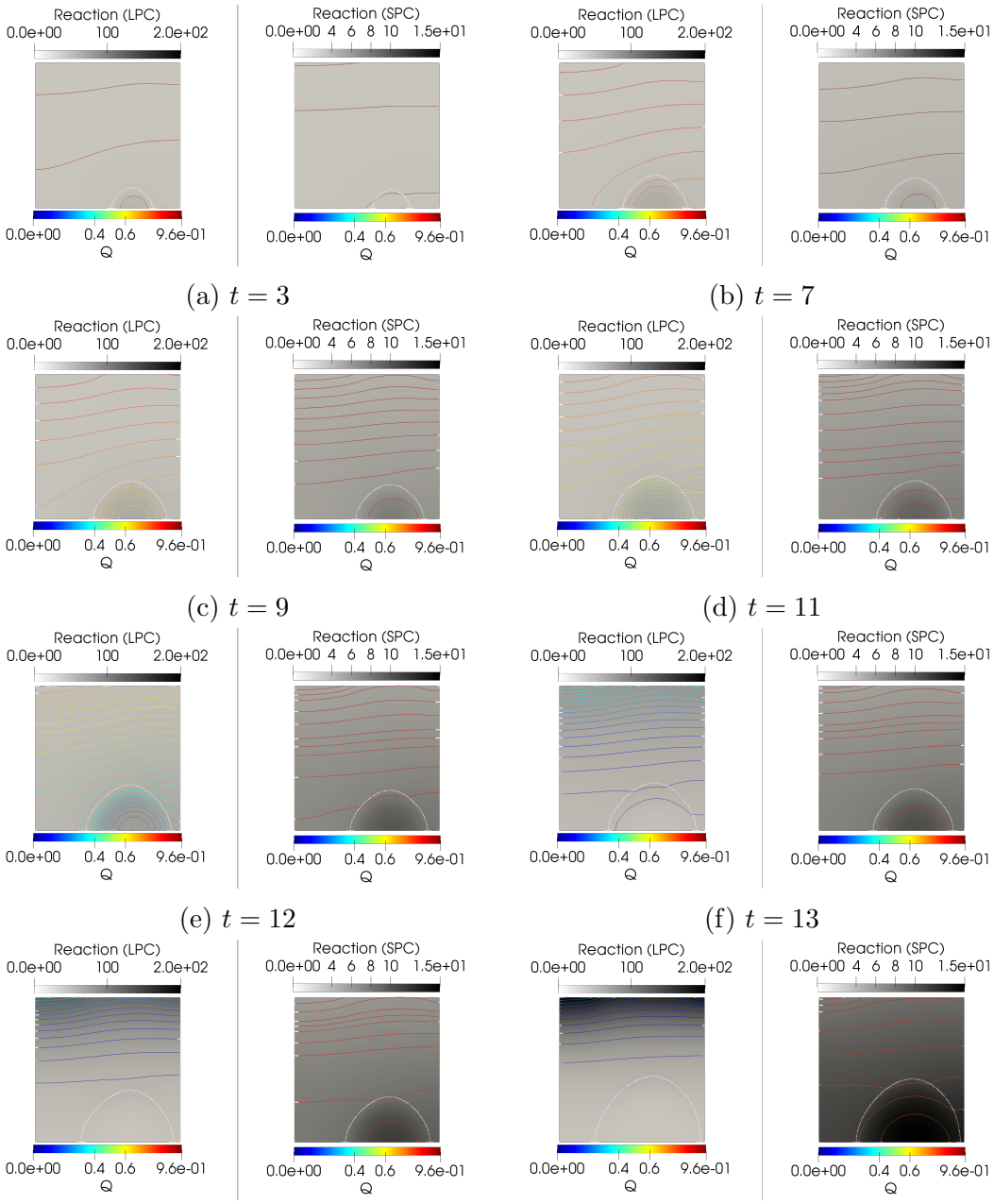

(a) $t = 3$ (b) $t = 7$

(c) $t = 9$ (d) $t = 11$

(e) $t = 12$ (f) $t = 13$

(g) $t = 15$ (h) $t = 24$ (LPC), $t = 26$ (SPC)

Figure 3.7: Location of reaction and QQM Q for both, a small (SPC) and a large performance constant (LPC) at different times

3.3.5 Sensitivity analysis with respect to the key parameters for the quorum quenching mechanism

Since the literature provides only little information on the reaction parameters, a sensitivity analysis for the reaction rate ν, the half rate constant k_Q and the conversion constant r will be conducted. In the following illustrations, Case 1 always refers to the reference case where parameters $\nu = 8640$, $k_Q = 100$ and $r = 25$ are used.

With increasing reaction rate, the time of up-regulation delays (Figure 3.8). When using a small reaction rate (Case 4 in Figure 3.8), the quorum quenching molecules cannot degrade the quorum sensing molecules fast enough to delay the up-regulation process. Subsequently, up-regulation happens, QSM are produced at an enhanced rate by up-regulated cells and thus, QQM are reduced quickly after the up-regulation. The QQM concentration is now too low in order to compensate the enhanced QSM production. If the reaction rate, however, is high (Case 2, 3 in Figure 3.8) the QQM efficiently degrade the QSM initially and the time of up-regulation increases significantly from $t \approx 13$ to $t \approx 18$.

With increasing half rate constant k_Q, the time of up-regulation decreases (Figure 3.9a, Figure 3.9b). Decrease k_Q by a factor of 10, changes the up-regulation time from $t \approx 13$ to $t \approx 18$ and thus, has the same effect as increasing the magnitude of the reaction rate by 10.

With increasing conversion rate r the time of up-regulation is also increasing (Figure 3.9c, Figure 3.9b). A conversion rate of $r = 1$ gives immediate up-regulation, almost as fast as in the case without the addition of QQM. For $r = 5$ the time of up-regulation is still close to the reference case without QQM, whereas it increases to $t \approx 13.5$ for $r = 25$ and $t \approx 18$ for $r = 100$.

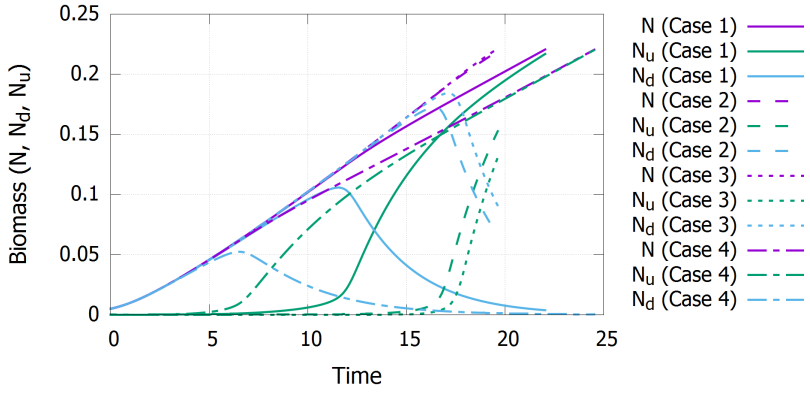

(a) Biomass N, N_d, N_u

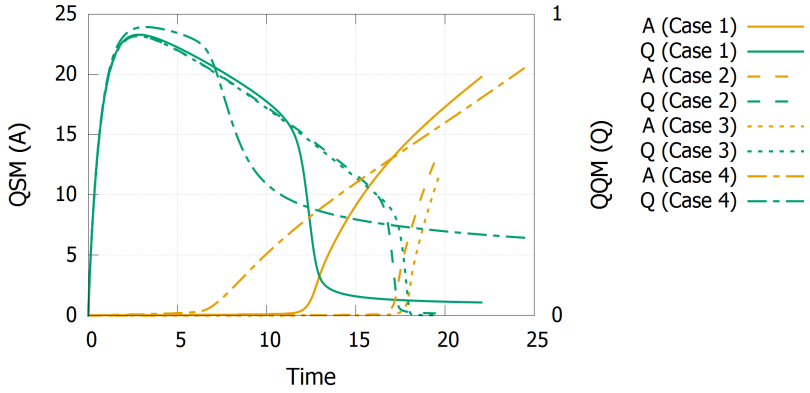

(b) QSM A and QQM Q

Figure 3.8: Sensitivity with respect to reaction rate ν - Case 1: $\nu = 8640$, Case 2: $\nu = 86400$, Case 3: $\nu = 864000$, Case 4: $\nu = 864$ ($k_Q = 100$ and $r = 25$)

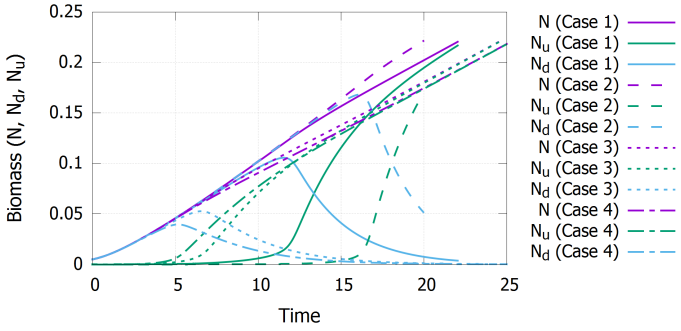

(a) Biomass N, N_d, N_u

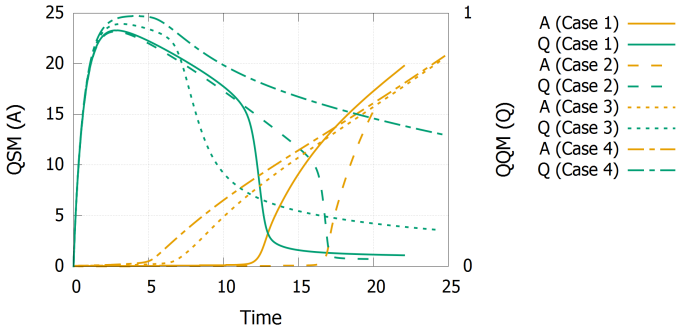

(b) QSM A and QQM Q

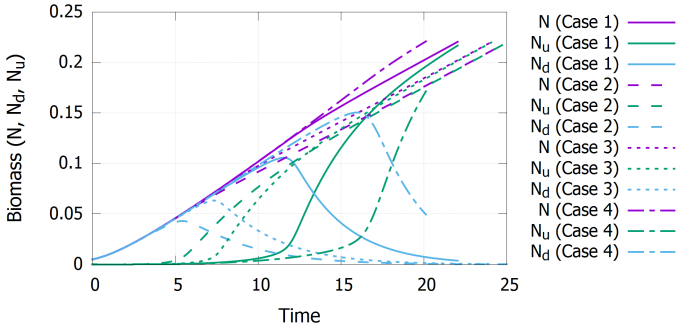

(c) Biomass N, N_d, N_u

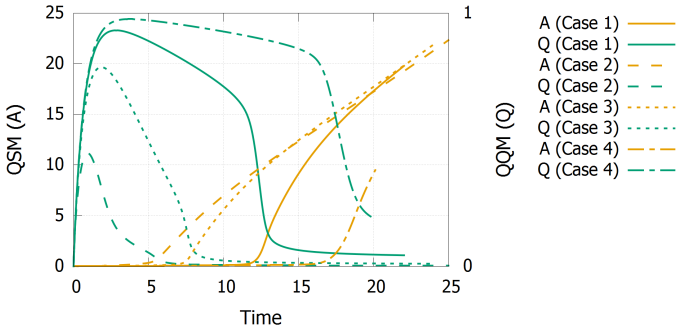

(d) QSM A and QQM Q

Figure 3.9: a), b): Sensitivity with respect to half rate constant k_Q - Case 1: $k_Q = 100$, Case 2: $k_Q = 10$, Case 3: $k_Q = 1000$, Case 4: $k_Q = 10000$ ($\nu = 8640$ and 25); c), d): Sensitivity with respect to conversion constant r - Case 1: $r = 25$, Case 2: $r = 1$, Case 3: $r = 5$, Case 4: $r = 100$ ($\nu = 8640$ and $k_Q = 100$)

3.4 Results

3.4.1 Effect of external conditions on the quenching mechanism

External mass transfer

The external mass transfer is modelled with Robin boundary conditions $I+\lambda\frac{\partial I}{\partial n} = I^{\infty}$ on the top boundary of the domain, where I^{∞} represents the substrate's bulk concentration and λ is the concentration boundary layer thickness. Nutrients and QQM enter the system here, meaning their bulk concentration is greater than zero, QSM are washed away, meaning their bulk concentration is set to 0. The degree of entry or ablation of substrates is represented by the concentration boundary layer thickness λ. A smaller λ allows more substrate to enter or to be washed away and a large value restrains the amount of substrate coming in or going out.
The amount of QQM added to the system can be changed by modifying either the QQM bulk concentration Q^{∞} or the concentration boundary layer thickness λ.

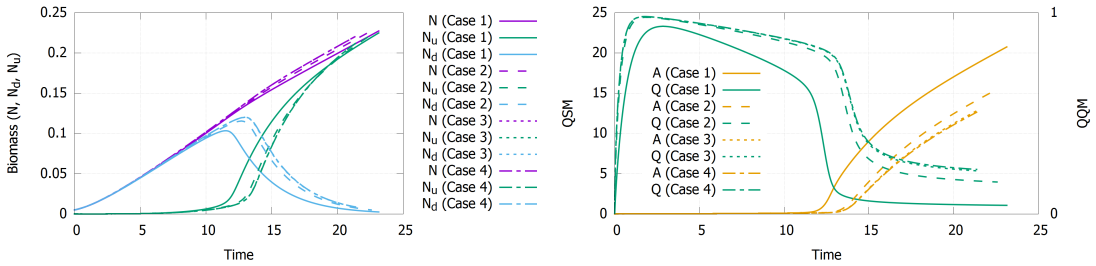

(a) Biomass N, N_d, N_u (b) QSM A and QQM Q

Figure 3.10: Case 1: Reference Case, Case 2: $\lambda_Q = 10^{-1}\lambda$, Case 3: $\lambda_Q = 10^{-2}\lambda$, Case 4: $\lambda_Q = 10^{-3}\lambda$

In the two-dimensional visualisations of the reaction, it can again (as in Figure 3.7 with LPC) be observed that there exist two different reaction locations. At first, the QQM have enough time to enter the system and spread through the whole domain before the QSM exceed its threshold for the up-regulation. This means the reaction occurs within the colony and uses up a significant amount of the QSM produced. The biofilm however grows and therefore, the total amount of QSM increases too. At some point, the up-regulation sets in and the amount of QSM abruptly increases such that the QQM are used up within and around

the colony. The QSM, diffusing faster than the QQM, spread to the outer area and further distribute through the whole domain leading to a shift of the reaction location to the top boundary, where the QQM enter the system. This observation is consistent for all the λ investigated.

QQ induced delay of up-regulation

The amount of QQM entering the system can also be modified by changing the QQM bulk concentration Q^{∞} in the Robin boundary condition $Q + \lambda \frac{\partial Q}{\partial n} = Q^{\infty}$.

In Figure 3.11, case 1 refers to a reference case without QQM, for case 2 and case 3 the bulk concentration for the QQM was set to $Q^{\infty} = 10$ and $Q^{\infty} = 50$ respectively. By increasing Q^{∞} by a 5-fold, the time of up-regulation is prohibited successfully in the observed time-period, however, previous simulations suggest that the system will get up-regulated eventually after enough QSMs are produced to use up a majority of the QQMs.

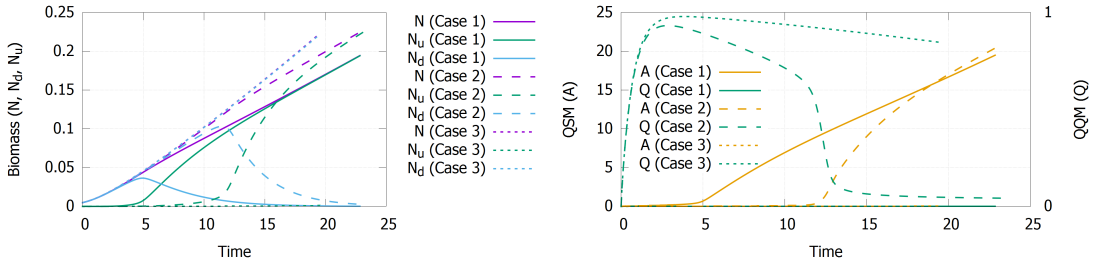

(a) Biomass N, N_d, N_u (b) QSM A and QQM Q

Figure 3.11: Case 1: Reference case without QQ, Case 2: $Q^{\infty} = 10$, Case 3: $Q\infty = 50$

3.4.2 Quorum quenching enzyme reaction

Several sources name special enzymes having quorum quenching abilities. Contrary to the reaction assumptions made in the simulations before, it is now assumed that only QSM but not QQ enzymes are degraded in the reaction. For that reason, the reaction rate ν_2 in the equation for the QQM was set to 0.

In Figure 3.12, case 1 refers to a reference case without the addition of QQM (dashed lines), case 2 represents the simulation considering the enzyme reaction

with a high performance (full lines) and case 3 a simulation with an enzyme reaction that has a small performance (dotted lines). The parameter sets for case 2 and case 3 can be found in Table 3.1. By choosing a high performance constant for the reaction term in the equation for the QSM, it can be demonstrated that up-regulation of the system can be prohibited during the time-period observed. The QQ enzymes reach the bulk concentration at $t = 3$ which stays constant afterwards. The QSMs are degraded, primarily inside and around the biofilm where they are produced and released. This effect can be seen in two-dimensional visualisations that are not given here due to their similarity to the case with the small performance constant (SPC) in Figure 3.7. The major part of the colony stays down-regulated due to the lack of signal molecules throughout the observed period. After $t = 10$ some up-regulated bacteria appear, making up only 5% of the total colony at $t = 21$.

An enzyme reaction with low efficiency (case 3) does not have the same result. The concentration of QQM is the same as for the high efficiency case. However, the reaction performance is too low in order to degrade enough QSM. As a result, the system gets up-regulated shortly after the reference case at around $t = 8$. This scenario resembles the SPC case in subsection 3.3.4. In both cases, there are would be enough QQM in the system but the reaction efficiency is too small to delay or prohibit up-regulation.

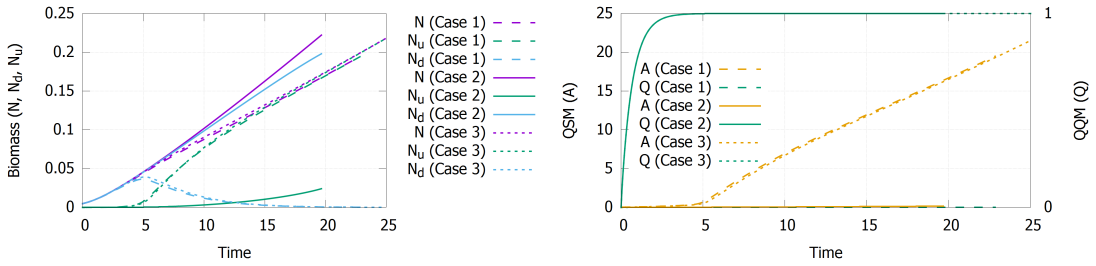

(a) Biomass N, N_d, N_u (b) QSM A and QQM Q

Figure 3.12: Case 1: Reference case without QQ, Case 2: Enzyme reaction ($\nu_2 = 0$) with high efficiency, Case 3: Enzyme reaction ($\nu_2 = 0$) with low efficiency

3.5 Application of QQ to a QS - Antibiotics - Model

3.5.1 Model extension

As an application for the quorum quenching model the coupling with the antibiotics-quorum sensing-model [20] is regarded. According to [28], resistance to antibiotics can be triggered by quorum sensing. Quorum quenching might be an supporting therapy in future treatment strategies.
For that, extra equations for the antibiotics and the biomass inactivated by the former have to be introduced. Following Ghasemi et al. [20], these assumptions are made:

1. **Antibiotics (B1)** The antibiotics enter the system, as the other dissolved substrates, from the top boundary and are transported by diffusion. They inactivate biomass at different rates, whereas up-regulated cells are more resistant against antibiotics than down-regulated cells. These inert biomass now represents the third biofilm forming part. It is further assumed, that antibiotics get consumed while eradicating the biomass. Furthermore, they decay naturally.

2. **Stress response (B2)** As a stress response, the quorum sensing molecule production is enhanced.

Table 3.3: Extended parameter description and values adapted from [20]

Parameter description	Parameter	Value	Unit
Decay rate for down-regulated cells by antibiotics	ψ_d	30	d^{-1}
Decay rate for up-regulated cells by antibiotics	ψ_d	3	d^{-1}
Half rate concentration for inactivation	k_{B1}	0.034	gm^{-3}
Exponent of Hill function for removal by antibiotic	m	2.5	-
Signal production rate as stress response	κ_B	55000	nMd^{-1}
Half rate concentration for stress response	k_{B2}	0.034	gm^{-3}
Antibiotic degradation rate (N_d)	ϕ_d	$4 \cdot 10^3$	$gm^{-3}d^{-1}$
Antibiotic degradation rate (N_u)	ϕ_u	$4 \cdot 10^3$	$gm^{-3}d^{-1}$
Antibiotic diffusion coefficient in water	d_B	10^{-4}	m^2d^{-1}
Biofilm/water diffusivity of antibiotics	ρ_B	0.1	-
Antibiotic bulk concentration	B^∞	-	gm^{-3}

The whole system writes now as follows:

$$
\begin{cases}
\dfrac{\partial N_d}{\partial t} = \nabla \cdot (D_N(N)\nabla N_d) + \mu_d N_d \dfrac{C}{k+C} - \alpha N_d \dfrac{A^n}{k_A^n + A^n} \\
\qquad\qquad + \beta N_u \dfrac{k_a^n}{k_a^n + A^n} - \sigma_N N_d \\
\qquad\qquad \underbrace{- \psi_d N_d \dfrac{B^m}{k_{B1}^m + B^m}}_{\text{inactivation by antibiotics}} \\
\dfrac{\partial N_u}{\partial t} = \nabla \cdot (D_N(N)\nabla N_u) + \mu_u N_u \dfrac{C}{k+C} + \alpha N_d \dfrac{A^n}{k_a^n + A^n} \\
\qquad\qquad - \beta N_u \dfrac{k_a^n}{k_a^n + A^n} - \sigma_N N_u \\
\qquad\qquad \underbrace{- \psi_u N_u \dfrac{B^m}{k_{B1}^m + B^m}}_{\text{inactivation by antibiotics}} \\
\dfrac{\partial I}{\partial t} = \nabla \cdot (D_N(N)\nabla I) + \underbrace{\psi_d N_d \dfrac{B^m}{k_{B1}^m + B^m} + \psi_u N_u \dfrac{B^m}{k_{B1}^m + B^m}}_{\text{inactivation of down- and up-regulated biomass}} \\
\dfrac{\partial C}{\partial t} = \nabla \cdot (D_C(N)\nabla C) - \omega_d \dfrac{C}{k+C} N_d - \omega_u \dfrac{C}{k+C} N_u \\
\dfrac{\partial A}{\partial t} = \nabla \cdot (D_A(N)\nabla A) + \kappa_0 (N_u + N_d) + \kappa_1 N_u \dfrac{A^n}{k_A^n + A^n} \\
\qquad\qquad - \sigma_A A - \nu Q \dfrac{A}{k_Q + A} \\
\qquad\qquad + \underbrace{\kappa_B (N_d + N_u) \dfrac{B}{k_{B2} + B}}_{\text{enhanced signal production as a stress response to antibiotics}} \\
\dfrac{\partial Q}{\partial t} = \nabla \cdot (D_Q(N)\nabla Q) - \dfrac{\nu}{r} Q \dfrac{A}{k_Q + A} \\
\dfrac{\partial B}{\partial t} = \nabla \cdot (D_B(N)\nabla B) \underbrace{- \phi_d N_d \dfrac{B^m}{k_{B1}^m + B^m} - \phi_u N_u \dfrac{B^m}{k_{B1}^m + B^m}}_{\text{degredation of antibiotics}} - \underbrace{\sigma_B B}_{\text{natural decay}}
\end{cases}
$$

With boundary conditions according to (A1) and (B1)

$$\begin{cases} \frac{\partial N_d}{\partial n} = \frac{\partial N_u}{\partial n} = \frac{\partial I}{\partial n} = 0 & \text{at} \quad x = 0 \quad \text{and} \quad y = 0, H \\ \frac{\partial C}{\partial n} = \frac{\partial A}{\partial n} = \frac{\partial Q}{\partial n} = \frac{\partial B}{\partial n} = 0 & \text{at} \quad x = 0 \quad \text{and} \quad y = 0, H \\ N_d = N_u = I = 0 & \text{at} \quad y = H \\ C + \lambda \frac{\partial C}{\partial n} = C^{\infty} & \text{at} \quad y = H \\ A + \lambda \frac{\partial A}{\partial n} = 0 & \text{at} \quad y = H \\ Q + \lambda \frac{\partial Q}{\partial n} = Q^{\infty} & \text{at} \quad y = H \\ B + \lambda \frac{\partial B}{\partial n} = B^{\infty} & \text{at} \quad y = H \end{cases}$$

and diffusion coefficients

$$D_N(N) = d_N \frac{N^a}{(1-N)^b} \quad \text{(A7)}$$

$$D_{C,A,Q,B} = d_{C,A,Q,B}(1 + N(\rho_{C,A,Q,B} - 1)) \quad \text{(A8,B1)}$$

The total system was again non-dimensionalised for computational reasons. The non-dimensional system for the new terms will not be given explicitly but can be found in [20]. For more details on the model for quorum sensing triggered resistance to antibiotics the reader is referred to [20]. The new parameters and their values used for simulations can be found in Table 3.3.

3.5.2 Results

According to assumption (A2), cells respond to the influence of antibiotics by producing QSM at an enhanced level. Now it is investigated whether quorum quenching can compensate that stress response.

For that purpose the colony is exposed to an amount of antibiotics small enough

not to kill the entire population. In case 1 of Figure 3.13 the parameter values in Table 3.3 are used and the antibiotic bulk concentration is set to $B^\infty = 1/30$. Case 2 uses the same values as the latter one, however, the stress response is switched off here, meaning $\kappa_B = 0$. In case 3 QQM are added and the stress response is switched on again.

Without stress response (case 1) the system gets up-regulated at around $t = 7.5$. The stress response (case 2) leads to an enhanced QSM production and thus to an earlier up-regulation at around $t = 5$. In Figure 3.13b the earlier start of QSM production can be observed for the case with stress response (case 2).
When QQMs are added to the system (case 3) the stress response can not only be compensated successfully, but the time of up-regulation can even be delayed (Figure 3.13a). The QSM production is suppressed until approximately $t = 9$.

Now an obvious question is whether and how the addition of QQM will affect the efficiency of antibiotics regarding the eradication of the biofilm.
As it was demonstrated in previous results, the addition of QQM delays the up-regulations, i.e. the time when more or less the whole colony is resistant. This means that one has more time to treat the biofilm with antibiotics in a less-protected state. However, timely treatment with antibiotics is important as the biofilm grows and up-regulation might happen eventually.

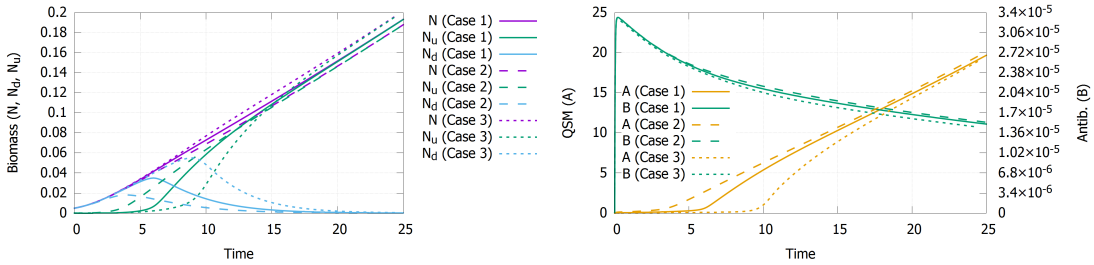

(a) Biomass N, N_d, N_u (b) QSM A and QQM Q

Figure 3.13: Case 1: Exposure to antibiotics without stress response ($B^\infty = 1/30$, $\kappa_B = 0$, $Q^\infty = 0$); Case 2: Exposure to antibiotics with stress response ($B^\infty = 1/30$, $\kappa_B > 0$, $Q^\infty = 0$); Case 3: Exposure to antibiotics and quorum quenching with stress response ($B^\infty = 1/30$, $\kappa_B > 0$, $Q^\infty = 10$)

3.6 Discussion

After the initial parameter investigation for the QSM-QQM reaction in the chemostat model, the spatial system was examined within a bacterial biofilm. In this two-dimensional setting the spatial effects of quorum quenching could be investigated properly.

In the chemostat model it was distinguished between two parameter sets: one for a high and one for a low affinity to the reaction. As it was shown that the outcome was more dependent on the "performance constant" than on the reaction affinity the focus in the two-dimensional model was set on the investigation of the performance constant. It was distinguished between two parameter sets, one for a low and one for a high performance constant.
When a low performance constant was used the time of up-regulation could only be slightly delayed and apart from that the system almost behaved as if the QQM would not be present. Due to the low performance the reaction hardly used up QSM or QQM. As a result the QQM concentration almost stayed constant and QSM were produced without restriction. Thus the whole system was up-regulated, i.e. resistant in a case of quorum sensing triggered resistance to antibiotics at the end. The reaction between QSM and QQM took place inside and closely around the colony for all observed times.
By using a high performance constant the QQM had an effect on both the colony and the QSM produced. The QSM were successfully degraded and thus the colony was kept down-regulated. This state could be maintained throughout the whole observation period when enough QQM were added. When less QQM were added, they were used up too fast to maintain the down-regulated state and the whole system went through up-regulation eventually. Nonetheless, the time of up-regulation could be significantly delayed. The reaction between QSM and QQM switched here to the top boundary where the QQM were added once the QQM were used up inside and closely around the biofilm.
According to some sources [7, 42, 23, 5, 14, 23] there are enzymes with quorum quenching abilities. An enzyme reaction is however different from the reaction that was considered in the beginning: The QQ enzyme would not be used up during the reaction process. To test the outcome with respect to that difference, it was assumed that QQM are not degraded. Again two parameter sets with high and low performance constant respectively were tested.

The low performance case again failed to prevent up regulation since QSM were not used up efficiently enough. This outcome was predictable considering the previous case where QQM could have been degraded too but was not due to the low reaction performance.
The up-regulation could again be successfully prohibited when a high performance constant was used. In these scenarios the QQM is not degraded and thus, a simpler version of the system would suffice for that model. The QQM concentration could be assumed to be constant and an additional equation for the QQM would be unnecessary.

In general it can be concluded that quorum quenching is an effective mechanism in order to delay or prohibit up-regulation if the performance of the reaction is high enough. A QQM with sufficiently high performance constant would therefore be a good choice for prohibiting or delaying unwanted bacterial group behaviours as resistance to antibiotics and thus could be considered as an adjuvant to traditional therapy methods.

The sensitivity analysis with respect to the three reaction parameters demonstrate that there can be a variety of outcomes for different combinations of the latter. With higher conversion rate, i.e. the number of QSM one QQM can degrade before the QQM itself decays, the reaction approaches an enzyme reaction. In general, a more profound knowledge of those parameter values would lead to much more accuracy in the model outcomes.

It was demonstrated that QQ can successfully prohibit up-regulation. In reality, this means that the expression of harmful bacterial group behaviours such as virulence could be delayed or even prevented with QQ. In this sense, QQ could be a means to make pathogenic bacteria less harmful.

As another application for QQ the system given in [20] is expanded with the equation for the QQM. In [20] the quorum sensing triggered resistance to antibiotics is investigated. The biofilm's exposure to antibiotics accelerates the production of QSM as a stress response and leads to an earlier up-regulation of the colony. An obvious application of QQ is thus the compensation of this stress response which could be successfully demonstrated with simulations. Since low efficiency reactions performed badly, this application was only tested with

a sufficiently efficient reaction. Quorum quenching with an effective molecule or enzyme thus seems to be a promising new strategy when targeting antimicrobial resistance.

Chapter 4

Conclusion

"Nothing in life is to be feared, it is only to be understood. Now is the time to understand more, so that we may fear less."
(M. Skłodowska Curie)

4.1 Summary

Facing the growing challenge of antimicrobial resistance - possibly triggered by quorum sensing - it is of great importance to study and understand potential alternative treatment strategies. Harmful bacterial group behaviours, e.g. virulence or antimicrobial resistance are often expressed due to a cell-to-cell communication pathway, called quorum sensing. Quorum quenching is an inhibition method of the latter and might be used as both, an anti-virulence therapy and an adjuvant to traditional antibiotics. Up until now, only a few mathematical models on quorum sensing inhibition and quorum quenching have been published. Some of them treated the detailed quorum sensing inhibition and quorum quenching mechanism on molecular scale. Others also investigated both, the molecular mechanism and its effect on a biofilm culture within complex multiscale models.
This work presents two models that take into account the simple but effective mechanism of quorum quenching and its effect on a bacterial community within both, a mesoscopic biofilm model and a chemostat model. The complex chemical mechanism of quorum sensing inhibition was neglected, allowing the use of a simpler model than in a multiscale approach. Hence, the aim of this work is to fill the empty gap in the literature by integrating quorum quenching into a mesoscopic biofilm model.

In the chemostat model, spatial effects could be neglected due to its well-mixed set up. For this, a system of non-linear ordinary differential equations was used.

This allowed for a comprehensive simulation based study of this phenomenon with low computational effort.
The chemostat provided a good environment for the initial investigation of the QQ mechanism. It could be demonstrated that the up-regulation of the system, i.e. the resistance of the bacterial colony, could be prohibited successfully under certain conditions. The amount of added QQM necessary to obtain this result depended on the performance constant of the reaction. The transition between up- and down-regulated outcome of the system appeared to be very abruptly and switch-like. Similar findings were made in [14]. The authors however also mention that the switch could only be demonstrated in simulations but not in real experiments.
Furthermore, a linear dependency of the amount of QQM needed in order to attain an down-regulated outcome from the reciprocal of the performance constant was found.
In the chemostat model also the inheritance of up-regulated phenotypes, i.e. the inheritance of resistance, was considered. The number of resistant heirs from a resistant "parent" cell was treated as unknown in [41]. Here it could be demonstrated that there exists an interval in which this parameter decides about the up- or down-regulation of the system's final state. Depending on the desired accuracy of the results, this parameter could be either neglected or integrated for more accurate results. The value of that parameter is however often unknown and right now subject of many biological investigations.

In the two-dimensional model builds on the quorum sensing part of the model in [20] and extends it with the additional equation for quorum quenching. Its aim is the observation of spatial effects of the quorum quenching mechanism.
The successful prohibition of the system's up-regulation could be shown here as well. The location of the reaction between QSM and QQM varied across different parameter sets with low or high reaction performance.
The success of QQ is highly dependent on the reaction efficiency. With a low performance the mechanism does not affect the colony and its QSM production. By using a high performance constant, quorum sensing could be successfully suppressed.
The time period in which up-regulation can be suppressed also depends on the amount of QQM added to the system, when more QQM are added the time of up-regulation can be delayed more.

In [20] the quorum sensing triggered resistance to antibiotics is investigated. When the bacteria are exposed to antibiotics they start to accelerate the production of signal molecules. In this work it was successfully demonstrated that the addition of QQM can compensate this kind of stress response.

The successful application of quorum quenching to a model where resistance to antibiotics was triggered by cell-to-cell communication shows its applicability for future models and biological experiments. Quorum quenching can delay or potentially prevent the resistance of a bacterial community and allow traditional antibiotics to function.

4.2 Lessons learnt

To conclude:

- **Extension of existing models with quorum quenching:**
  Existing models of quorum sensing in bacterial populations can be extended to include quorum quenching, both in the contexts of suspended populations in chemostats, and spatially structured biofilm colonies. In the former case this leads to systems of ODEs, in the latter case to systems of nonlinear PDEs. Also the numerical techniques that have been used previously to simulate such models can be extended in a straightforward manner. While it has often been suggested in the biological literature that quorum sensing inhibition (including quorum quenching) might provide a way to support antimicrobial therapies, specific quantitative experimental evidence seems scarce. Mathematical models like the ones developed here might be a useful tool to explore and analyse this.

- **Experimental data:**
  There is currently only little quantitative information available in the experimental literature to parametrise quorum quenching models such as the ones that are proposed here. Moreover, the quantitative information available suggests that some key parameter may be highly variable across several orders of magnitudes. Therefore, the predictive capabilities of these models are currently limited. Nevertheless, by conducting a sensitivity analysis we could identify some key parameters, on which one should focus to improve the accuracies of predictions. The interplay of bacterial population

dynamics, quorum sensing, and quorum quenching, possibly coupled with further processes such as population response to antibiotics is complex. Our simulations suggests that the efficiency for quorum quenching to suppress up-regulation and thus stress mechanisms might depend on several factors, however a key parameter here is the performance constant of the QQ reaction.

- **Simplification of the system:**
  The simulation results suggest that there are certain circumstances under which the model could be substantially simplified, for example because it might not be necessary to actually track the quorum quenching component explicitly if the QQMs do not become low enough to be reaction limiting. Also, if the QQM is actually an enzyme an additional equation for the QQM might even be omitted.

4.3 Future work

The scope of this work was very comprehensive, a lot of aspects had to be neglected and there remains still a lot to be uncovered. This work provides only a short glance of what would be possible with quorum quenching as a quorum sensing inhibiting method. As quorum sensing appears in many different contexts, there are many possible areas of application for quorum quenching (modelling). Here are suggestions of what could be done in the future regarding the investigation of quorum quenching:

- **Optimal control for chemostat model:**
  Here, always a constant inflow of QQM into the system was assumed. A biologically more relevant approach would be to administer QQM only discretely at certain times. To calculate the optimal strategy, the chemostat ODE model could be reformulated into an optimal control problem.

- **Proof of well-posedness for biofilm model:**
  In [35, 36] the well-posedness for similar multi-dimensional QS systems without QQ was proven. The authors suggest that those systems can be expanded analogously, however, a formal proof of the well-posedness for the two-dimensional QS-QQ model as it was introduced here remains to be formulated.

- **Experimental data:**
  As already mentioned before, there was only little quantitative information from experimental data. In order to properly parametrise a whole quorum sensing - quorum quenching model a broader set of measures would allow for more accuracy in mathematical models. Some parameters to further investigate would be the diffusion coefficient for the QQM, the inheritance of the up-regulated phenotype, as well as the reaction parameters for the QS-QQ reaction.

- **Model elaboration:**
  In [15, 16] the importance of mass transfer of signal molecules was demonstrated when it comes to quorum sensing. The same might be true for quorum quenching mechanisms. This could be done by adding a second colony once the first one has grown to a certain size.

In this work the applicability of quorum quenching to a quorum sensing operating bacterial community was successfully demonstrated. Now it remains that the model is refined and used in a broad range of possible applications.

Appendix A

Chemostat model

Mathematical preliminaries

Consider the initial value problem

$$y' = f(x, y), \quad y(\xi) = \eta \tag{A.1}$$

Definition A.0.1. *[4, §10.I] A vector function $y(t)$ is a solution of (2.1) in the interval J if $y(t)$ is differentiable in J and if (2.1) is satisfied identically by $y(t)$.*

Proposition A.0.2. *[4, §10.XVI] Let $M \subset \mathrm{R}^n$ be closed, $f(x, y) : [\xi, \xi+a] \times M \to \mathrm{R}^n$ bounded and continuous, and assume that a tangent condition (T_i) or (T_d) holds.*

$$lim_{h \to 0+} \frac{1}{h} dist(z + hf(x, z), M) = 0 \quad for \quad z \in \bar{M}, \quad x \in J = [a, b] \quad (T_d)$$

$$n(z), f(x, z) \leq 0 \quad for \quad x \in J, \quad z \in \partial M \qquad (T_i)$$

where $n(z)$ is the outer normal to M at z. Then, for any $\eta \in M$, the initial value problem (A) has a solution y such that $y(x) \in M$ for $\xi \leq x \leq \xi + a$.
In particular, if M is compact and if f is continuous in $[\xi, \infty) \times M$, then there exists a global solution satisfying $y(x) \in M$ for all $x \geq \xi$.

Proposition A.0.3. *[4, §10.VI] Let $f(y)$ be continuous in a domain $D \subset \mathbb{R}^n$ and satisfy a local Lipschitz condition with respect to y in D (this hypothesis is satisfied, for instance, if $\partial f / \partial y \in C(D)$). If $(\xi, \eta) \in D$, then the initial value problem*

$$y\prime = f(y), \quad y(\xi) = \eta \tag{A.2}$$

has exactly one solution. The solution can be extended to the left and right up to the boundary of D.

Definition A.0.4. ***Lipschitz Condition.*** *([4], §5,VI) Let E, F be two real or complex normed spaces and $T : D \to F$ a function with $D \subset E$. The operator T satisfies a* ***Lipschitz condition*** *in D (with* ***Lipschitz constant*** *q) if*

$$||Tx - Ty||_F \leq q||x - y||_E \quad for \quad x, y \in D. \tag{A.3}$$

Proposition A.0.5. ***Mean Value Theorem.*** *[4, Appendix B,I]*

Proposition A.0.6. ***Theorem on Continuous Dependence.*** *([4], §12,VI) Let J be a compact interval with $\xi \in J$ and let the function $y = y_0(t)$ be a solution of the initial value problem*

$$y\prime = f(t, y) \quad in \quad J, \quad y(\xi) = \eta. \tag{A.4}$$

The α-neighbourhood ($\alpha > 0$) of graph y_0 (definition: the set of all points (t, y) with $t \in J, |y - y_0(t)| \leq \alpha$) will be denoted by S_α. Suppose there exists $\alpha > 0$ such that $f(t, y)$ is continuous and satisfies the Lipschitz condition (A.3) *in S_α. Then the solution $y_0(t)$ depends continuously on the initial values and on the right-hand side f. In other words: For every $\epsilon > 0$, there exists $\delta > 0$ such that if g is continuous in S_α, and the inequalities*

$$|g(t, y) - f(t, y)| < \delta \quad in \quad S_\alpha, \quad |\zeta - \eta| < \delta \tag{A.5}$$

are satisfied, then every solution $z(t)$ of the "perturbed" initial value problem

$$z\prime = g(t, z), \quad z(\xi) = \zeta \tag{A.6}$$

exists in all of J and satisfies the inequality

$$|z(t) - y_0(t)| < \epsilon \quad in \quad J \tag{A.7}$$

Non-dimensionalisation

For the non-dimensionalisation of the ODE system, the following non-dimensional variables were used:

$$\bar{t} := qt, \quad \bar{N_d} := \frac{N_d \kappa_0}{q k_A}, \quad \bar{N_u} := \frac{N_u \kappa_0}{q k_A}, \quad \bar{C} := \frac{C}{C^\infty}, \quad \bar{A} := \frac{A}{k_A}, \quad \bar{Q} := \frac{Q}{Q^\infty},$$

And let

$$\begin{aligned}
&\bar{\mu_d} := \frac{\mu_d}{q}, \quad \bar{\mu_u} := \frac{\mu_u}{q}, \quad \bar{\alpha} := \frac{\alpha}{q}, \quad \bar{\beta} := \frac{\beta}{q}, \quad \bar{\nu_1} := \frac{\nu Q^\infty}{q k_A}, \quad \bar{\nu_2} := \frac{\nu}{rq}, \\
&\bar{k_C} := \frac{k_C}{C^\infty}, \quad \bar{k_Q} := \frac{k_Q}{k_A}, \quad \bar{\kappa} := \frac{\kappa_1}{\kappa_0}, \\
&m_d := \frac{\mu_d k_A}{y_d C^\infty \kappa_0}, \quad m_u := \frac{\mu_u k_A}{y_u C^\infty \kappa_0}
\end{aligned}$$

For readability, the bars were dropped in the following text. The system transforms as follows:

$$\begin{cases}
\dfrac{\mathrm{d}N_d}{\mathrm{d}t} = & \mu_d N_d \dfrac{C}{k_C + C} + \mu_u (2-\gamma) N_u \dfrac{C}{k_C + C} - N_d \\
& -\alpha N_d \dfrac{A^n}{1 + A^n} + \beta N_u \dfrac{1}{1 + A^n} \\
\dfrac{\mathrm{d}N_u}{\mathrm{d}t} = & \mu_u (\gamma - 1) N_u \dfrac{C}{k_C + C} - N_u \\
& +\alpha N_d \dfrac{A^n}{1 + A^n} - \beta N_u \dfrac{1}{1 + A^n} \\
\dfrac{\mathrm{d}C}{\mathrm{d}t} = & (1 - C) - (m_d N_d + m_u N_u) \dfrac{C}{k_C + C} \\
\dfrac{\mathrm{d}A}{\mathrm{d}t} = & (N_u + N_d) + \kappa N_u \dfrac{A^n}{1 + A^n} - \nu_1 Q \dfrac{A}{k_Q + A} - A \\
\dfrac{\mathrm{d}Q}{\mathrm{d}t} = & (1 - Q) - \nu_2 Q \dfrac{A}{k_Q + A}
\end{cases}$$

Appendix B

Biofilm model

Numerical treatment and non-dimensionalisation

The numerical method for solving this system needs to cope with the two non-linear properties of the diffusion coefficient for the biomass: $D_N(N)$ vanishes as $N \approx 0$ and approaches a super-diffusion singularity as $N \to 1$. The numerical method used for these simulations is the same as the one used by Ghasemi et al. in [20]. This method is an extension of [18] and [19], developed by the same authors. For the time integration, an error-controlled, time-adaptive Rosenbrock-Wanner method was used, whereas the spatial discretisation was performed on a Finite Volume scheme on a uniform grid. The non-dimensionalisation of the system is given below. For detailed information on the numerical scheme, it is referred to [18, 19, 20].

Let

$$\tilde{t} := \mu_d t, \quad \tilde{x} := \frac{x}{L}, \quad \tilde{C} := \frac{C}{C^\infty}, \quad \tilde{A} := \frac{A}{k_A}, \quad \tilde{Q} := \frac{Q}{Q^\infty}$$

The dependent variables N_d and N_u are already defined as dimensionless. The new model parameters are defined as follows:

$$\begin{cases} \tilde{\mu_u} = \dfrac{\mu_u}{\mu_d}, \quad \tilde{\alpha} = \dfrac{\alpha}{\mu_d}, \quad \tilde{\beta} = \dfrac{\beta}{\mu_d}, \quad \tilde{\sigma_N} = \dfrac{\sigma_N}{\mu_d}, \quad \tilde{\sigma_A} = \dfrac{\sigma_A}{\mu_d}, \quad \tilde{\nu_1} = \dfrac{\nu Q^\infty}{k_A \mu_d} \\ \tilde{k} = \dfrac{k}{C^\infty}, \quad \tilde{k_Q} = \dfrac{k_Q}{k_A}, \quad \tilde{\omega_d} = \dfrac{\omega_d}{\mu_d C^\infty}, \quad \omega_u = \dfrac{\omega_u}{\mu_d C^\infty} \\ \tilde{\kappa_0} = \dfrac{\kappa_0}{\mu_d k_A}, \quad \tilde{\kappa_1} = \dfrac{\kappa_1}{\mu_d k_A}, \quad \tilde{\nu_2} = \dfrac{\nu}{r \mu_d} \\ \tilde{D}_{N,C,A,Q}(N) = \dfrac{D_{N,C,A,Q}(N)}{\mu_d L^2} \end{cases}$$

The non-dimensionalised system can be written as:

$$
\begin{cases}
\dfrac{\partial N_d}{\partial t}(\tilde{x},\tilde{t}) = \nabla(\tilde{D}_N(N)\nabla N) & + & \dfrac{\tilde{C}}{\tilde{k}+C}N_d & - & \tilde{\alpha}\dfrac{\tilde{A}^n}{1+\tilde{A}^n}N_d \\
& + & \tilde{\beta}\dfrac{1}{1+\tilde{A}^n}N_u & - & \tilde{\sigma}N_d \\
\dfrac{\partial N_u}{\partial t}(\tilde{x},\tilde{t}) = \nabla(\tilde{D}_N(N)\nabla N) & + & \tilde{\mu_u}\dfrac{\tilde{C}}{\tilde{k}+C}N_d & + & \tilde{\alpha}\dfrac{\tilde{A}^n}{1+\tilde{A}^n}N_d \\
& - & \tilde{\beta}\dfrac{1}{1+\tilde{A}^n}N_u & - & \tilde{\sigma}N_u \\
\dfrac{\partial \tilde{C}}{\partial t}(\tilde{x},\tilde{t}) = \nabla(\tilde{D}_{\tilde{C}}(N)\nabla \tilde{C}) & - & \omega_d\dfrac{\tilde{C}}{\tilde{k}+C}N_d & - & \omega_u\dfrac{\tilde{C}}{\tilde{k}+C}N_u \\
\dfrac{\partial \tilde{A}}{\partial t}(\tilde{x},\tilde{t}) = \nabla(\tilde{D}_{\tilde{A}}(N)\nabla \tilde{A}) & + & \tilde{\kappa_0}(N_d+N_u) & + & \tilde{\kappa_1}N_u\dfrac{\tilde{A}^n}{1+\tilde{A}^n} \\
& - & \tilde{\sigma_A}\tilde{A} & - & \tilde{\nu_1}\dfrac{\tilde{A}}{\tilde{k_Q}+\tilde{A}}\tilde{Q} \\
\dfrac{\partial \tilde{Q}}{\partial t}(\tilde{x},\tilde{t}) = \nabla(\tilde{D}_{\tilde{Q}}(N)\nabla \tilde{Q}) & - & \tilde{\nu_2}\dfrac{\tilde{A}}{\tilde{k_Q}+\tilde{A}}\tilde{Q} &&
\end{cases}
\tag{B.1}
$$

List of Figures

List of Tables

Bibliography

[1] Definition of 'quorum', https://www.merriam-webster.com/dictionary/quorum.

[2] K Anguige, JR King, JP Ward, and P Williams. Mathematical modelling of therapies targeted at bacterial quorum sensing. *Mathematical biosciences*, 192(1):39–83, 2004.

[3] Arren Bar-Even, Elad Noor, Yonatan Savir, Wolfram Liebermeister, Dan Davidi, Dan S Tawfik, and Ron Milo. The moderately efficient enzyme: evolutionary and physicochemical trends shaping enzyme parameters. *Biochemistry*, 50(21):4402–4410, 2011.

[4] A. Browder, W. Walter, R. Thompson, W. Wolfgang, W.L. Walter, S.J. Axler, F.W. Gehring, and P.R. Halmos. *Ordinary Differential Equations*. Graduate Texts in Mathematics. Springer New York, 1998.

[5] Weihua Chu, Shuxin Zhou, Wei Zhu, and Xiyi Zhuang. Quorum quenching bacteria bacillus sp. qsi-1 protect zebrafish (danio rerio) from aeromonas hydrophila infection. *Scientific reports*, 4:5446, 2014.

[6] J William Costerton, Zbigniew Lewandowski, Douglas E Caldwell, Darren R Korber, and Hilary M Lappin-Scott. Microbial biofilms. *Annual Reviews in Microbiology*, 49(1):711–745, 1995.

[7] Weiwei Dong, Jie Zhu, Xiang Guo, Delong Kong, Qi Zhang, Yiqing Zhou, Xiaoyang Liu, Shumiao Zhao, and Zhiyong Ruan. Characterization of aiik, an ahl lactonase, from kurthia huakui lam0618 t and its application in quorum quenching on pseudomonas aeruginosa pao1. *Scientific reports*, 8(1):6013, 2018.

[8] Yi-Hu Dong and Lian-Hui Zhang. Quorum sensing and quorum-quenching enzymes. *The Journal of Microbiology*, 43(1):101–109, 2005.

[9] Antonija Duvnjak and Hermann J Eberl. Time-discretisation of a degenerate reaction-diffusion equation arising in biofilm modeling, el. *Trans Num. Analysis*, 23:15–38, 2006.

[10] Herman J Eberl, David F Parker, and Mark Van Loosdrecht. A new deterministic spatio-temporal continuum model for biofilm development. *Computational and Mathematical Methods in Medicine*, 3(3):161–175, 2001.

[11] Hermann J Eberl and Laurent Demaret. A finite difference scheme for a degenerated diffusion equation arising in microbial ecology. *Electron. J. Differ. Equ*, 15:77–95, 2007.

[12] Messoud A Efendiev, Sergey V Zelik, and Hermann J Eberl. Existence and longtime behavior of a biofilm model. *Comm. Pure Appl. Analysis*, 8(2):509–531, 2009.

[13] Blessing O Emerenini, Burkhard A Hense, Christina Kuttler, and Hermann J Eberl. A mathematical model of quorum sensing induced biofilm detachment. *PloS one*, 10(7):e0132385, 2015.

[14] July Fong, Chaodong Zhang, Renliang Yang, Zhao Zhi Boo, Soon Keat Tan, Thomas E Nielsen, Michael Givskov, Xue-Wei Liu, Wu Bin, Haibin Su, et al. Combination therapy strategy of quorum quenching enzyme and quorum sensing inhibitor in suppressing multiple quorum sensing pathways of p. aeruginosa. *Scientific reports*, 8(1):1155, 2018.

[15] Mallory R Frederick, C Kuttler, BA Hense, J Müller, and HJ Eberl. A mathematical model of quorum sensing in patchy biofilm communities with slow background flow. *Can Appl Math Q*, 18(3):267–298, 2010.

[16] Mallory R Frederick, Christina Kuttler, Burkhard A Hense, and Hermann J Eberl. A mathematical model of quorum sensing regulated eps production in biofilm communities. *Theoretical Biology and Medical Modelling*, 8(1):8, 2011.

[17] W Claiborne Fuqua, Stephen C Winans, and E Peter Greenberg. Quorum sensing in bacteria: the luxr-luxi family of cell density-responsive transcriptional regulators. *Journal of bacteriology*, 176(2):269, 1994.

[18] Maryam Ghasemi and Hermann J Eberl. Extension of a regularization based time-adaptive numerical method for a degenerate diffusion-reaction biofilm growth model to systems involving quorum sensing. *Proc Comput Sci*, 108:1893–1902, 2017.

[19] Maryam Ghasemi and Hermann J Eberl. Time adaptive numerical solution of a highly degenerate diffusion–reaction biofilm model based on regularisation. *Journal of Scientific Computing*, 74(2):1060–1090, 2018.

[20] Maryam Ghasemi, Burkhard A Hense, Hermann J Eberl, and Christina Kuttler. Simulation-based exploration of quorum sensing triggered resistance of biofilms to antibiotics. *Bulletin of mathematical biology*, pages 1–40, 2018.

[21] Denis Herbert, R Elsworth, and RC Telling. The continuous culture of bacteria; a theoretical and experimental study. *Microbiology*, 14(3):601–622, 1956.

[22] Ronald L Iman, James M Davenport, and Diane K Zeigler. Latin hypercube sampling (program user's guide).[lhc, in fortran]. Technical report, Sandia Labs., Albuquerque, NM (USA), 1980.

[23] Vipin Chandra Kalia. Quorum sensing inhibitors: an overview. *Biotechnology advances*, 31(2):224–245, 2013.

[24] Daniel E Koshland Jr. The application and usefulness of the ratio kcat/km. *Bioorganic chemistry*, 30(3):211–213, 2002.

[25] Kim Lewis. Persister cells, dormancy and infectious disease. *Nature Reviews Microbiology*, 5(1):48, 2007.

[26] MR Mattei, L Frunzo, B DAcunto, Y Pechaud, F Pirozzi, and G Esposito. Continuum and discrete approach in modeling biofilm development and structure: a review. *Journal of mathematical biology*, 76(4):945–1003, 2018.

[27] Pontus Melke, Patrik Sahlin, Andre Levchenko, and Henrik Jönsson. A cell-based model for quorum sensing in heterogeneous bacterial colonies. *PLoS computational biology*, 6(6):e1000819, 2010.

[28] Melissa B Miller and Bonnie L Bassler. Quorum sensing in bacteria. *Annual Reviews in Microbiology*, 55(1):165–199, 2001.

[29] I.W.A.T.G.B. Modeling. *Mathematical Modeling of Biofilms*. Scientific and Technical Report Series. IWA Publishing, 2006.

[30] Jacques Monod. The growth of bacterial cultures. *Annual Reviews in Microbiology*, 3(1):371–394, 1949.

[31] Kenneth H Nealson, Terry Platt, and J Woodland Hastings. Cellular control of the synthesis and activity of the bacterial luminescent system. *Journal of bacteriology*, 104(1):313–322, 1970.

[32] Aaron Novick and Leo Szilard. Description of the chemostat. *Science*, 112(2920):715–716, 1950.

[33] Merle E Olson, Howard Ceri, Douglas W Morck, Andre G Buret, and Ronald R Read. Biofilm bacteria: formation and comparative susceptibility to antibiotics. *Canadian Journal of Veterinary Research*, 66(2):86, 2002.

[34] Martin Schuster, D Joseph Sexton, Stephen P Diggle, and E Peter Greenberg. Acyl-homoserine lactone quorum sensing: from evolution to application. *Annual review of microbiology*, 67:43–63, 2013.

[35] Stefanie Sonner, Messoud A Efendiev, and Hermann J Eberl. On the well-posedness of a mathematical model of quorum-sensing in patchy biofilm communities. *Mathematical Methods in the Applied Sciences*, 34(13):1667–1684, 2011.

[36] Stefanie Sonner, Messoud A Efendiev, and Hermann J Eberl. On the well-posedness of mathematical models for multicomponent biofilms. *Mathematical Methods in the Applied Sciences*, 38(17):3753–3775, 2015.

[37] ME Stroppolo, M Falconi, AM Caccuri, and A Desideri. Superefficient enzymes. *Cellular and Molecular Life Sciences CMLS*, 58(10):1451–1460, 2001.

[38] MCM Van Loosdrecht, D Eikelboom, A Gjaltema, A Mulder, L Tijhuis, and JJ Heijnen. Biofilm structures. *Water science and technology*, 32(8):35–43, 1995.

[39] Lian-Hui Wang, Li-Xing Weng, Yi-Hu Dong, and Lian-Hui Zhang. Specificity and enzyme kinetics of the quorum-quenching n-acyl homoserine lactone lactonase (ahl-lactonase). *Journal of Biological Chemistry*, 279(14):13645–13651, 2004.

[40] Qi Wang and Tianyu Zhang. Review of mathematical models for biofilms. *Solid State Communications*, 150(21-22):1009–1022, 2010.

[41] John P Ward, John R King, AJ Koerber, P Williams, JM Croft, and RE Sockett. Mathematical modelling of quorum sensing in bacteria. *Mathematical Medicine and Biology*, 18(3):263–292, 2001.

[42] Guopeng Wei, Chieh Lo, Connor Walsh, N Luisa Hiller, and Radu Marculescu. In silico evaluation of the impacts of quorum sensing inhibition (qsi) on strain competition and development of qsi resistance. *Scientific reports*, 6:35136, 2016.

[43] Neil A Whitehead, Anne ML Barnard, Holly Slater, Natalie JL Simpson, and George PC Salmond. Quorum-sensing in gram-negative bacteria. *FEMS microbiology reviews*, 25(4):365–404, 2001.

[44] Joshua W Williams, Xiaohui Cui, Andre Levchenko, and Ann M Stevens. Robust and sensitive control of a quorum-sensing circuit by two interlocked feedback loops. *Molecular systems biology*, 4(1):234, 2008.